Dynamics of Knotted DNA Molecules Confined in Nanochannels

A DISSERTATION SUBMITTED TO THE FACULTY OF THE GRADUATE SCHOOL OF THE UNIVERSITY OF MINNESOTA
BY

Zixue Ma

IN PARTIAL FULFILLMENT OF THE REQUIREMENT FOR THE DEGREE OF DOCTOR OF PHILOSOPHY

Advisor: **Kevin D. Dorfman**

March, 2022

Acknowledgements

I am deeply grateful to so many people for their support at every stage of my research projects and throughout graduate school. First and foremost, I would like to express my sincere gratitude to my advisor, Prof. Kevin Dorfman, for accepting me into his research group and providing invaluable scientific guidance to me during the past four and a half years of my PhD study. He encouraged me to explore ideas that interested me and guided me in developing the ideas into scientific projects. Apart from training me as an independent researcher, he was also very supportive in my career path development. I feel extremely grateful for being Kevin's graduate student and he is a great advisor. I would also like to thank my other committee members, Prof. Satish Kumar, Prof. Mahesh Mahanthappa, and Prof. Vincent Noireaux for their scientific comments and suggestions on my thesis work.

The dissertation work would have been impossibe without the help and support from Dorfman group members. I was very lucky to have the opportunity to work and spent greatly enjoyable time with them. Thanks to all my colleagues in the Dorfman group, Hui-Min Chuang, Paridhi Agrawal, Aditya Bikram Bhandari, GK Cheong, Pranav Agrawal, Xiaolan Li, Vaidyanathan Sethuraman, Akash Arora, Seunghwan Shin, Mathew Thomas, Demetra Adrahtas, Logan Case, Anshul Chawla, Kexin Chen,

Pengyu Chen, Ryan Collanton, Ben Magruder, Clive Onyango, Sojung Park, and Sarah Seeger. I would like to offer my special thanks to my mentor, Dr. Hui-Min Chuang for teaching me research skills, assistance in the nanofluidic device protocols and helpful discussion about DNA in nanochannels in the formative years of my PhD.

I would like to acknowledge the funding sources for all the work in this thesis. This work was supported by NIH (R01-HG006851) and NSF (CBET-2016879). Device fabrication was conducted in the Minnesota Nano Center, which is supported by the National Science Foundation through the National Nano Coordinated Infrastructure Network (NNCI) under Award Number ECCS-1542202.

Thanks to all my CEMS friends and friends in Buffalo and China for your company and encouragement during my PhD. Special thanks to my roommates, Qiaomiao Tu and Jane Shi, and my cute cat, TangTang, for supporting me during my frustrated time.

Finally, I would like to express my sincere gratitude to my family for their encouragement, love and support during my life.

Abstract

Knots are intriguing topological objects and ubiquitous in biopolymers such as DNA molecules. The occurrence of knots in DNA confounds the accuracy of genomics technologies, such as nanochannel-based genome mapping and nanopore sequencing, that require uniformly stretching the DNA molecules. Knots existing in vivo also influence biological processes, such as DNA replication, and hence leads to cellular malfunction. The control of DNA knots is, thus, significant for genomics technologies and cell survival, which require first understanding the fundamental properties of knotted DNA in a crowded environment. The aim of this thesis is to address fundamental questions related to knot transport in nanochannel-confined DNA molecules, particularly the knot diffusion mechanism, the effect of knots on DNA diffusion in nanochannels and the interactions between two knots.

We first determined the knot diffusive behavior along DNA confined in nanochannels to distinguish between two predicted knot diffusion mechanisms, self-reptation and knot region breathing. With a recently developed nanofluidic "knot factory" device, we generated knots in DNA molecules with a formation probability of $48 \pm 20\%$. The experimental results of knot motion along DNA chains show that knots undergo subdiffusion, i.e. their mean-squared displacement grows sublinearly with time, which

supports the knot diffusion mechanism of self-reptation.

We then investigated the effects of knots on DNA center-of-mass diffusion in nanochannels, thus resolving the open question which of these competing effects, the shortening of DNA chains or the increased DNA-wall friction, dominates knotted DNA diffusion in nanochannels. To address this question, we measured the diffusivity of DNA molecules before and after knot formation via a combination of the nanofluidic knot factory device for knot generation and laser-induced fluorescence microscopy for DNA observation. The experimental results show that the presence of knots decreases the diffusivity of DNA chains confined in nanochannels. The reduced diffusivity indicates that the DNA-wall friction, rather than the shortening of the confined chain size, dominates the friction of knotted DNA in nanochannels.

Our previous work focused on the dynamical properties of single knots. Long DNA molecules are susceptible to form multiple knots in the chains. In the third research project, we investigated the interactions between two knots in nanochannel-confined DNA by analyzing the motion of the two knots along DNA chains. The free energy profiles of knot-knot interactions show that the separated knot state is more stable than the intertwined knot state, with dynamics in the separated knot state that are consistent with independent diffusion of the two knots.

The thesis work provides deep insights into the dynamical properties of DNA knots under nanochannel confinement. We hope such fundamental knowledge gained in this dissertation could prescribe avenues for suppression and removal of knots under nanofluidic systems and crowded environments, thereby improving the genomic technologies and controlling knots in living cells.

Contents

List of Figures

Chapter 1

Introduction

1.1 Knots

Knots are topological objects that consist of a set of continuous circles embedded together in a three-dimensional space [1]. These topological objects have a plethora of applications in daily activities of humankind, from tying shoelaces to creation of fishing knots; from boating to camping; from weaving cloth to decorative construction of wall-hangings.

Due to the practical and ornamental usage of knots, knots have sparked interest of scientists to develop the topological knot theory for centuries [2]. The knot theory was first developed by Vandermode, who specifically described knots in the subject of the geometry of position in 1771. A mathematical study of knots probably was first identified in the early part of the 19th century by Gauss, who defined the concept of linking numbers in topology. By 1900, there were published tables listing knots with up to 11 crossings which establish a basis for the development of a formalized knot theory in the 20th century [3]. The mathematical knot theory provides basic

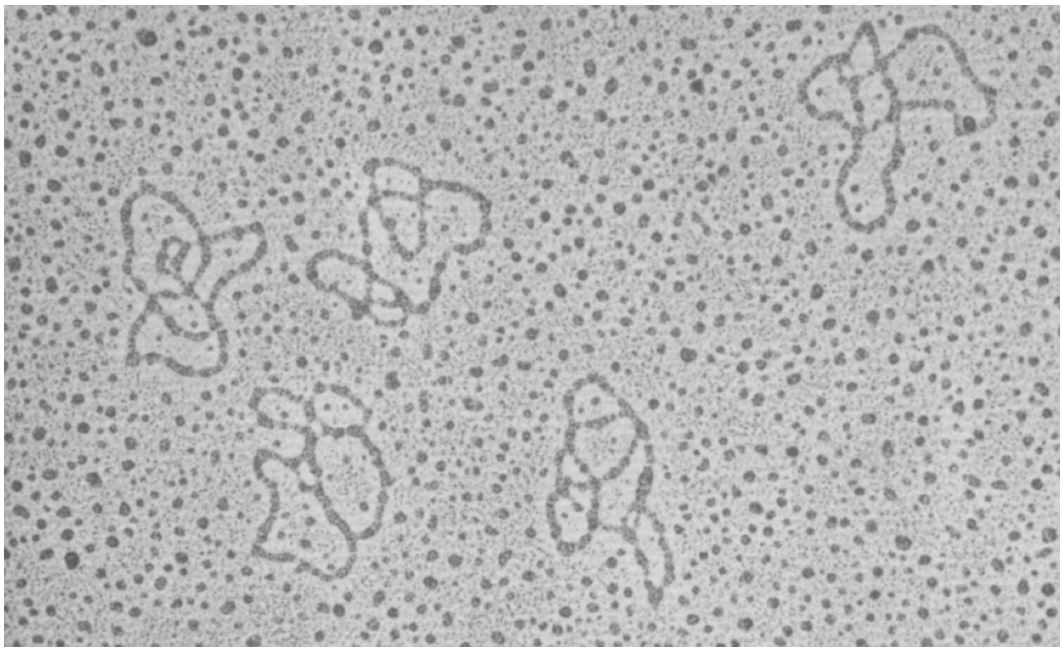

Figure 1.1: An electron microscopy image of knotted single-stranded DNA molecules. Reproduced from Ref. [4].

concepts, terminology and knot diagrams which guided scientists in the studies of physical knots.

Physical knots such as deoxyribonucleic acid (DNA) knots have been the focus of significant study in fields as diverse as polymer physics, topology, biology, fluid mechanics and nanotechnology from the late 20th century. The first DNA knots were identified in 1976 as shown in the electron microscopy image of knotted DNA rings in Figure 1.1 [4]. With the development of simulations and experimental techniques, the equilibrium properties of DNA knots, such as knot formation probability [5–12] and knot tightness [13–17], have been extensively investigated by simulations, and somewhat by experimental studies. The dynamical properties of knotted DNA, however, remain relatively unexplored and are primarily studied by simulations and theoretical work [18–21]. Understanding the dynamics of knotted DNA is an intriguing question

that spans multiple scientific disciplines including polymer physics, topology, biology, and fluid mechanics.

Besides the scientific interest in studying the dynamics of DNA knots, the fundamental knowledge about dynamical properties of DNA knots under confinement will permit developing rational strategies to improve genomic technologies, nanochannel-based genome mapping and nanopore sequencing, in which knots play a confounding effect on the genomic data. From a biological perspective, the fundamental understanding of DNA knots in crowded environments will also help to control DNA knotting in vivo, which is essential for cell survival.

1.2 DNA Knots in Genomic Technologies

Decoding of DNA that comprises the human genome is of great significance for explaining human evolution and diseases such as cancers [22, 23]. In 1990, a 15-year Human Genome Project (HGP) was launched to sequence around 3 billion base pairs (bp) of the euchromatic human genome [22]. Sanger sequencing [24], the major sequencing technique used in the HGP, was successful in reading encoded base pair sequences of single DNA molecules up to 900 bp in length [25]. With the increasing demand to quickly and accurately sequence genomes in large quantities, it was no more practicable to use the time-consuming and expensive Sanger sequencing technology [26]. On the other hand, the development of next-generation sequencing (NGS) technologies showed very promising results [27, 28] by sequencing the human genome at a cost of around $1000 in 24 hours [29, 30].

Despite the ultra-high throughput of NGS technologies, NGS can only read DNA molecules that are limited to lengths ranging from 50 to 150 bp [31, 32]. As a result,

it is very challenging for NGS to identify genomic structural variations that comprise of deletions, inversions, insertions, duplications and translocations, which generally span from 1 kbp to 1 Mbp in the human genome. These structural variations are responsible for human diseases such as autism and schizophrenia [33]. Additionally, nearly half of human genome have repetitive genomes which cause technical challenges in *de novo* genome assembly [34–36]. These challenges are being tackled by long-read genomic technologies such as nanochannel-based genome mapping [37, 38], nanopore sequencing [39–42] and linked-read sequencing [43, 44]. DNA knots, however, were observed in the nanofluidic systems, nanochannels [45] and nanopores [12]. The detected DNA knots have been shown to affect the accuracy of the two genomic technologies, genome mapping in nanochannels [45] and nanopore sequencing [12, 46–49].

1.2.1 Genome Mapping in Nanochannels

Nanochannel-based genome mapping is a genomic technology that can create a genomic map of DNA molecules up to Mbp in length, thus detecting genomic structural variations and also improving genome assemblies by scaffolding the genomic map with sequencing data from NGS [37, 38, 50, 51]. In the genome mapping technique (Figure 1.2), a fluorescent sequence-specific labeled long DNA molecule is linearized via confinement in a nanochannel. Images of the labeling barcodes along the DNA backbone are produced using laser-induced fluorescence microscopy. The fluorescence intensity of the DNA molecule along the nanochannel obtained from the image is then analyzed to provide the genomic distance between each of the labeled sites. The genomic distance between the labels on the DNA molecule and the position of label patterns

can be used to detect structural variations by comparing the experimental data with a reference genome. The genomic distances also provide the DNA barcode, which are then aligned onto the genome to assemble the genomic map [38].

While the nanochannel-based genome mapping requires uniformly stretching DNA molecules in nanochannels by confinement, the presence of knots along the long DNA molecules detected as bright spots challenges the accuracy of genome mapping data because such a topological event could be misinterpreted as a deletion, one of the major structural variation types, as illustrated in Figure 1.3 [45]. Here, the occurrence of a knot reduces the genomic distance between label "2" and "3" by pulling the two labels closer, giving rise to a misinterpretation of deletion [8]. To reduce the confounding effect of knots on the resulting genome map, two currently available methods in the nanochannel-based genome mapping technique are (i) to remove the bright spots through expensive image processing and (ii) to work at very high coverage [45]. The nanochannel array technology from Bionano Genomics is capable of obtaining genomic maps of thousands of molecules per loading cycle. However, knots also affect the accuracy of other genome mapping methods based on stretching DNA in a nanofluidic system by an elongational flow [53, 54] and formation of DNA dumbbells within nanoslits to stretch DNA [55, 56]. The throughput of such approaches is not high enough to obtain sufficient coverage. It is thus highly desirable to develop new strategies to suppress knot formation or to remove knots in DNA molecules, which requires the understanding of dynamical properties of knotted DNA molecules in nanochannels.

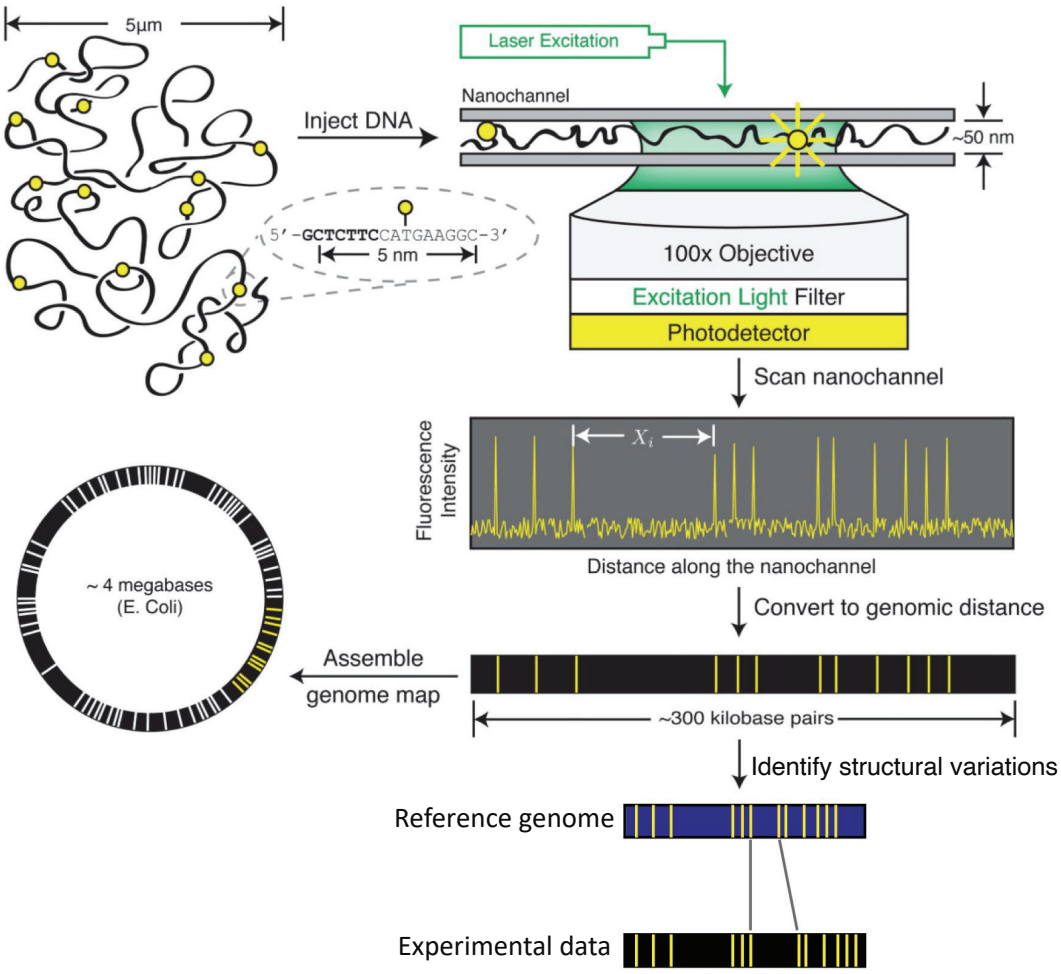

Figure 1.2: Schematic illustration of workflow of geonme mapping in nanochannels for creating a genomic map from single DNA molecules and for detecting structural variations of genome. A fluorescent sequence-specific labeled long DNA molecules is injected into a nanochannel and is then linearized by confinement along the channel axis. The DNA molecule and the labeled sites are imaged using laser-induce fluorescence microscopy. The fluorescence intensity of the DNA molecule along the channel obtained from the image is then analyzed to provide the distance between each of the labeled sites. The distance is then converted to genomic distance which can be used to assemble genome map by aligning onto the genome and detect structural variations by comparing with a reference genome. Reproduced from Ref. [52].

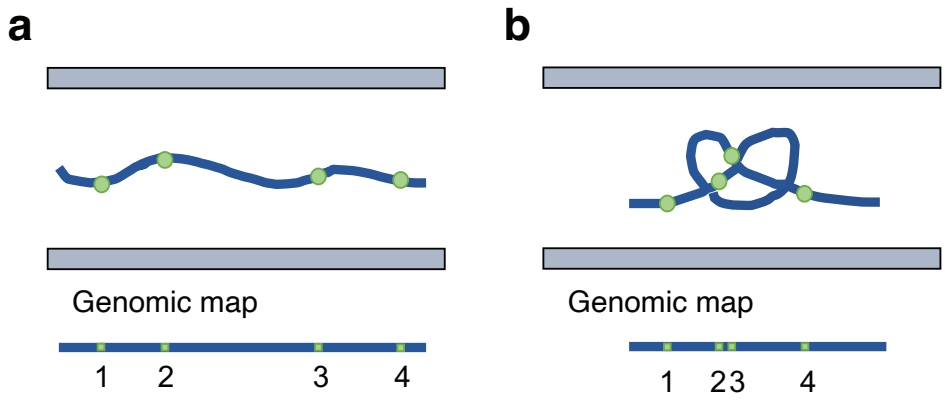

Figure 1.3: Schematics of the effects of knot formation on nanochannel-based genome mapping. The schematics illustrate a DNA chain (blue line) with sequence-specific labels (green dot) confined in a nanochannel and a genomic map corresponding to the position of labels along the DNA molecule. (a) The unknotted DNA generates a reference genomic map. (b) The knot mimics a deletion in the genomic map by pulling the two labels "2" and "3" closer. Adapted from Ref. [8]

1.2.2 Nanopore Sequencing

Nanopore-based DNA sequencing is the long-read genomic sequencing technology that could read nucleotides, one-by-one, of single-stranded DNA molecules up to Mbp in length [39–42, 57]. With the real-time individual base detection of long DNA molecules, the sequencing technology allows detecting DNA base modifications directly and capturing structural variations in genomes [39]. In nanopore sequencing, single DNA molecules are translocated through a narrow pore, typically several nanometer in size, by applying an electric field [42]. The ionic current changes as the single-stranded DNA pass through the pore due to the differences in electrical resistances of the four nucleotides, adenine (A), thymine (T), guanine (G) and cytosine (C). The changes in the electrical current are measured and then decoded to provide the specific DNA sequence as shown in Figure 1.4a [39, 57].

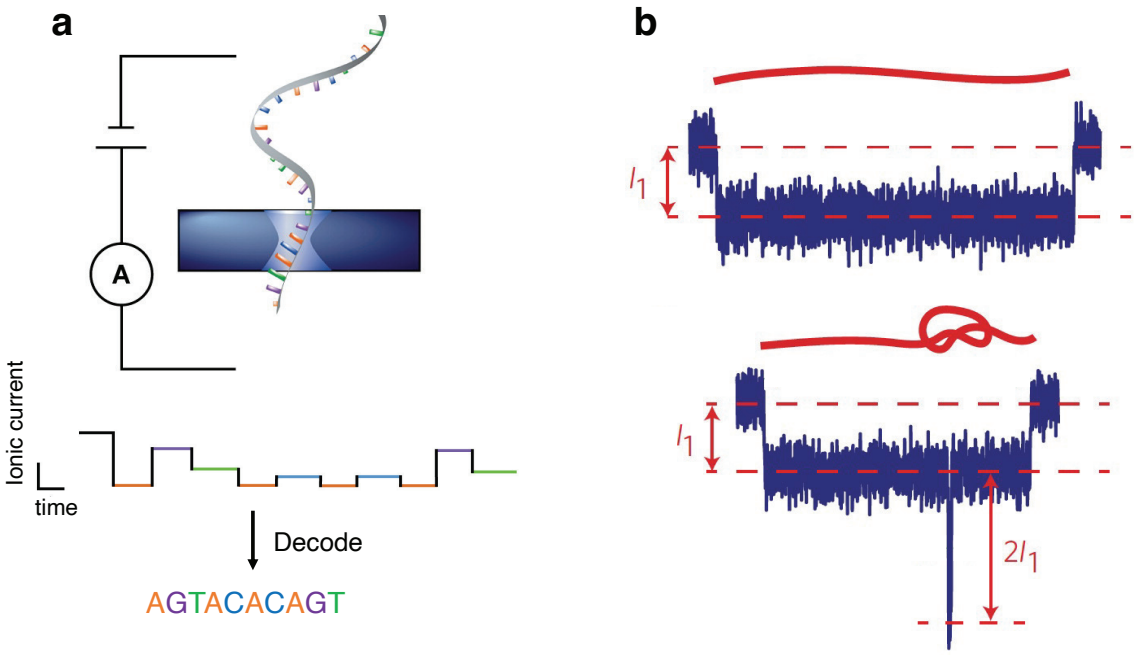

Figure 1.4: Schematics of the effect of knots on current blockage in nanopore sequencing. (a) Simplified schematic illustration of nanopore-based DNA sequencing principle. The changes in the ionic current are detected when individual single-stranded DNA molecules are driven through nanopores by applying an electric field. The red, purple, blue and green lines represent the signals of the four different bases of DNA which are adenine (A), guanine (G), cytosine (C), and thymine (T), respectively. (b) Current trace of an unknotted DNA (top) and a DNA with a trefoil knot (bottom). The knot produces a current blockage with $2I_1$ amplitude higher than the current blockage of I_1 generated by the linear chain. Reproduced from Ref. [58] and Ref. [12].

The formation of knots in DNA chains, however, affects the changes in the ionic current when DNA molecules are passing through the nanopores as shown in Figure 1.4b [12, 46–49]. When a linear unknotted DNA chain is translocating through a nanopore, the molecule produces an ionic current blockage of I_1. A DNA molecule with a trefoil knot, however, generates a higher ionic current blockage with an additional amplitude of $2I_1$ compared with the unknotted part of the linear DNA chain. Such blockage of the nanopore due to the formation of knots with a higher electric

resistance compared with the unknotted DNA chain confounds the accuracy of DNA sequencing data produced from the changes in the ionic current. In nanopore sequencing, knots may even impede DNA translocation through the narrow pore, which might block the nanopores for future usage of DNA sequencing [12, 47–49]. Thus, rational strategies are highly desirable to be developed to suppress knot formation or remove knots in DNA molecules in the nanopore-based sequencing which first requires the understanding of the dynamics of knotted DNA under confinement.

1.3 DNA knots in biological systems

In biological systems, DNA molecules are likely to form knots by passing the free chain ends through loops within the same DNA chain [59]. Random cyclization of linear DNA molecules with cohesive ends illustrates the knotting mechanism. The free ends in linear DNA first pass through loops within the same molecule to form pseudo-knots and then the closed knotted rings arise from joining the cohesive ends during the cyclization process [60]. The knotting process of DNA in vivo can also be regulated by enzymes such as topoisomerases and recombinases which operate by breaking and rejoining of single or double strands of DNA chains [59].

DNA knotting in vivo, however, affects the biological processes such as DNA replication, and hence the cell survival. DNA molecules within bacteriophage capsids, typically 50 - 80 nm in size, exemplify the problems caused by knotting. The DNA inside the capsids of bacteriophage P2 are likely to self-entangle into knots which hinder the viral DNA ejection into an infected bacterial cell. The affected infection efficiency of bacteriophages plays a significant role in replication of bacteriophages, and hence survival of the host bacterial cell [61, 62]. Nanochannel-confined DNA

molecules provide ideal model systems to explore DNA knots in crowded environments which are relevant for DNA packing in cells. The fundamental knowledge gained in the study of dynamics of knotted DNA under confinement will permit understanding of DNA knots in living cells, hence paving a way to manipulate DNA knotting in biological systems which is important for cell survival.

1.4 Thesis Organization

Knots are topological objects that are of special interests for centuries due to their practical and decorative usage in our everyday life. Knots are also ubiquitous in biological systems such as DNA molecules. The occurrence of knots along DNA molecules confounds the accuracy of genomics technologies, such as nanochannel-based genome mapping and nanopore sequencing. Understanding the dynamical properties of DNA knots could prescribe avenues for suppression and removal of knots in the techniques, thereby improving the genomics technologies. More broadly, the knotted DNA under confinement provides an ideal model to study DNA knotting in living cells, which is significant for cell survival. Additionally, knotting dynamics in confinement is an intriguing topic that confluences various scientific disciplines including polymer physics, biology, fluid mechanics, topology and nanotechnology. *As such, my dissertation research focuses on fundamental questions related to the dynamics of knotted DNA molecules in nanochannel confinement.*

In line with above goals, **Chapter 2** provides background information for the research focusing on dynamical properties of DNA knots under nanochannel confinement. The chapter starts to introduce the physical properties of DNA molecules and the physcial regimes in nanochannel confinement, particularly focusing on the

extended de Gennes regime which is relevant to the dissertation research. Then, the chapter reviews the DNA knots including the knot types and the experimental techniques for DNA knot generation.

Chapter 3 describes the determination of knot diffusive behavior along nanochannel-confined DNA molecules. To study DNA knot diffusion, we take advantage of the nanofluidic "knot factory" devices described in **Chapter 2** to generate knots in DNA molecules under nanochannel confinement and laser-induced fluorescence microscopy to detect DNA knots. With the knot factory device and fluorescence microscopy, we determined the knot diffusive behavior, and thus the knot diffusion mechanism by analyzing the single knot motion along nanochannel-confined DNA chains.

Chapter 4 explores the effect of knots on DNA center-of-mass diffusion confined in nanochannels in the extended de Gennes regime. We compare the diffusivity of DNA molecules before and after knot formation and show that the formation of knots decreases the knotted DNA center-of-mass diffusion in nanochannels which indicates that the DNA-wall friction, rather than the shortening of the confined chain, dominates the friction of knotted DNA in nanochannels in the extended de Gennes regime.

Chapter 5 investigates the interactions between two knots in nanochannel-confined DNA molecules. We image the movement of two knots in DNA molecules and analyze the interactions between two knots by obtaining the free energy profiles of knot-knot separations. The experimental results show that the separated knot state is more stable than the intertwined knot state which contradicts the experimental results of long-range attraction between two knots in DNA under elongational flow. This inconsistency is postulated to result from a weaker transverse fluctuations-induced

attraction force between knots in DNA under confinement compared with DNA under flow.

Chapter 6 summarizes the conclusions of this dissertation research and presents an outlook on future directions related to knot formation and knot transport. We propose the experimental methods for the exploration of knot formation mechanisms under confinement and also several topics related to dynamical properties of knotted DNA in different-sized nanochannels and different ionic strengths of buffer solution that may be interest for the future study.

Chapter 2

Background

The important part of this chapter is an introduction to fundamental physical properties of DNA in nanochannels and DNA knots, which helps to understand the studies of knotted DNA under nanochannel confinement presented in the following chapters. Section 2.1 provides background on physical properties of DNA molecules and equilibirum and dynamical properties of DNA in different physical regimes in nanochannel confinement with a focus on the extended de Gennes regime. Section 2.2 presents an overview of knots and then introduces various experimental techniques to study DNA knots, particularly the nanofluidic knot factory device for efficient DNA knot formation in nanochannels, which is the technique used in the thesis work.

2.1 Polymer Physics

Polymers are macromolecules that are composed of chains of repeat units [63]. DNA molecules are biopolymers and the repeat unit for DNA is a nucleotide which consists of a sugar-phosphate backbone and a nitrogenuous base. The nitrogen-containing

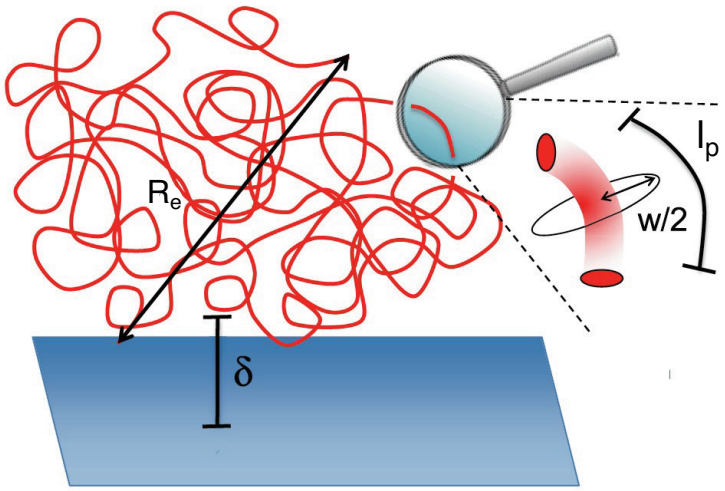

Figure 2.1: Schematic illustration of a single linear DNA chain with physical parameters including end-to-end length (R_e), persistence length (l_p), effective width (w), and DNA-wall depletion length (δ). Reproduced from Ref. [65].

bases for DNA are adenine, guanine, cytosine, and thymine. Long polymers such as DNA molecules are susceptible to self-entangle into knots [59, 60, 64]. Understanding the dynamical properties of knotted DNA in nanochannels which is the focus of the dissertation research requires the fundamental knowledge of physical properties of DNA and the equilibrium and dynamical properties of DNA under nanochannel confinement.

2.1.1 Physical Properties of DNA

The fundamental physical properties characterizing DNA include contour length (L), persistence length (l_p), effective width (w), and DNA-wall depletion length (δ). Figure 2.1 shows a typical conformation of a linear DNA molecule and a schematic illustration of the persistence length, effective width, and DNA-wall depletion length. Below, we provide an overview of the four physical parameters.

Contour Length (L)

The contour length (L) is the maximum end-to-end length (R_e) of a DNA chain when the DNA is stretched without thermal fluctuations. The contour length of a DNA molecule can be calculated as the product of the total number of base pairs in the DNA and the average height of a base pair. The average height of a base pair is approximately to be 0.34 nm for B-state DNA [66]. For T4 GT7 DNA molecules with 166 kilobase pairs (kbp) used in this dissertation research, the contour length is calculated to be 56 μm. These contour lengths are for unstained DNA molecules. To image DNA using fluorescence microscopy, the DNA molecules are typically stained with fluorescent dyes such as YOYO-1 due to its large signal enhancement upon binding. When DNA are stained with fluorescent dyes, the contour length of DNA is increased due to the intercalation of the dyes in DNA molecules [67, 68]. The increased length is assumed to be 0.51 nm per bound dye molecule [68, 69]. Let us take T4 GT7 DNA again as an example, the stained T4 GT7 DNA with a dye-to-DNA base pair ratio of 1:10 is estimated to be 65 μm.

Persistence Length (l_p)

DNA molecules are semiflexible chains which have random configurations due to thermal fluctuations. The persistence length (l_p), which quantifies the rigidity of DNA chains, is a distance along the backbone over which the DNA has to go before the orientation changes appreciably as shown in Figure 2.1 [63, 65]. The persistence length of DNA can be obtained experimentally using single molecules in elasticity studies [70, 71]. In the studies, DNA is stretched between two polystyrene beads in an optical tweezers apparatus and the force-extension measurements are conducted

by measuring the force on the trapped bead while moving the other bead with a known distance. An estimation of the persistence length is then obtained by fitting the force-extension curve with the worm-like chain elastic behavior model [70–72]. The persistence length of DNA obtained from the single molecules elasticity study increases from 46 to 59 nm as the sodium ion concentration decreases from 1000 to 2.57 mM [70]. The persistence length of DNA molecules strongly depends on the ionic strength of buffer solution [70, 71, 73, 74].

Classic theory suggests that the persistence length is the sum of bare persistence length (l_{p0}), which can be estimated as the persistence length of DNA in high ionic strength buffer solution, and the electrostatic persistence length [73–75]. In the classical theory, the electrostatic contribution to $l_p \sim \lambda_D^2$, where λ_D is the Debye length which is affected by the ionic strength of buffer solution [73, 74]. Other theories, however, argue that the electrostatic contribution to $l_p \sim \lambda_D$ instead of $\sim \lambda_D^2$ [75, 76]. Dobrynin [75, 76] suggests an empirical formula

$$\mathrm{l_p} \approx 461 + \frac{607}{\sqrt{I}} \tag{2.1}$$

where l_p has the unit of Angstrom and I is the ionic strength of buffer solution in unit of mM. The equation is obtained by fitting of available DNA persistence length data at different ionic strength of buffer solutions. In our experimental work described in the dissertation research, we use Eq. 2.1 to estimate the persistence length of DNA molecules which is 60 nm, in buffer solution with an ionic strength of 18 mM.

Effective Width (w)

The effective width (w) is used to account for the repulsive interactions between DNA chain segments as shown in Figure 2.1. The quantity can be estimated using a theoretical model of interactions between two charged cylinders in salt solutions. The idea to predict the effective width is first to calculate the effective interaction potentials between the two charged cylinders using Poisson-Boltzmann theory. With the calculated interaction potentials, the excluded volume between the two cylinders is then evaluated to obtain the effective with [77]. The theoretically predictions of the effective width are consistent with the values obtained using experimental techniques such as light scattering [78], sedimentation [79] and studies of the probability of DNA trefoil knot formation during cyclization [60]. The experiments and theory suggest that the effective width depends on the ionic strength of buffer solution. In the thesis work, the effective width of DNA in a buffer with an ionic strength of 18 mM is estimated to be 12 nm based on the formula by Stiger [77].

DNA-wall Depletion Length (δ)

The DNA-wall depletion length (δ) is a quantity that account for the DNA-wall excluded volume and electrostatic interactions as shown in Figure 2.1 [80–82]. When DNA are confined in nanochannels, the depletion length characterizes the reduction in the region of the nanochannels that is inaccessible to the DNA molecules. An accurate estimation of DNA-wall depletion length is important for approximating the effective channel size which is the actual space available to DNA inside nanochannels.

The effective channel size is estimated as D_{eff}, using the equation

$$D_{\text{eff}} = \sqrt{(D_1 - \delta)(D_2 - \delta)} \tag{2.2}$$

where D_1 and D_2 are the height and width of the nanochannels. Many studies estimate the DNA-wall depletion length as the effective width of DNA molecules [82, 83]. The approximation, however, is not an accurate estimation. A study has shown that there is typically a 10% error between simulation and experimental results using the approximation [84]. A model was developed by Bhandari *et al.* [80] to estimate the DNA-wall depletion length based on more than 5 million experimental measurements of the DNA fractional extension in square nanochannels with size of 38 nm. The DNA-wall depletion length in our experimental work presented in the following chapters is computed to be 14 nm for DNA in nanochannels at buffer solutions with an ionic strength of 18 mM using the recently developed model [80].

2.1.2 DNA in Nanochannel Confinement

DNA as a polymer model has been the focus of significant study in polymer physics. Nanochannel confinement is emerging as an important technique to study the static and dynamical properties of DNA for single molecule genomics. When DNA molecules are confined in nanochannels whose size are smaller than the radius of gyration of DNA molecules (R_g) in the bulk, the DNA chain extends along the channel axis which allows to access the genomic information contained in the single DNA molecules.

In nanochannel confinement, there are four physical regimes to a polymer confined in nanochannels with geometric average channel size D_c as shown in Figure 2.2. As

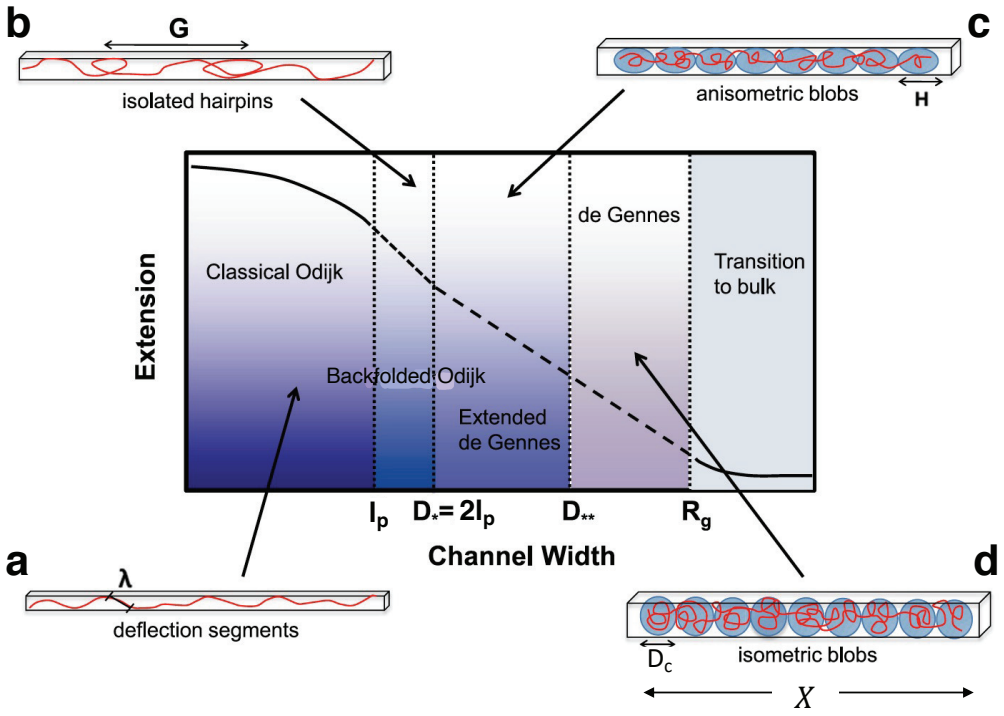

Figure 2.2: Schematic illustration of DNA confined in nanochannels in (a) the Odijk regime, (b) the backfolded Odijk regime, (c) the extended de Gennes, and (d) the de Gennes regimes. Reproduced from Ref. [65].

the channel size D_c decreases, the polymer chains feel a stronger effect of confinement and the chains change from weakly compressed coils to strongly elongated filaments. De Gennes [85, 86] developed the blob theory to describe the properties of polymers confined in the classic de Gennes regime where $D_c \gg l_p$. In the regime as shown in Figure 2.2d, the polymer chain is envisioned as being a series of isometric blobs with dimension proportional to D_c. The DNA chains on length scales less than D_c are unaware of the channel compression and each blob has the conformation of self-avoiding random walk in a good solvent. The extension, X, of the chain parallel to the channel axis scales as $X \sim D_c^{-2/3}$. For channel sizes between Kuhn length of $2l_p$ and thermal blob size l_p^2/w of DNA molecules, corresponding to the extended de

Gennes regime, the conformation of DNA chains consist of a series of linearly ordered anisometric blobs with length of $H = (D_c l_p)^{2/3} w^{-1/3}$ as shown in Figure 2.2c [87, 88]. The blob theory developed by de Gennes [85, 86] can also be applied to the extended de Gennes regime. The extension of the DNA chain scales exactly like the scaling in the classic de Gennes regime [65, 89]. As the channel size decreases to approximately Kuhn length, the polymer chain enters the backfolded Odijk regime, where the polymer chain forms isolated hairpins with a global persistence length G as shown in Figure 2.2c [88]. When the channel size is less than the persistence length l_p, the polymer chain feels a stronger confinement and the confined chain forms deflection segments with length of λ instead of hairpins and coils as shown in Figure 2.2a [90].

The experimental data in the dissertation work fall in the extended de Gennes regime. The effective channel size, D_{eff}, of our knot factory device is calculated to be 307 nm using the equation 2.2 described in the previous section. The effective channel size is in the extended de Gennes regime boundaries of 241 and 694 nm as determined by simulations [91]. The focus of the dissertation work is the dynamical properties of knotted DNA chains in the regime, in particular the diffusion of knotted DNA in the extended de Gennes regime as described in Chapter 4. The diffusion coefficient, D_t, of a linear unknotted polymer chain confined in the extended de Gennes regime is estimated as

$$\mathrm{D_t} \approx D_R \left[c_1 + c_2 \left(\frac{X}{L} \right)^{-1} \right] \tag{2.3}$$

based on the modified blob theory that incorporates the effect of local chain stiffness on semiflexible polymer diffusion in nanochannels [81, 92]. D_R is the Rouse diffusivity of a freely draining chain and is calculated as $D_R = k_B T/(6\pi\eta L)$, where k_B is the Boltzmann constant, T is the absolute temperature, η is the solvent viscosity and L

is the contour length of polymer chains. Gupta *et al.* [81] measured the diffusivity of λ-DNA in nanochannels with effective sizes ranging from 117 to 260 nm and obtained the coefficients $c_1 = 0.86 \pm 0.79$ and $c_2 = 1.2 \pm 0.19$ of the modified blob theory model by fitting the experimental data at 95% confidence interval. They also fit Eq. 2.3 to the simulation data of Kirkwood diffusivity of a discrete wormlike chain model and obtained the coefficients to be $c_1 = 1.4 \pm 0.4$ and $c_2 = 1.0 \pm 0.1$ [81, 92].

2.2 Knots

To understand the experimental study of dynamical properties of DNA pseudo-knots in this dissertation research, the basic issues are what knots and knot types are and how to generate DNA knots experimentally. In the section, we will provide background on the concepts of knots and knot types and experimental techniques to study DNA knots.

2.2.1 Knot Types

In mathematics, a knot is defined to be a set of continuous circles that are embedded together in a three-dimensional space [1]. Strictly speaking, the mathematical definition of a knot can only be applied on a closed chain. Linear DNA chains, however, can form pseudo-knots, which can be mapped to the mathematical knots by connecting the two chain ends together to form closed loops [1, 93]. Knots can form diverse types and the corresponding complexity of knots is illustrated in Figure 2.3. The characterization of such knot types is significant in understanding the effect of knot complexity on the dynamical properties of knotted DNA. One useful description for the type of

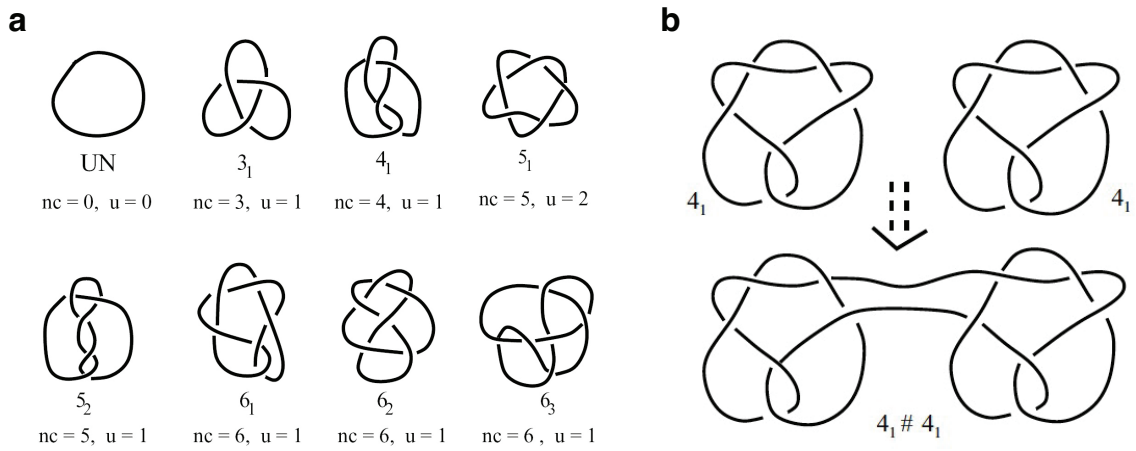

Figure 2.3: Knot diagrams for prime and composite knots. (a) Knot diagrams for prime knots with crossings up to 6. Mirror images are not shown here. The nc and u represent crossing number and unknotting number, respectively. (b) Schematic illustration of a composite knot (4_1 # 4_1) which is formed by the connection of two figure eight knots (4_1). Reproduced from Ref. [1]

a knot is the crossing number (nc) of a knot in a knot diagram. A knot diagram is a planar representation of a knot in a three-dimensional space when projected onto a plane. Typical prime knot types with six crossings or fewer are shown in Figure 2.3a, where nc denotes the crossing number and u represents the unknotting number, namely the minimal number of crossing changes that a knot in the knot diagram is turned into an unknot. The knot type with nc = 0 is the unknot (UN), also called the trivial knot. The trefoil knot (3_1) with three crossings is the simplest non-trivial knot. The 4_1 represents the figure eight knot. The 5_1 and 5_2 are two knot types with nc = 5. For nc = 6, there are three prime knots, 6_1, 6_2 and 6_3 [1]. All the knots shown in the Figure 2.3a are prime knots, which are not the combination of two non-trivial knots. A knot which is the connected sum of two non-trivial knots is defined as a composite knot [94]. An example of a composite knot which is the composition of two figure eight knots is shown in Figure 2.3b.

2.2.2 Experimental Techniques of DNA Knot Generation & Analysis

A number of techniques for DNA knot generation and analysis have been developed, including alternating current (AC) electric field [96–99], optical tweezers [95, 100], and solid-state nanopores [12]. Examples of the techniques studying DNA knots are shown in Figure 2.4a-c. Each of the techniques has advantages and disadvantages. The technique using AC electric field to introduce knots allows to generate knots efficiently and study DNA knots in stretched molecules as shown in Figure 2.4a. The imposed tension used to stretch DNA molecules in the technique, however, may confound the dynamical properties of knotted DNA. In the optical tweezer technique as illustrated in Figure 2.4b, knots can be formed with known type using optical tweezers to mechanically tie single DNA molecules with beads at the ends as handles for optical tweezers [95, 100]. Although the experimental technique can generate knots with known topology, the experimental method for knotting is not efficient to acquire enough single knotted DNA molecules for the dynamics of knotted DNA study. The solid-state nanopore shown in Figure 2.4c provides an efficient method to detect knots by measuring the ionic current when knotted DNA translocate through the nanopore [12]. This solid-state nanopore techniques allow to study the equilibrium properties of DNA knots, such as knot size and knotting probability [12], and also the dynamics of knotted DNA translocating through the narrow pore [46]. In this nanopore confinement, the DNA molecules are pulled by electric field gradient outside the nanopore. The dynamical properties of knotted DNA may be confounded by the external force to linearize the knotted DNA molecules in the solid-state nanopore.

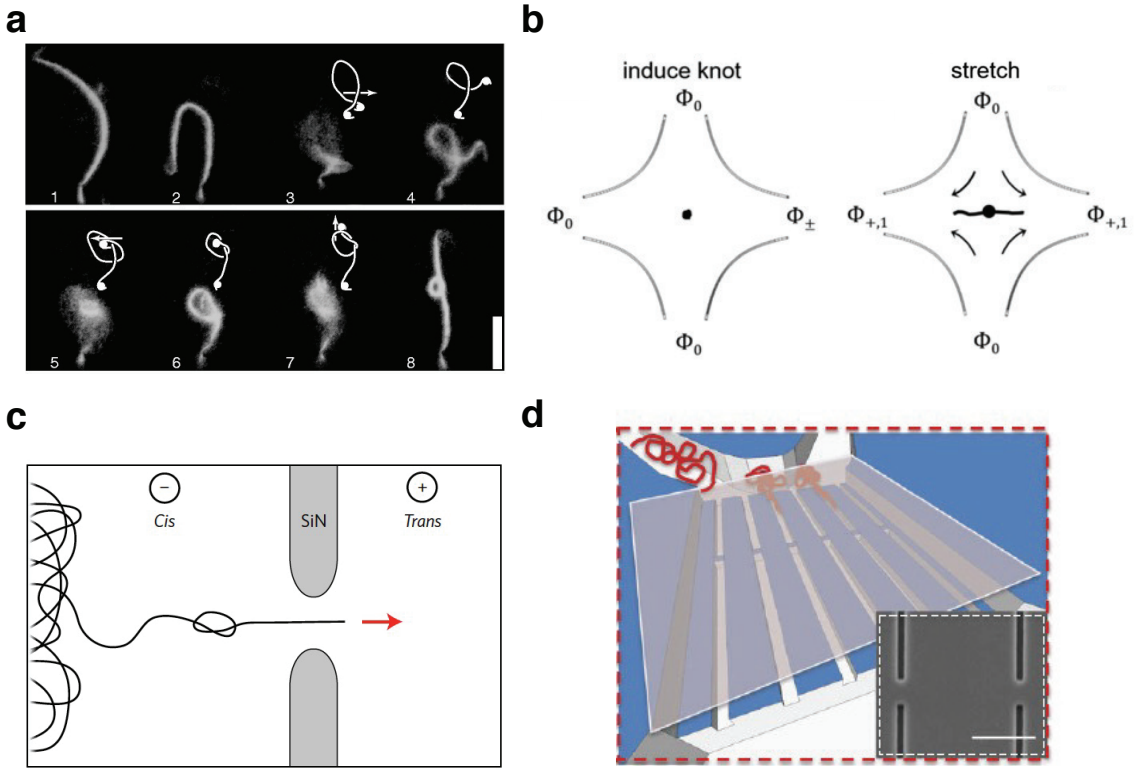

Figure 2.4: Experimental techniques to study DNA knots. (a) The process of knot generation using optical tweezers. The trefoil knot is mechanically tied using beads at the ends as handles for optical tweezers [95]. The scale bar is 10 μm. (b) A schematic illustration of application of AC electric fields to introduce a knot. An AC electric field is applied to compress a DNA molecule and induce a knot in the molecule. The knotted DNA is stretched by an elongational field [96]. (c) A schematic illustration of a knotted DNA translocating through a nanopore by applying an electric field gradient [12]. (d) Schematics of the center of the nanofluidic knot factory device with nanochannels and slit barriers. The DNA molecules (red curves) are loading from microchannels to nanochannels. Inset: an SEM image of the nanochannels and nanoslits. The scare bar is 3 μm. Reproduced from [11, 12, 95, 96].

All the previous introduced experimental techniques, AC electric fields, optical tweezers, and solid-state nanopores, use external forces to stretch DNA which may confound the dynamical properties of knotted DNA. Thus, it is desirable to develop a technique which can generate and detect knots efficiently and stretch DNA molecules without imposing tension. A nanofluidic knot factory device shown in Figure 2.4d was recently developed by Amin *et al.* [11]. In this techniques, knots can be generated and detected efficiently in nanochannels which linearize DNA by confinement without imposing tension [101], enabling investigation of dynamical properties of knotted DNA molecules.

The knot factory device is composed of nanochannel arrays with slit-barriers in the center of nanochannels as shown in Figure 2.4d, and it has been demonstrated to produce knots using pressure driven flow to compress a single DNA molecule against the slit-barrier in a nanochannel. The schematic of DNA knot generation process is illustrated in Figure 2.5. Initially, single DNA molecules are confined in nanochannels. Then, a pressure driven flow is applied to compress the DNA molecules against slit-barriers. In the compression process, DNA segments adjacent to the barriers first become concentrated with unconstrained free DNA ends away from the barriers. Then, the DNA chain undergo transient compression. After the pressure is released, the DNA molecule begin to relax and eventually reach equilibrium state with the presence of knots in the DNA chains. In the knot factory, the knot formation probability can be controlled by adjusting the applied pressure and the waiting time during the compression process. The working principle of the system to generate knots and the dynamics of knot generation, however, are still not well understood. Three possible knot-formation mechanisms were proposed for the knot factory. One of the possi-

bilities is that the chain ends are forced to pass through loops to generate knots in the compression process. The other two possible mechanisms are that hydrodynamic flows near the slit-barrier which show curving streamlines or thermal fluctuations drive chain ends to form knots along single DNA molecules [11]. To understand the knot formation mechanism in the nanofluidic systems, we propose an experimental study of knotting in the knot factory device which is described in detail in Chapter 6.

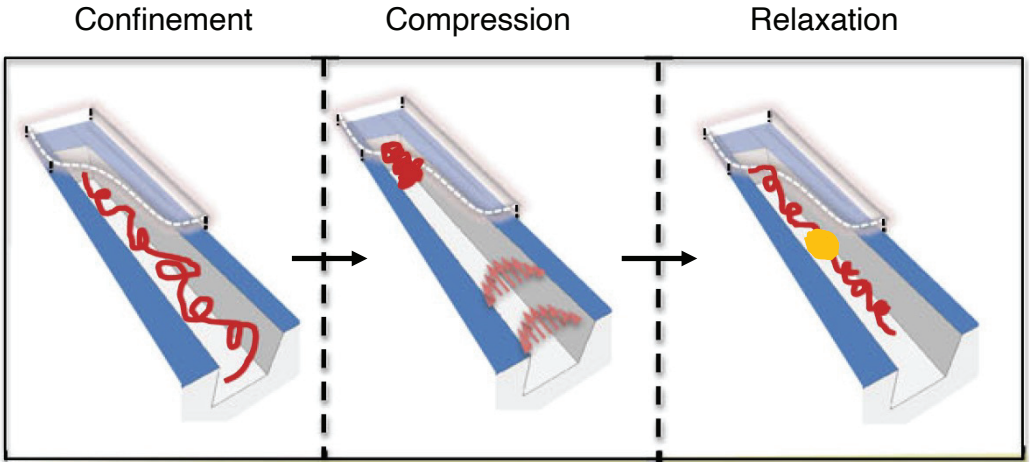

Figure 2.5: Schematics of knot generation process in the nanofluidic knot factory device. Initially, a DNA molecule confined in a nanochannel is in its equilibrium state. The DNA molecule is then compressed against a silt-barrier with a free end away from the barrier. After pressure is released, the DNA is relaxed with a knot (yellow) formed in the DNA molecule. The arrow indicates the direction of fluid flow. Reproduced from [11].

The knot factory device allows to generate knots with high probability in the nanochannel-confined DNA molecules. The formed knots can also be detected efficiently in the devices using fluorescence microscopy. In the knot factory device, knots are identified as bright spots in DNA images and spikes in intensity profiles of DNA backbones. Such bright spots could also be associated with a folded configuration as both of the folds and knots show spikes in the DNA intensity profiles as shown in

Figure 2.6 [45]. The differences in the unravelling process of knots and folds, however, allow us to distinguish between knots and folds. In the nanofluidic knot factory, knots are observed to be persistent as well as localized, and can only be destroyed by diffusing to the chain ends [11]. In contrast, folds unravel spontaneously via an entropic force [102]. The typical unfolding time is about 30 s for a folded configuration with an initial length of about 8 μm [45]. Thus, the argument that the bright features can be determined as knots in the knot factory is strongly supported by the differences between knots and folds in their unravelling processes. Although the knot type can not be detected in the nanofluidic knot factory device, the complexity of knots can be correlated with knot size, which can be estimated as the difference in the extension of nanochannel-confined DNA molecules before and after knot formation. Such an efficient technique for DNA knot generation and detection in nanochannels allows us to study the dynamical properties of knotted DNA molecules under nanochannel confinement which are presented in the following chapters.

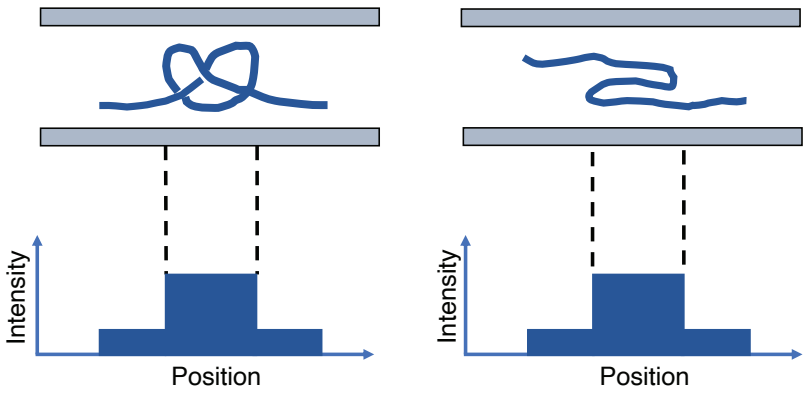

Figure 2.6: Schematic of a trefoil knot (left) and a fold (right) with their DNA-intensity profiles (bottom). The schematic illustrates a DNA chain (a thick blue line) confined in a nanochannel. Both the knots and the folds show the same DNA-intensity profiles. Reproduced from Ref. [45]

Chapter 3

Diffusion of Knots along DNA Confined in Nanochannels

This chapter is based on the publication

Z. Ma and K. D. Dorfman, "Diffusion of knots along DNA confined in nanochannels," *Macromolecules* **53**, 6461–6468 (2020). [103]

3.1 Introduction

Knots are intriguing topological objects, ubiquitous *in vivo* for polymeric materials such as DNA and proteins [59, 64, 104], and the subject of considerable work in the context of polymer physics [1]. In particular, knot diffusion was first studied by simulations in linear DNA under tension [105] and nanochannel confinement [19]. Our study addresses the mechanism of knot diffusion, which remains an open question. Two diffusion mechanisms for knots in polymers have been proposed. The first is self-reptation [13, 106], where the diffusion of a knot originates from a snakelike motion

of the polymer chain. Meltzer *et al.* [18], however, proposed an additional knot diffusion mechanism: knot region breathing. This second mechanism posits that the diffusive motion of a knot is due to knot size fluctuations, locally exchanging DNA chain inside the knot region with its neighborhood. In their analysis of knot diffusion, Meltzer *et al.* [18] predicted the time-scales of a knot moving along a polymer chain for these two mechanisms. The knot diffusion time for the self-reptation mechanism scales as L^3, where L is the contour length of the polymer. In contrast, knot region breathing gives an L^2 scaling. As a consequence, this scaling argument predicts that, for long chains, the diffusion time for knot region breathing dominates self-reptation. Simulations, which provide a more detailed model of the knot diffusion, indicated that the diffusion mechanism of knots is a mix of the two mechanisms [107], and are thus inconclusive.

While measuring knot diffusion as a function of polymer molecular weight is one possible way to distinguish between the two diffusion mechanisms, this is a challenging approach because a wide range of molecular weights are needed. A less technically difficult option is to examine the nature of the diffusion process. Knot region breathing is suggested to show normal diffusion [18]. Self-reptation, however, is thought to be subdiffusive in long polymers owing to an analogy between the reptation of the polymer through the knotted region and the translocation of a polymer through a narrow pore [18]. In the latter case, simulations [108, 109] of a long polymer translocating through a narrow pore exhibit subdiffusive behavior with an exponent of 0.92 arising from the aggregate motion of the long polymer constraining the translocation process [109].

Ultimately, it is desirable to resolve the question of the dynamical properties of

knots in unconfined polymers experimentally, but this is challenging because the polymers in free solutions undergo a random walk in three dimensions, giving rise to a difficulty detecting knots and tracking knot motion along single polymers. This challenge has been tackled by using optical tweezers [100] or by entraining the polymers in an extensional flow where polymers are trapped at the stagnation point to keep the knot within the focal plane and linearize the polymer [97, 98, 110–112]. Bao *et al.* [100] have examined the motion of knots along DNA linearized by optical tweezers and indicated that the knot diffusion mechanism is self-reptation. The self-reptation mechanism also agrees with the study of knot motion in DNA stretched by an extensional flow field [98]. The subdiffusive behavior of the knot, however, may be confounded by the external force used to linearize polymers. Thus, it is desirable to perform similar measurements on relaxed DNA.

Nanochannel confinement provides an approach to linearize DNA by compression instead of tension [101], leading to relaxed DNA ends. While confinement affects the friction opposing DNA motion [92], the increased resistance to motion would only affect the time-scale for knot diffusion and not the underlying mechanism. It is possible that confinement could also affect the knots, but this is unlikely due to the tightness of the knots [13–17]. Our experiments take advantage of the knot factory device developed by Amin *et al.* [11], composed of nanochannel arrays with slit barriers in the center of the nanochannels. This device produces knots when a pressure-driven flow compresses a single DNA molecule against the slit barrier, where the applied pressure and waiting time can be adjusted to control the knotting probability.

Here we use T4 DNA confined in nanochannels to determine whether knot diffusion

is dominated by self-reptation or knot region breathing. There are two reasons for using this molecule. First, T4 DNA, which has higher molecular weight compared with λ-DNA, was chosen to provide a high knotting probability [113, 114]. Second, in the theory of Meltzer *et al.* [18], the knot diffusion time for self-reptation is predicted to be an order of magnitude larger than that of the knot region breathing mechanism for this molecular weight [18]. Such a large difference in predicted knot diffusion times permits an unambiguous test of the knot diffusion mechanism by inspection of the exponent governing the growth of the ensemble-averaged mean-squared displacement of the knots on time lag, where normal diffusion indicates a knot region breathing mode and subdiffusion indicates a self-reptation mode.

3.2 Experimental Methods

3.2.1 Device fabrication

The nanofluidic device shown in Figure 3.1a, consisting of 89 nanochannels (450 μm long) with 1 μm breaks in the channel centers and adjoining nanoslits, was designed based on the knot factory concept [11]. The arm length and the width of the two U-shaped microchannels are 8 mm and 50 μm, respectively. The devices were fabricated on fused silica substrates (University Wafers) using two steps of electron beam lithography to create first the nanochannels and then the slit barriers, and subsequent photolithography to fabricate two parallel U-shaped microchannels connecting the ends of the nanochannel array to inlet and outlet reservoirs. The connecting slits were wider than the nanochannels to simplify the alignment process during the second step of electron beam lithography. Each patterning step was followed by a

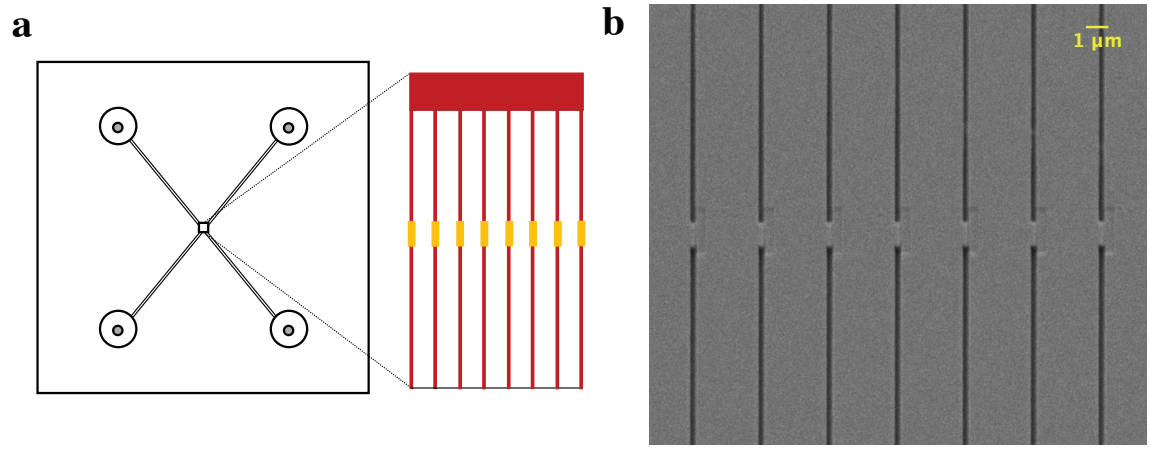

Figure 3.1: Knot factory device design [11]. (a) Schematic layout of the nanofluidic device with a magnified view of the nanochannels and nanoslits (not to scale). (b) SEM image of the nanochannel pattern in the nanofluidic device for knot generation. Nanochannels (black lines) are connected by slit barriers.

fluorine (CF_4:CHF_3) reactive ion etching (RIE) step to transfer the pattern into the substrate. Scanning electron microscopy (SEM) imaging of the nanofluidic device (Figure 3.1b) reveals that the nanochannels are 304 nm wide and nanoslits are 500 nm wide. The depths of microchannels, nanochannels and nanoslits were measured to be 0.8 µm, 340 nm and 32 nm, respectively, using a KLA Tensor P-7 profilometer. After a standard RCA clean, the device with sand-blasted holes for sample loading was sealed with a 170 µm thick fused silica coverslip (University Wafers) via fusion bonding.

3.2.2 DNA preparation

The T4 GT7 DNA molecules (166 kilobase pairs, Nippon Gene) were stained with YOYO-1 fluorescent dye (Invitrogen) at a dye to DNA base pair ratio of 1:10 in a 5× TBE buffer solution and subsequently diluted to 0.25× TBE. The contour length, L, of the stained T4 GT7 DNA was estimated to be 65 µm by assuming

an increase in the rise of 0.51 nm per intercalated YOYO-1 molecule [68, 69]. The stained solution was heated at 50 °C for three hours to accelerate the equilibration of YOYO-1 binding to DNA molecules and melt any annealed DNA sticky ends [115–117]. β-mercaptoethanol (Sigma-Aldrich, 4% v/v) was added to the solution before the start of the knot diffusion experiments to suppress photobleaching of YOYO-1. The ionic strength of the final DNA sample solution is 18 mM, calculated following a previous approach [84, 118].

3.2.3 Knot diffusion experiments

At the start of the experiment, one microchannel of the nanofluidic device shown in Figure 3.1a was filled by capillary action with a buffer solution containing β-mercaptoethanol (Sigma-Aldrich, 4% v/v) with the same ionic strength as the DNA sample solution. The DNA sample solution was then loaded to the other microchannel using a pipette. The wet device was assembled into a chuck that allows pressure actuation [84, 119]. T4 DNA molecules in the microchannel were drawn into the nanochannels by applying 35 kPa pressure for around 10 s and then reducing the pressure to 10 kPa until the DNA reach the slit barriers. The DNA were then imaged prior to compression using a blue laser (Coherent OBIS, 473 nm) with a power of 2.5 mW and a 100× (1.4 N.A.) oil immersion objective on an inverted epifluorescene microscope (Olympus IX73). The images of the DNA were recorded by an EMCCD camera (Photometrics, Cascade II:512) at 20 fps with a 50 ms exposure time for 60 s to measure the DNA extension prior to compression. The T4 DNA were then compressed against the nanoslits by applying 5 kPa pressure for 60 s. Subsequently, the DNA were moved away from the nanoslit by imposing 10 kPa pressure in the

opposite direction and then relaxed in the absence of any imposed pressure for 120 s before imaging. To obtain data for knot diffusion, the DNA with knots were imaged at 5 fps with a 200 ms exposure time for 8 minutes in a quiescent fluid. After video acquisition, the DNA were driven out of the nanochannels by applying 10 kPa pressure for 120 s and new DNA were loaded into the nanochannels.

After each experiment, which consists of multiple loading and compression cycles, the device was cleaned and dried to be reused for the next experiment. First, the device was immersed in DI water overnight to reduce the ionic strength of the solution in the channels. Then, the device was submerged in base piranha solution heated at 80 °C for 40 minutes to remove organic residues. The cleaned device was subsequently heated at 1000 °C for 6 hours for drying.

3.2.4 Data processing

The videos were processed using a custom-written MATLAB script [120] that outputs the time evolution of each DNA molecule's intensity profile. The location of left end, x_{end}, and the total extension, X, of the DNA molecule are identified by fitting the intensity profile to a dual error-function algorithm, which is the result of a Gaussian point-spread function convolved with a box function [121]. The longest relaxtion time is computed by fitting the extension autocorrelation function with an exponential function, following a previous method [84]. The longest relaxation times of unknotted DNA and knotted DNA are 2.7 $\pm$ 0.3 s and 4.6 $\pm$ 0.4 s, respectively. The average extension of the DNA is then determined from uncorrelated measurements of its extension by using a time sampling of 5 s for unknotted DNA and 10 s for knotted DNA.

When a molecule with a knot is produced from the first image processing program, the knot position, x_{knot}, is located by using a second custom-written MATLAB program following the method described in Ref. [45]. The dimensionless knot position, x_{KNOT}, is defined as

$$x_{\mathrm{KNOT}}(t) = \frac{x_{\mathrm{knot}}(t) - \langle x_{\mathrm{end}}(t) \rangle_{1\mathrm{s}}}{\langle \mathrm{X}(t) \rangle_{1\mathrm{s}}} \tag{3.1}$$

where $\langle \ldots \rangle_{1\mathrm{s}}$ operation is a moving average with a window length of one second to reduce the impact of chain end fluctuations.

The time evolution of independent measurements of the dimensionless knot position with a time sampling of 5 s, x_{KNOT}, is used to compute the ensemble-averaged mean-squared displacement (MSD)

$$\mathrm{MSD}(\delta t) = L^2 \left\langle [x_{\mathrm{KNOT}}(t) - x_{\mathrm{KNOT}}(t - \delta t)]^2 \right\rangle_{\mathrm{t,n}} \tag{3.2}$$

where $\langle \ldots \rangle_{\mathrm{t,n}}$ is an average over time t and the ensemble of n DNA molecules and δt is the time lag between images [81]. When useful, we will also refer to a time-averaged MSD, which corresponds to applying Eq. 3.2 to a single knot's trajectory without averaging over n.

To analyze the diffusive behavior of the ensemble of knots, we computed the scaling exponent β of the ensemble-averaged data for the MSD by fitting the logarithm of the data with a linear function

$$\log_{10} \mathrm{MSD}(\delta t) = \beta \log_{10} \delta t + c \tag{3.3}$$

where both β and c are fitted constants. At short time lags, the dynamic diffusion coefficient, $\mathrm{MSD}/2\delta t$, decays continuously until the time lag of 60 s, as shown in Figure

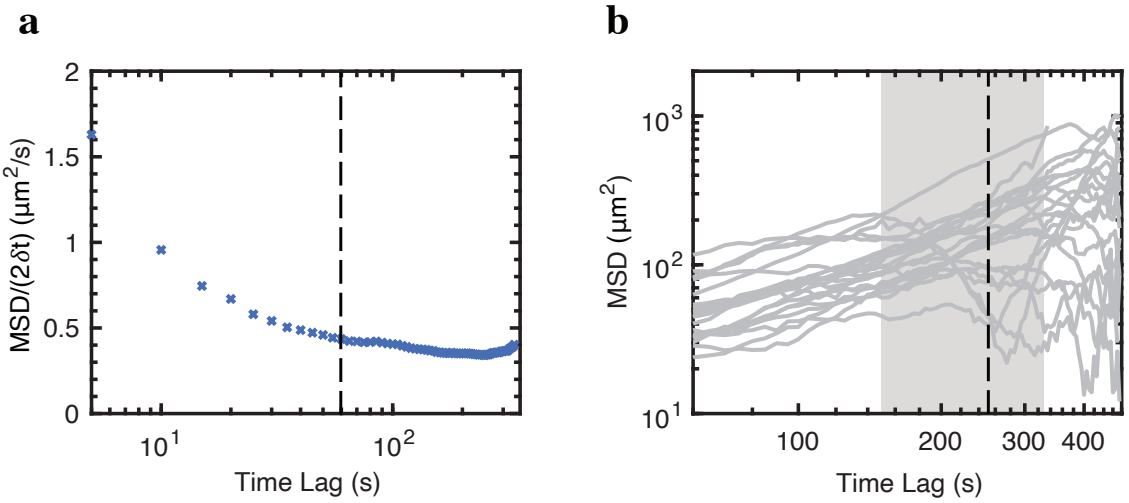

Figure 3.2: Determination of lower and upper bounds of the time lag used for fitting the scaling exponent β. (a) Dynamic diffusion coefficient, MSD/$2\delta t$, as a function of time lag. The MSD/$2\delta t$ decays continuously to a constant value of around 0.4 $\mu m^2/s$ at the time lag of 60 s, indicated by the vertical black dashed line. (b) Time-averaged MSDs as a function of time lag for individual knots. The figure shows the large fluctuations of the time-averaged MSDs for individual knots at time lags larger than 150 s. The vertical black dashed line indicates the first choice of the upper bound of 255 s for estimating the random error. The shaded region corresponds to the second choice of the range of upper bounds from 150 s to 325 s for estimating the systematic error.

3.2a, due to a dynamic error in the MSD [122]. Thus, the lower bound for the time lag used for the calculation of the exponent β is determined to be 60 s. The choice of upper bounds requires a quantitative approach. We first calculated the correlation coefficient, R^2, of the linear fit line with different upper bounds and a fixed lower bound of 60 s. We then performed two analyses, by considering the random error and the systematic error caused by the choice of the upper bound separately. The upper bound determined from the first analysis is 255 s, which is the point with the highest R^2 value. For the second analysis, the upper bounds larger than 150 s are selected where R^2 value is greater than 0.99. Thus, the upper bound has a range [150 s, 325 s] for estimation of systematic errors. The minimum upper bound is determined to

be 150 s because the time-averaged MSDs of the various knots fluctuate significantly when time lags are greater than 150 s, as shown in Figure 3.2b. This fluctuation is mainly caused by limited statistics [81]. As a result, two choices of the upper bound are 255 s for estimating the random error and [150 s, 325 s] for estimating the systematic error.

3.3 Results

Our device was designed based on the nanofluidic knot factory device developed by Amin *et al.* [11] to generate knots with high probability. The effective size of our nanochannels, corresponding to the geometric mean of channel sizes after correcting for the DNA-wall excluded volume and electrostatic interactions, is 308 nm [80–82]. This effective size is close to the knot factory device effective channel size of 346 nm from Amin *et al.* [11], which we computed from their reported channel sizes and the ionic strength of their buffer solution. With this effective channel size, the knotting probability of our device is expected to be close to prior work [11] because the knotting probability is presumed to be a function of channel size [8–10]. For the applied pressure and waiting time used in our experiments, we anticipated a knotting probability of around 60% based on the model for the probability of forming a single knot from Amin *et al.* [11]. The probability of knot generation in our experiments on 42 molecules was 48 $\pm$ 20% calculated using a Clopper-Pearson interval with a 95% confidence interval [123]. Our knotting probability is consistent with the prediction from previous work [11].

The T4 DNA molecules with an estimated contour length of 65 μm [68, 69] are susceptible to shear cleavage by hydrodynamic forces during the compression required

to generate knots [124]. We thus performed two control analyses, one measuring the effect of the compression step and the other checking the quality of the DNA initially loaded into the device, to confirm that shear cleavage was sufficiently small that it would not affect the knot diffusion mechanism, which is expected to be a function of the polymer chain length [18].

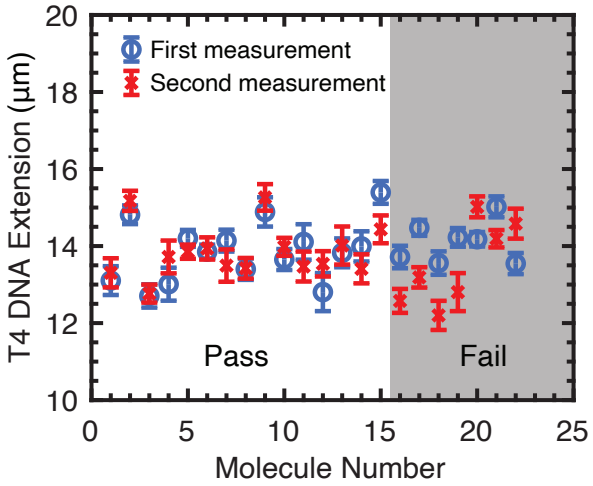

Figure 3.3: Average extension for unknotted T4 DNA molecules from uncorrelated measurements of their extension before and after compressed against the nanoslits. The error bars are the standard error of the mean. The shaded region represents the 7 rejected molecules, which are 1.1 $\pm$ 0.1 μm shorter after being compressed against the nanoslits.

The first test we performed was to analyze the change in DNA length after compression against the slit barrier. Since only half of our molecules are knotted, we can examine whether T4 DNA molecules are sheared significantly by compression against the nanoslits by examining those DNA molecules that do not form knots during the compression. To this end, Figure 3.3 compares the average extension for 22 unknotted T4 DNA molecules before and after being compressed against the nanoslits. An unpaired two-sample t test with 5% significance level was used to determine if the two-measurement means are equal. The test result shows that 15 molecules passed the

hypothesis test. The rejected 7 molecules are 1.1 ± 0.1 μm shorter after compressed against the nanoslits. This is a relatively small effect on the DNA size.

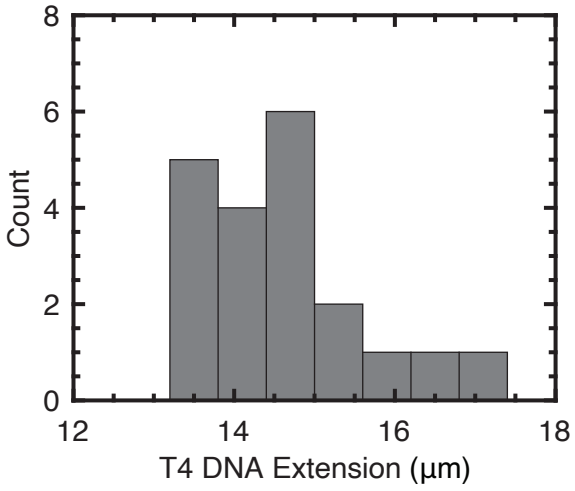

Figure 3.4: Histogram of the extension distribution of the T4 DNA before knot generation. The mean value of the extensions is 14.6 μm with a standard error of 0.2 μm, corresponding to a fractional extension of 0.22 based on a contour length of 65 μm.

In addition to the average extension of unknotted DNA before and after compression, we also measured the chain extension distribution of the T4 DNA molecules before knots are formed in those DNA. The extension of long DNA molecules is linear in chain length [125]. Figure 3.4 provides the distribution of T4 DNA extension in nanochannels from uncorrelated measurements of their extension, showing that the T4 DNA extension values are spread around the mean value 14.6 μm with a standard error of 0.2 μm. Our effective channel size of 308 nm is in the extended de Gennes regime, which corresponds to effective channel sizes ranging from 241 nm to 694 nm estimated based on simulations [91]. Theory for confined polymers in the extended de Gennes regime predicts a fractional extension of 0.23 for our channel size [126]. The corresponding average contour length of these observed T4 DNA

molecules is estimated to be 63.5 $\pm$ 0.9 μm based on the measured average extension and the theory-based prediction of fractional extension, remarkably close to the expected value for intact, stained T4 DNA [126]. While the theory of knot diffusion mechanisms suggests a strong scaling of knot diffusion time with polymer chain length [18], this narrow range of observed T4 DNA chain length in Figure 3.4 and the small amount of shear cleavage during compression observed in Figure 3.3 lead us to conclude that variations in molecular weight between different molecules are not expected to affect the mechanism of knot diffusion.

Figure 3.5a shows an example of knot diffusion along a DNA chain confined in a nanochannel; the knot is visualized as a bright spot that moves along the less bright background of the unknotted portion of the DNA chain with time, and the white streak is the knot trajectory. Such a bright feature could also be associated with a fold [45, 127]. A folded configuration, however, unfolds spontaneously via an entropic force [102]. The typical unfolding time is about 30 s for a fold with an initial length of about 8 μm [127]. Such folds were also observed in our experiments after the compression process, but they were unfolded before the knot diffusion measurements. Knots, on the other hand, are persistent, localized and only unravel at the chain end [11, 98, 100]. Thus, the argument that the bright feature is a knot in our device is strongly supported by the differences between knots and folds in their unravelling processes. Figure 3.5b illustrates a time trace of position of the knot produced by processing the kymograph shown in Figure 3.5a.

The evolution of the dimensionless single knot positions in time allows us to compute the time-averaged mean-squared displacement (MSD) of each knot. Figure 3.6 shows the time-averaged MSDs for individual knots along with the ensemble-averaged

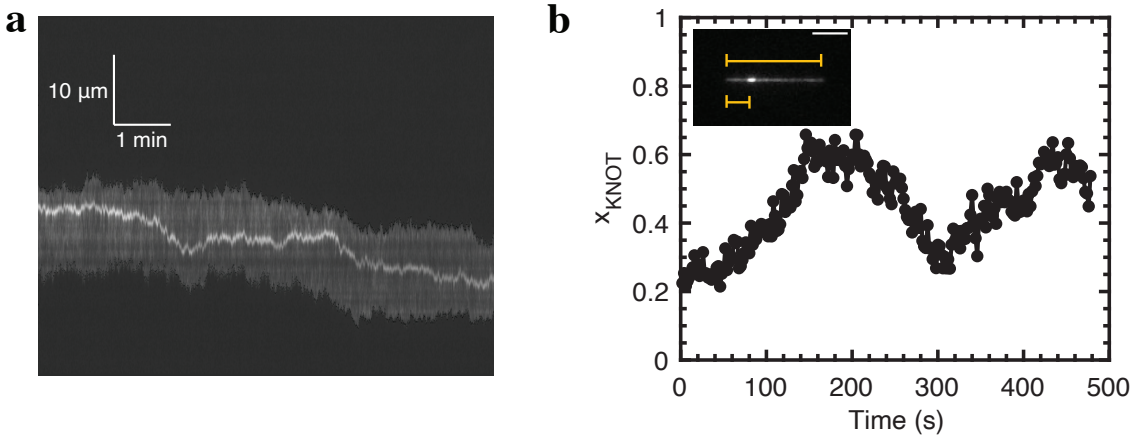

Figure 3.5: Trajectory of a knot along the DNA molecule. (a) Kymograph of a T4 DNA after a knot is formed in our device. The vertical axis is intensity along the nanochannel and the horizontal axis is time. The knot is observed as a bright spot that diffuses along the less bright background of the unknotted portion of DNA chain. Black boxes at the ends of the DNA images are created by the imaging processing code to locate the DNA molecule. (b) Time trace of the knot in (a) diffusing along the DNA chain confined in a nanochannel. The dimensionless knot position, x_{KNOT}, is defined as the ratio of the knot's distance from DNA left end to the DNA extension in Eq. 3.1, as illustrated in the inset of a knotted DNA molecule image. The scale bar is 5 μm.

MSD as a function of time lag; time-averaged MSDs reveal greater statistical uncertainty than the ensemble-averaged MSD. Thus, knot diffusive behavior is quantified by using the ensemble-averaged MSD to improve the estimation of the scaling exponent characterizing the knot diffusive behavior [128]. The apparent scaling exponent extracted by fitting the ensemble-averaged MSD data between 60 s and 255 s in Figure 3.6 is 0.82 ± 0.01, where the error refers to a 95% confidence interval from the linear regression. For upper bounds from 150 s to 325 s, the range of the scaling exponent is [0.79, 0.88], where the range indicates the systematic error due to the choice of the upper bound for the linear regression. Both results indicate a subdiffusive behavior of knots along T4 DNA chains confined in nanochannels.

Two potential sources of systematic error are that each knot generated in the

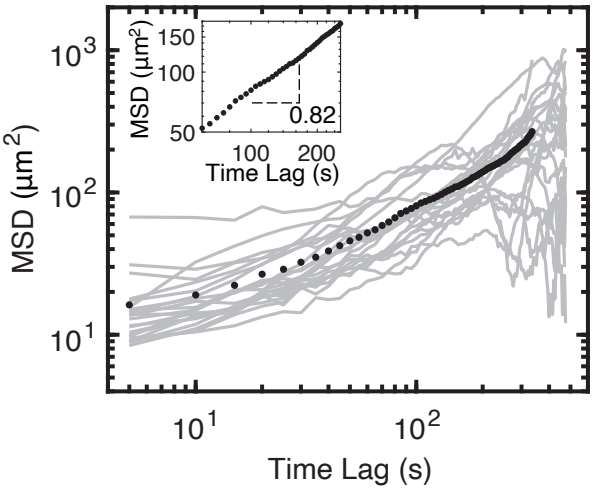

Figure 3.6: Mean-squared displacements as a function of time lag. The gray solid lines, which also appear in Figure 3.2b, are time-averaged MSDs for individual knots. The black dots are the ensemble-averaged MSD of the ensemble of knots as a function of time lag. The linear fit to the logarithm of ensemble-averaged MSD and time lag data between 60 s and 255 s yields a scaling exponent of 0.82 $\pm$ 0.01, as illustrated in the inset. The error is estimated using a 95% confidence interval. The determinations of lower and upper bounds of the time lag used in the inset for fitting were described in Figure 3.2.

knot factory device may have (i) a different topology [60, 129] and (ii) a different initial position relative to the chain ends. While we expect the scaling exponent, which characterizes the knot diffusive behavior, is insensitive to the type of knot [100, 130], checking the topological complexity of analyzed knots could further verify the accuracy of the scaling exponent of the ensemble-averaged MSD. We cannot directly ascertain the knot complexity from the images, but we can create a proxy for the knot complexity by comparing the knot dynamic diffusion constants in Figure 3.7 because the dynamic diffusion constant is suggested to decrease with complexity of knots, consistent with slower diffusion for larger knots [100]. The dynamic diffusion constant is calculated as MSD/$2\delta t$ at a fixed time lag of 60 s to avoid tracking noise and limited statistics [98, 131]. The scatter plot illustrates no apparent correlation between knot

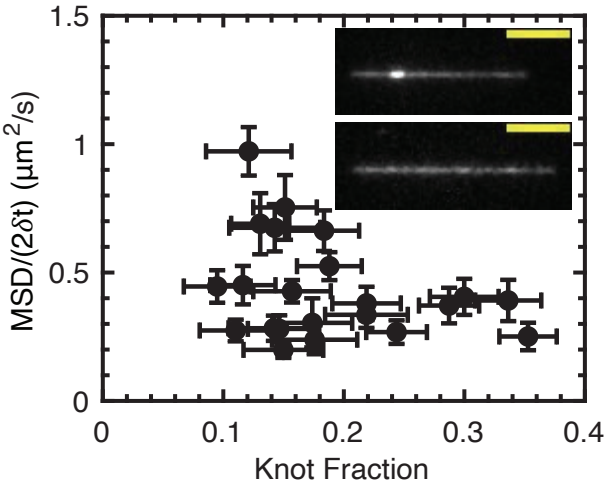

Figure 3.7: Scatter plot of the knot dynamic diffusion constants, defined as MSD/$2\delta t$, at a time lag of 60 s and knot fractions for an ensemble of measured knots. The knot fraction is defined as a ratio of extension difference between unknotted and knotted DNA chain to the unknotted DNA chain extension. The inset shows the images of nanochannel confined knotted T4 DNA (top) and the DNA before knot generation (bottom). The scale bars are 5 μm.

dynamic diffusion constant and knot fraction for the ensemble of observed knots, suggesting that the knots we observe are of similar (but unknown) complexity. The position of a knot relative to the chain ends, however, is expected to affect the scaling exponent of knot diffusion. The knot mobility is thought to increase when a knot moves towards one of the chain ends [18, 98]. Figure 3.8 shows that there is no apparent relationship between the MSD at a time lag of 60 s and the initial knot position relative to the chain ends for the ensemble measured knots. The experimental result of our observed knots is inconclusive for the effect of initial knot positions on knot diffusion due to insufficient data.

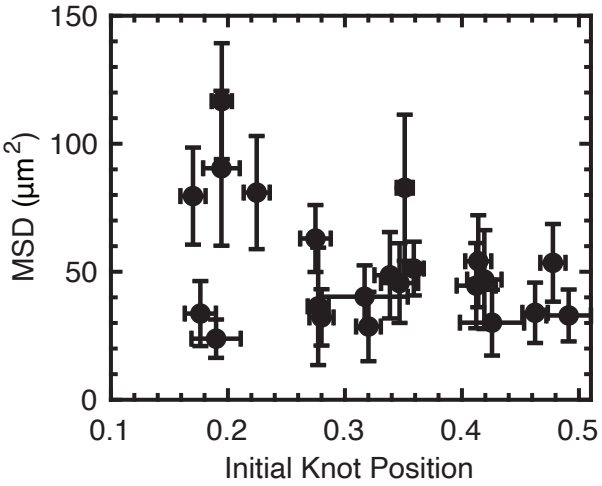

Figure 3.8: Scatter plot of the time-averaged MSDs at a time lag of 60 s and initial positions relative to the chain ends for the observed knots. The initial dimensionless knot position is defined as the ratio of the knot's distance from either of the chain ends to the DNA extension at 0 s.

3.4 Discussion

Our observations of knot movement along T4 DNA chains reveal that the motion of knots is subdiffusive with an apparent scaling exponent of 0.82 ± 0.01 at the range of time lags between 60 s and 255 s, where the uncertainty is an estimate of the random error, and a scaling exponent range [0.79, 0.88] produced by the possible systematic errors from the choice of the upper bound for the exponent. Those values are not the same as the predicted value of 0.92 from simulations of long self-avoiding polymers translocating through a narrow pore [108]. The translocation process is analogous to the knot self-reptation mechanism [108, 109], but it is difficult to rigorously compare the two scaling exponents due to the differences between the two systems. In our experiment, DNA knots translate along extended chains under nanochannel confinement. The pore translocation, however, is a process that polymers move through a

narrow pore in a membrane with infinite space on both sides of the membrane.

The subdiffusive behavior of knots observed in our experiments contradicts the theory proposed by Meltzer *et al.* [18] for the diffusion of DNA knots in nanochannels. At the contour length of T4 DNA, the rate of knot region breathing prediction by Meltzer *et al.* [18] is about an order of magnitude faster than self-reptation, implying that knot region breathing should dominate knot diffusion along T4 DNA. Based on their theory, the knot movement along T4 DNA should be regular diffusion, inconsistent with our results of knot subdiffusive behavior. The inconsistency is plausibly due to the assumption of Brownian diffusion by Meltzer *et al.* [18] for both diffusion mechanisms when predicting the scaling of knot diffusion time with polymer chain length, a point which is noted in their analysis. Another factor accounting for this discrepancy might be the narrow range of the measured knot diffusion due to experimental limitations. Surmounting these limitations is non-trivial, requiring very even longer DNA molecules (e.g., yeast choromosomes), very high stability of the stage, and the use of stroboscopic imaging to provide adequate coverage over the full range of time lags. The knot diffusive behavior at later time lags larger than the upper bound $\delta t = 325$ s from our experiments is thus inconclusive due to the lack of sufficient data at such long time lags.

Our observation of subdiffusion of knots agrees with the results from experimental [98] and theoretical [21] studies of dynamics of knots along polymers under tension. Klotz *et al.*[98] found anomalous behavior of knots in T4 DNA stretched by an elongational field in a microfluidic device. The MSD of the knot position measured in their experiments [98] shows subdiffusive behavior at short time lags and superdiffusion at long time lags. The superdiffusive behavior agrees with a prediction from

an asymmetric self-reptation mechanism, where knots are expected to move faster towards one of the chain ends [18, 98]. Their observation [98] of knot subdiffusive behavior in T4 DNA at short time lags less than around 50 s is consistent with our experimental results. Our experimental results are also supported by simulations by Matthews *et al.* [21], who found subdiffusive motion of knots along strected polymer chains at short times.

The observed subdiffusive behavior of knots, however, is not consistent with the simulation results of Matthews *et al.* [21] at larger times and computational studies on knot diffusion along stretched DNA chain under tension [105], which show normal diffusive behavior. This discrepancy may be due to the difference between stretched chains under tension and nanochannel confined chains in the extended de Gennes regime. In stretched chains, the knot moves along the polymer contour, which is aligned along the observed axis. A confined polymer in the extended de Gennes regime, however, corresponds to a series of anisometric blobs with a tortuous chain [126]. Our experiments measure the knot diffusion projected onto the channel axis, which is not necessarily the same as the knot diffusion along the chain contour. A study of more extended DNA chains in Odijk regime is a potential method to reduce the difference of measured knot diffusion track between stretched and confined chains, since the chain tortuosity would be largely eliminated [132].

Our experimental results also suggest directions in modeling DNA knot diffusion for further theoretical studies. One issue is the low effective ionic strength of the buffer solution of 18 mM in our experiment, lower than the salt condition of 100 mM assumed in previous simulations [19, 21, 105]. The effect of electrostatics might need to be incorporated into simulation models for DNA knot diffusion, which typically

treat the polymer as neutral with an increased persistence length (and, where applicable, effective width) due to electrostatic repulsion. However, the more important consideration is that the analysis of simulation data likely do not discriminate between small and large knots. Indeed, the identification of small knots is relatively straightforward in simulations but challenging for experiments [5, 19, 21, 105, 130, 133, 134]. The knots generated in our experiment are estimated to contain several microns of contour length. Simulations with complex and large knots are needed to make a thorough comparison to our experimental data. At the same time, if computational studies of small knots indicate a measurable difference in diffusive behavior between small and large knots, they could motivate developing experimental methods to visualize those small knots.

3.5 Conclusion

We have examined the diffusion of knots along DNA molecules confined in nanochannels by using a nanofluidic device to generate knots and fluorescence microscopy to observe knot movement. The knot diffusive behavior was quantified by a scaling exponent of ensemble-averaged mean-squared displacement on time lag. The apparent scaling exponent and the range of scaling exponents were found to be 0.82 ± 0.01, where the uncertainty refers to the random error, and [0.79, 0.88], where the range indicates the systematic error, both indicating a subdiffusive behavior of knots along DNA molecules. Our finding contradicts the theory [18] that knot diffusion is dominated by knot region breathing, but agrees with observations of the short-time dynamics of knots on DNA under tension [21, 98]. Our experimental work also provides guidelines to model knot diffusion along DNA for future simulation studies.

While the observation of knot subdiffusive behavior supports the self-reptation mechanism, it is desirable in the future to measure diffusion time of knots along DNA molecules with different contour length to test definitively the two knot diffusion models; it may be the case that the crossover between knot region breathing and self-reptation takes place at a higher molecular weight than predicted by Meltzer *et al.* [18]. Other open questions related to knot dynamics still remain, particularly the details surrounding the effect of confinement, which is controlled by channel size and the ionic strength of buffer solution, on knot diffusion. The effect of knots on DNA chain diffusion in different confinement regimes [88, 91] is also a particularly intriguing question.

Chapter 4

Diffusion of Knotted DNA Molecules in Nanochannels in the Extended de Gennes Regime

This chapter is based on the publication

Z. Ma and K. D. Dorfman, "Diffusion of knotted DNA molecules in nanochannels in the extended de Gennes regime," *Macromolecules* **54**, 4211–4218 (2021). [135]

4.1 Introduction

Long polymers such as deoxyribonucleic acid (DNA) are likely to self-entangle into knots [59, 60, 64]. This topological object affects the mechanical and dynamical properties of the polymers [1, 59]; in particular, the presence of knots increases the mobility of the polymer chain in free solution [136–138]. The corresponding effect of knot formation on diffusion of DNA confined in nanochannels, however, remains an

open question.

Unknotted DNA under the weak confinement conditions considered here is described by blob theory [139], with a friction that is proportional to the extension of the polymer along the channel axis [140]. In other words, the confined DNA is a non-draining object. Two competing factors are expected to change the DNA friction, which is inverse to the diffusivity, due to the presence of a knot. The formation of a knot in a DNA molecule decreases the extension of the confined molecule as illustrated in Figure 4.1, thus decreasing the friction of the non-draining object by reducing its size. A potential counteracting effect is the increased friction between the knotted part of the DNA chain and the nanochannel surface. The DNA knot fills the hydrodynamic screening volume in a more compact way, giving rise to the DNA chain closer to the channel wall as shown in Figure 4.1b and increases DNA-wall friction. It is not obvious, *a priori*, which of these competing mechanisms is more important.

Here we measured the center-of-mass diffusivity of T4 DNA molecules confined in nanochannels with an effective size of 307 nm before and after knot formation to address which of these competing effects dominates knotted DNA diffusion in the extended de Gennes regime, i.e., for channel sizes that lie between the Kuhn length and thermal blob size of the DNA [87]. The diffusivity scaling of semiflexible polymers under the extended de Gennes regime in nanochannel confinement is described by a modified blob theory which incorporates the effect of local chain stiffness [81, 92, 141]. In this confinement regime, the polymer chain remains a non-draining object with a small correction due to the stiffness of the chain [81, 92]. We use a nanofluidic knot factory device introduced by Amin *et al.* [11] for efficient large knot generation. The knot factory device consists of nanochannels with nanoslits that enables us to

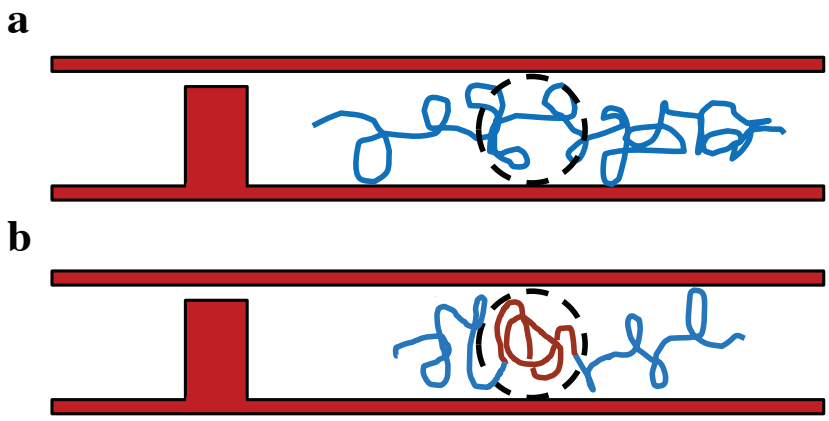

Figure 4.1: Schematic illustration of a cross-sectional view of a DNA molecule confined in a nanochannel (340 nm deep) with a 32 nm deep nanoslit (not to scale) before and after knot formation in the chain. (a) A single DNA chain (blue curve) confined in a nanochannel before being compressed against a nanoslit for knot generation. (b) A knot shown in red is formed along the DNA chain (blue curve). The black dashed line represents the screening volume of hydrodynamic interactions.

use a pressure-driven flow to compress the DNA against the nanoslits to generate knots efficiently. T4 DNA molecules are chosen as the model system due to their higher molecular weight relative to the other standard model system, λ-DNA. Such long T4 DNA chains lead to a higher probability of knot formation [113, 114] and a longer diffusion time of knots along the DNA chains [98, 103], which allows us to have sufficient time to investigate the knotted DNA diffusion before the knots unravel at the end of the chains. Our results show that the presence of knots decreases the DNA chain diffusivity in nanochannels, which demonstrates that the increase in DNA-wall friction dominates the reduction in chain extension for the knotted DNA chain diffusion under the extended de Gennes regime in nanochannel confinement.

4.2 Experimental Methods

4.2.1 Device fabrication

The nanochannel devices designed based on the concept of the knot factory [11] were fabricated on fused silica substrates (University Wafers) by a combination of electron beam lithography and photolithography followed by a fluorine (CF_4:CHF_3) reactive ion etching step as described in Ref. [103]. The nanofluidic device consists of two U-shaped microchannels (50 μm wide, 0.8 μm deep) with an arm length of 8 mm adjoining the reservoirs and the nanochannles with height, D_1, of 340 nm and width, D_2, of 304 nm. The nanochannels are 450 μm long with nanoslits (500 nm wide, 32 nm deep) in the channel centers. A cross-sectional view of a nanochannel at the device center with a nanoslit is shown in Figure 4.1. Additional details of the device fabrication and design are reported in Ref. [103].

4.2.2 DNA diffusion experiments

The nanofluidic device was filled with a DNA sample solution by capillary action. The solution contains 0.25× TBE buffer, β-mercaptoethanol (Sigma-Aldrich, 4% v/v) to suppress photobleaching, and T4 GT7 DNA molecules (166 kilobase pairs, Nippon Gene) stained with YOYO-1 fluorescent dye (Invitrogen) at a dye to DNA base pair ratio of 1:10, resulting in a contour length, L, of 65 μm [68, 69]. The ionic strength of this solution is 18 mM, calculated following a previous approach [84, 118]. The wet device was assembled into a chuck with inlets that allow for applying pressure [84, 119]. The pressure was controlled using a microfluidic flow control system (Fluigent

MFCS-EZ). Following the loading of the DNA solution, 6 μL of buffer solution with the same ionic strength as the DNA sample solution was subsequently added to each port of the chuck, linked to the reservoirs on the nanofluidic device, to prevent fluid flow through channels. The chuck was then mounted on an inverted epifluorescene microscope (Olympus IX73) with a 100× (1.4 N.A.) oil immersion objective. Imaging of DNA diffusion before and after compression was performed using a blue laser (Coherent OBIS, 473 nm) with a power of 1 mW and an EMCCD camera (Photometrics, Cascade II:512) at 2 fps with a 200 ms exposure time for 1000 s. The compression step for knot generation was conducted using the method described in Ref. [103]. After the experiment, the device was cleaned and dried to allow it to be reused for the next experiment [103].

4.2.3 Data processing

The movies of DNA molecules in nanochannels were analyzed using a custom-written MATLAB program [120]. The positions of the edges of the DNA molecules, $x_1(t)$ and $x_2(t)$, were extracted by fitting the intensity profile, $I(x,t)$, to a convolution of a box function with a Gaussian point-spread function [121]. The intensity-weighted center of mass of the DNA molecules [81, 142], $x_{\mathrm{com}}(t)$, was then calculated as

$$x_{\mathrm{com}}(t) = \frac{\int_{x_1(t)}^{x_2(t)} xI(x,t)\,dx}{\int_{x_1(t)}^{x_2(t)} I(x,t)\,dx} \tag{4.1}$$

In the experiment, we measured the center of mass motion for individual DNA molecules over a relatively short time due to unknotting of DNA molecules, stage drift and photocleavage of YOYO-stained DNA in long exposure times [143]. The

motion of a single DNA molecule provides a measurement of the time-averaged mean-squared displacement (MSD) with localization errors under a particular configuration, which does not provide sufficient statistics to obtain the long-time chain diffusivity. To sample molecules with diverse configurations, an ensemble of DNA molecules is required to calculate the ensemble-averaged MSD with standard errors as measured over the ensemble of molecules. The time evolution of the center of mass, $x_{\mathrm{com}}(t)$, was used to compute the ensemble-averaged MSD

$$\mathrm{MSD}(\delta t) = \left\langle [x_{\mathrm{com}}(t) - x_{\mathrm{com}}(t - \delta t)]^2 \right\rangle_{\mathrm{t,n}} \tag{4.2}$$

where $\langle \ldots \rangle_{\mathrm{t,n}}$ denotes an average over all times t and the ensemble of n DNA molecules, and δt is the time lag between images [81]. A time-averaged MSD was also calculated using Eq. 4.2 without averaging over n to show each DNA molecule's trajectory.

In the experiment, the DNA molecules are susceptible to drift towards one direction caused by a pressure drop from unequal fluid levels in reservoirs [81, 142]. To ensure that measurements are free of this artifact, we performed an analysis to detect the systematic errors due to DNA drift in nanochannels. First, we computed the scaling exponent β of the ensemble-averaged MSD for DNA molecules in each video by fitting the logarithm of the data with a linear function

$$\log_{10} \mathrm{MSD}(\delta t) = \beta \log_{10} \delta t + c_\beta \tag{4.3}$$

following the method from York [144], where c_β is a fitted constant. We also calculated the cross correlation coefficient, $C_{A,B}$ between DNA molecules A and B in a given

video

$$\mathrm{C_{A,B}} = \frac{\left\langle [x_{\mathrm{com,A}}(t) - \langle x_{\mathrm{com,A}}(t)\rangle_{\mathrm{t}}][x_{\mathrm{com,B}}(t) - \langle x_{\mathrm{com,B}}(t)\rangle_{\mathrm{t}}]\right\rangle_{\mathrm{t}}}{\sigma_{\mathrm{x_{com,A}}}\sigma_{\mathrm{x_{com,B}}}} \tag{4.4}$$

where $x_{\mathrm{com,A}}(t)$ and $x_{\mathrm{com,B}}(t)$ are the centers of mass of different DNA molecules at time t, and $\sigma_{\mathrm{x_{com,A}}}$ and $\sigma_{\mathrm{x_{com,B}}}$ are their standard deviations. We then define an overall correlation coefficient for an ensemble of molecules in each movie, denoted as C, that is computed as the average of $C_{A,B}$ obtained for all possible molecules in the movie; if each molecule is highly cross-correlated with every other molecule in its movie, this is indicative of a fluid flow. A k-means clustering analysis partitioned the data for β and C into three clusters as shown in Figure A.1. The cluster with high β and C values are highly correlated DNA molecules with superdiffusive behavior, consistent with the effect of fluid flow. These molecules were excluded from the subsequent analysis.

The DNA chain diffusivity, D, was then obtained by fitting the ensemble-averaged MSD data of the non-drifting DNA molecules with a linear function

$$\mathrm{MSD}(\delta t) = 2D\delta t + c_{\mathrm{D}} \tag{4.5}$$

using the least-squares fitting method from York [144], where c_{D} is a fitted constant. The ensemble-averaged MSD of unknotted DNA molecules was fit from 50 to 227 s to extract the diffusivity of DNA before compression. For the knotted DNA molecules, their ensemble-averaged MSD data was fit from 200 to 418 s. The lower and upper bounds for fitting the data were determined using the method described previously [103]. The details of determination of the bounds are shown in Figure A.2.

4.3 Results

The modified blob theory applies to the polymer chains under the extended de Gennes regime in nanochannel confinement [81, 92]. A necessary step before the analysis of T4 DNA diffusion in nanochannels is to confirm that our experiments of confined DNA are located in the extended de Gennes regime. We thus calculate the effective channel size D_{eff}, using the equation $D_{\text{eff}} = \sqrt{(D_1 - \delta)(D_2 - \delta)}$. The wall depletion length, δ, is an offset to account for the DNA-wall excluded volume and electrostatic interactions [80–82], which is computed to be 14 nm in our experiments using the model developed by Bhandari *et al.* [80] The effective channel size of our nanochannels is 307 nm, which is in the extended de Gennes regime boundaries of 241 and 694 nm as determined by simulations [91]. We also confirm that our measured average extension of stained T4 DNA molecules is consistent with the theoretically predicted extension of nanochannel confined T4 DNA in the extended de Gennes regime. The fractional extension of semiflexible polymers in the extended de Gennes regime is predicted to be 0.23 for our effective channel size [126], corresponding to an extension of 15 μm for intact, stained T4 DNA molecules with a contour length of 65 μm [68, 69]. The measured average extension estimated from uncorrelated measurements of the extensions of T4 DNA molecules before knotting is 14.8 μm with a standard error of 0.3 μm, within experimental error of the predicted value of 15 μm.

The stained T4 DNA with a contour length of about 65 μm [68, 69] are long DNA molecules. Thus, the molecules are susceptible to breakage by hydrodynamic forces when being compressed against nanoslits for knot generation [124]. To confirm that the shortening of knotted DNA is due to knot formation, we examine T4 DNA

molecules without knot generation from the compression process to study whether T4 DNA are sheared after being compressed against nanoslits. An unpaired two-sample t-test at a 5% significance level was used to compare the average extension of 10 molecules that do not form knots before and after the compression step. The test results show that three molecules are rejected in the hypothesis test, but the change in average extension of those rejected molecules is 0.4 μm with a standard error of 0.03 μm. This small value relative to the average extension of T4 DNA suggests that the T4 DNA molecules are not significantly shortened after the compression step, consistent with the experimental result from our previous work [103]. As a consequence, our experimental results lead to a conclusion that the measured T4 DNA molecules for diffusion analysis are intact. The observed shortening of 2 μm, with a standard error of 0.5 μm, for the knotted DNA after being compressed against nanoslits is thus due to knot formation, not any shearing due to the compression process. The knot contour length is estimated to be 9 μm with a standard error of 2 μm, computed from the reduced extension and a theoretically predicted fractional extension of 0.23 [126].

Figure 4.2 provides an example of a single T4 DNA diffusing in a nanochannel before and after a knot, observed as a bright spot in Figure 4.2c, is formed in the chain. In the kymograph of the knotted DNA as seen in Figure 4.2c, the bright streak is the trajectory of the knot moving along the DNA chain. Such a bright feature is associated with a knot because knots are persistent and can only unravel at the end of a chain, which is different from other topological events such as folds [11, 98, 100, 102, 103, 127]. Folded configurations also occur in our experiments during injection of the DNA into the nanochannels [102, 127], but the molecules unfold before the start

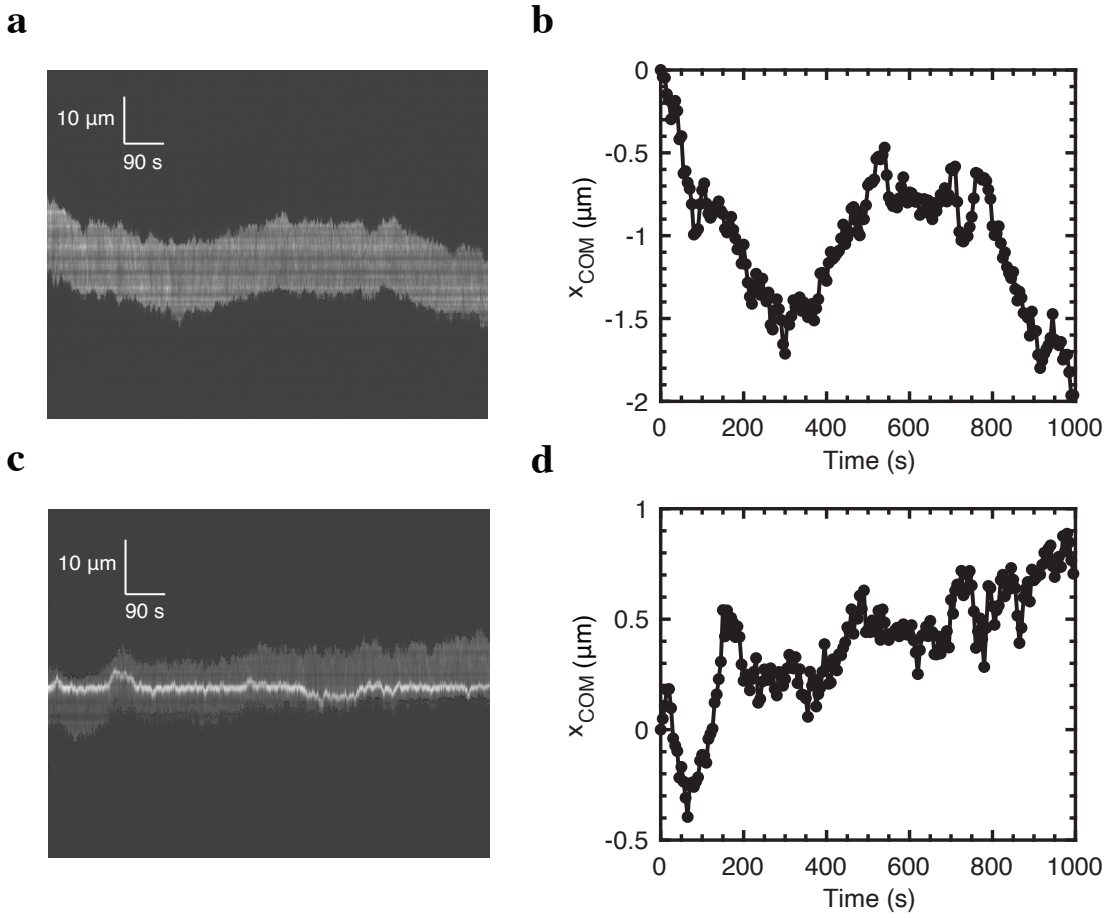

Figure 4.2: Trajectory of a single T4 DNA confined in a nanochannel before and after a knot was generated in the DNA chain. (a, c) Kymograph and (b, d) time evolution of the intensity-weighted center of mass for an unknotted T4 DNA (a, b) and a T4 knotted DNA (c, d) confined in a nanochannel. In the kymographs, the vertical axis is the intensity along the nanochannel and the horizontal axis is the time. The knot is identified as a bright spot. Black dots superimposed on the ends of the DNA are produced by the imaging processing code to locate the DNA.

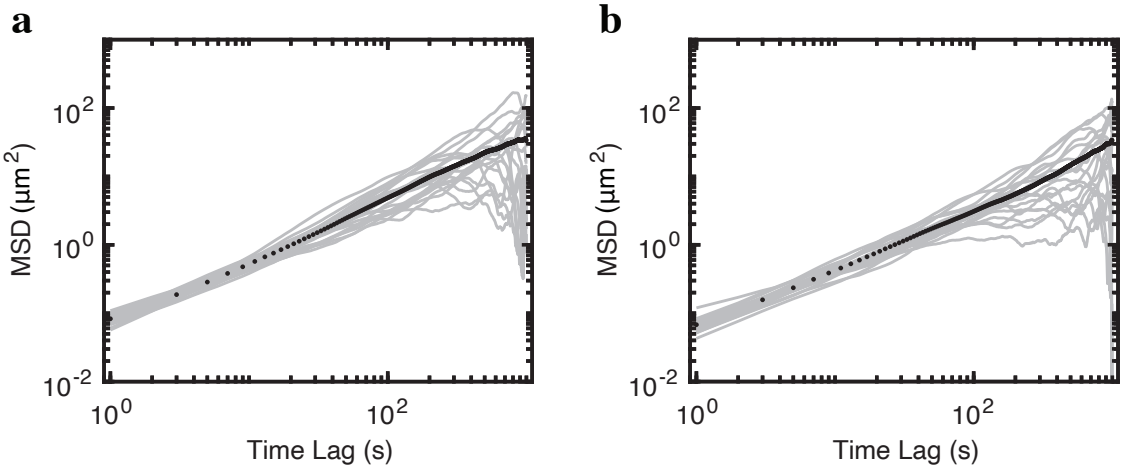

Figure 4.3: A log-log plot of mean-squared displacement (MSD) of 20 T4 DNA confined in nanochannels as a function of time lag. (a) The time-averaged MSDs (gray lines) and the ensemble-averaged MSD (black dots) of T4 DNA molecules before compression as a function of time lag. The scaling exponent, β, extracted by fitting the ensemble-averaged MSD data for $\delta t \in$ [50 s, 227 s] is 1.00 $\pm$ 0.03. (b) T4 DNA molecules with knots, same type of plot as in panel a. The β value obtained by fitting the ensemble-averaged MSD curve for $\delta t \in$ [200 s, 418 s] is 1.0 $\pm$ 0.1. The errors are calculated using 95% confidence interval.

of image acquisition. In addition, we produce the time evolution of the intensity-weighted center of mass for the unknotted (Figure 4.2b) and knotted DNA molecule (Figure 4.2d) by processing the kymographs.

Figure 4.3 shows the time-averaged MSDs computed from the time evolution of center of mass of 20 molecules along with the ensemble-averaged MSD as a function of time lag for the measured T4 DNA molecules before and after knot formation. The ensemble-averaged MSD allows us to obtain the diffusivity of DNA chain confined in nanochannels. One potential systematic error in the measurement of DNA diffusivity is anomalous diffusive behavior of DNA molecules due to induced motion of DNA by fluid flow or adsorption of DNA onto nanochannel surface [81]. We already performed

a k-means clustering analysis to identify correlated, superdiffusive molecules due to flow. To confirm that our data set is indeed free of this artifact, we computed the scaling exponent β of the ensemble-averaged MSD before and after knotting for the molecules that were not removed by the k-means clustering. Fitting of the linear function Eq. 4.3 to the logarithm of the ensemble-averaged MSD yields a scaling exponent of 1.00 ± 0.03 for DNA molecules before compression and a scaling exponent of 1.0 ± 0.1 for the DNA with knots after being compressed against nanoslits at a 95% confidence level. Both values of the scaling exponent at 95% confidence indicate a normal diffusive behavior of the observed DNA molecules before and after knot generation.

We thus proceed to investigate the effect of knots on the DNA chain diffusion by comparing the diffusivity of DNA molecules before and after knots are formed along the DNA chains. Figure 4.4 shows the ensemble-averaged MSD as a function of time lag and the linear fits to the data for observed DNA molecules before and after knot generation. The diffusivity for the unknotted DNA chains is 0.0243 ± 0.0009 $\mu m^2/s$ by fitting the ensemble-averaged MSD curve between 50 and 227 s. For the DNA molecules that contain knots, the ensemble-averaged MSD was fit from 200 to 418 s to extract the diffusivity value which is 0.014 ± 0.001 $\mu m^2/s$. Note that the errors are calculated using a 95% confidence interval. The diffusion constant of the knotted DNA molecules is smaller than the value of the DNA without knots. The result indicates that the formation of knots decreases the diffusivity of DNA chain in the extended de Gennes regime.

Two potential sources of systematic error in the measurement of knotted DNA diffusivity in nanochannels are that (i) the knot factory device produces knots with

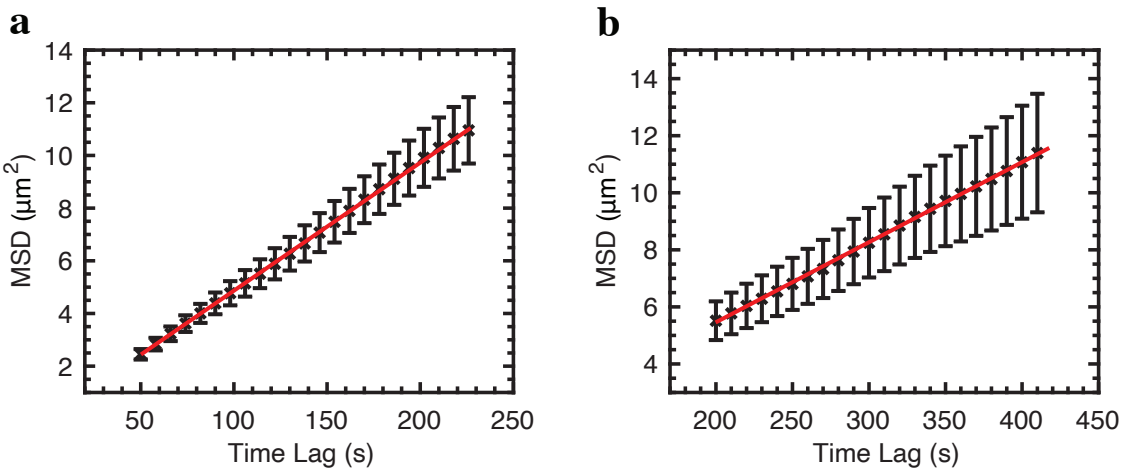

Figure 4.4: Ensemble-averaged MSDs of 20 measured T4 DNA molecules before and after knot formation as a function of time lag. (a) The ensemble-averaged MSD of unknotted DNA molecules was fit to a linear line (solid red line) for $\delta t \in$ [50 s, 227 s] to extract the diffusivity which is 0.0243 $\pm$ 0.0009 $\mu m^2/s$. (b) A linear fit (solid red line) to the ensemble-averaged MSD data of knotted DNA in nanochannels for $\delta t \in$ [200 s, 418 s] yields a diffusivity value of 0.014 $\pm$ 0.001 $\mu m^2/s$. The errors in the linear regression are estimated using a 95% confidence interval. Error on the ensemble-averaged MSD for a given time lag is the standard error.

varying sizes and (ii) multiple knots can be generated along a T4 DNA chain. Examples of both effects are shown in Figure 4.5. Figure 4.6 illustrates the relationship between knotted DNA chain diffusivity and knot contour length for the 20 measured knotted T4 DNA molecules. The knotted DNA chain diffusivity decreases as the knot contour length increases. This result supports our claim that the presence of knots decreases the DNA chain diffusivity in nanochannels in the extended de Gennes regime. The number of knots in a DNA molecule may also affect the knotted DNA chain diffusivity. We observed that two of the 20 measured T4 DNA molecules formed two knots. The chain diffusivity of one molecule containing two knots with a contour length of 4.7 $\pm$ 0.6 μm is 0.0224 $\pm$ 0.0002 $\mu m^2/s$, which is larger than the averaged

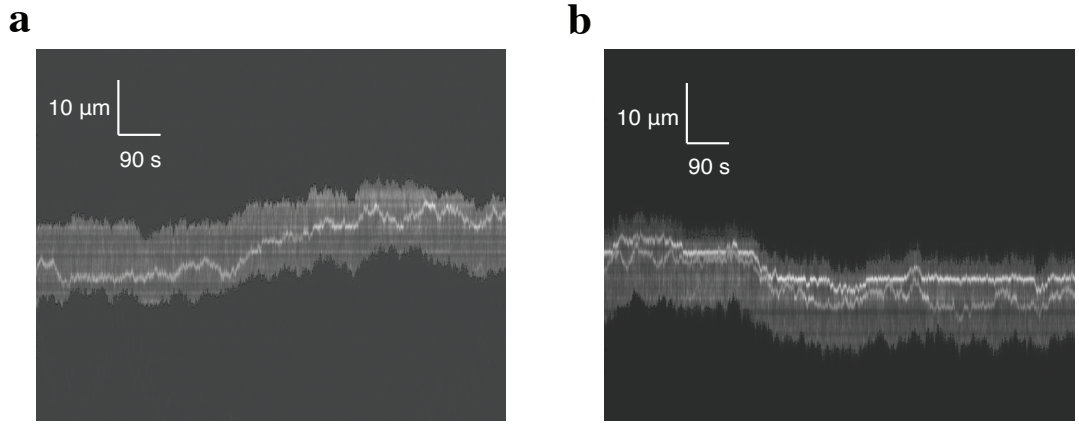

Figure 4.5: Examples of kymographs for (a) a knotted T4 DNA molecule with a smaller knot compared with the molecule in Figure 4.2c and (b) a knotted T4 DNA molecule with two knots formed in the chain. The intensity along the nanochannel (vertical axis) is plotted versus time (horizontal axis). Knots are visualized as bright spots along the DNA chains. Black dots at the ends of DNA chains are created by the image processing code to locate the DNA molecule.

chain diffusivity of 0.0163 $\pm$ 0.0003 $\mu m^2/s$ for molecules containing a single knot with a contour length of 5.2 $\pm$ 0.3 μm. However, the chain diffusivity of 0.0127 $\pm$ 0.0002 $\mu m^2/s$ for the other molecule involving two knots with a contour length of 9.9 $\pm$ 0.7 μm is within the uncertainty of the DNA chain diffusivity of 0.015 $\pm$ 0.003 $\mu m^2/s$ for molecules containing a single knot with a knot contour length of 10.3 $\pm$ 0.5 μm. The experimental result is inconclusive for the effect of knot number on knotted DNA chain diffusivity due to insufficient data because, even though the center-of-mass errors are small, adequate sampling of the full configuration space requires observing more molecules since long tracks are not possible.

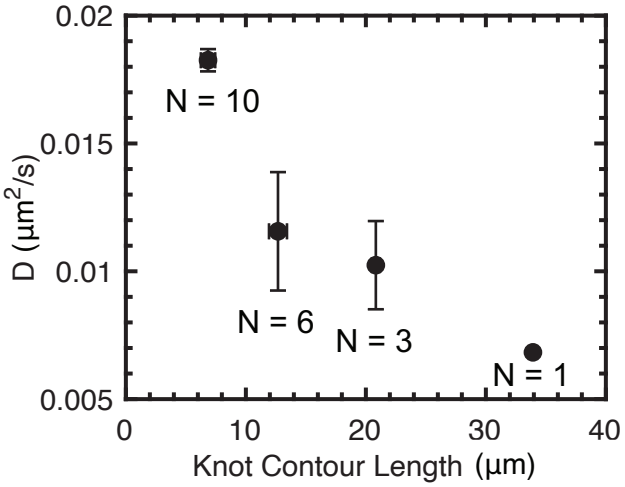

Figure 4.6: The knotted DNA chain diffusivity as a function of knot contour length. The N value represents the ensemble size of knotted T4 DNA molecules for calculating the knotted DNA chain diffusivity. Errors on the knotted DNA chain diffusivity are calculated using 95% confidence interval. Error bar on the knot contour length represents the standard error as measured over multiple knotted DNA molecules. The uncertainty is not estimated for the point with N = 1 due to insufficient number of molecules with such large knot contour length of 34 μm.

4.4 Discussion

We observed the T4 DNA diffusion in nanochannels before and after knot formation to study the effect of knots on the DNA chain diffusion under the extended de Genne regime in nanochannel confinement. The DNA chain diffusivity is found to be 0.0243 $\pm$ 0.0009 $\mu m^2/s$ for T4 DNA molecules without knots. The measured unknotted T4 DNA chain diffusivity is in good agreement with the value predicted by the modified blob theory that incorporates the effect of local stiffness of chains on semiflexible polymer diffusion in nanochannels [81, 92]. Gupta *et al.* [81] measured the diffusivity of λ-DNA in nanochannels with effective sizes from 117 to 260 nm and obtained the coefficients of the modified blob theory model by fitting the exper-

imental data. The value of T4 DNA diffusivity in nanochannels predicted using the modified blob theory model from Gupta *et al.* [81] is 0.023 ± 0.006 $\mu m^2/s$. Companion simulations of the Kirkwood diffusivity of nanochannel confined, long semiflexible chains suggest that the diffusivity of T4 DNA chain confined in our nanochannels is 0.022 ± 0.003 $\mu m^2/s$ [81, 92]. Note that these values are computed using a fractional extension of 0.23 predicted by a model for semiflexible polymers in the extended de Gennes regime [126] and a Rouse diffusivity of 0.00377 $\mu m^2/s$ for T4 DNA with a contour length of 65 μm in water at room temperature of 25 °C [81]. Our experimentally measured diffusivity of unknotted T4 DNA in nanochannels is close to the predicted values from both previous experiments and simulations.

The T4 DNA chain diffusivity is decreased to 0.014 ± 0.001 $\mu m^2/s$ after knots are generated in the molecules. The decrease in the chain diffusivity of nanochannel confined DNA molecules after knot formation reveals that the DNA-wall friction dominates the knotted DNA diffusion in the extended de Gennes regime. The presence of knots decreases the size of DNA molecules in nanochannel confinement, thus decreasing the friction of the DNA chains. The knots, however, fill the screening volume of hydrodynamic interactions more densely, leading parts of the DNA chain to be closer to the channel surface. Thus, the friction between the DNA chain and channel wall is increased, more than counteracting the effect of decreased DNA size.

The formation of a knot, on average, increases the DNA friction by a factor of 1.7. To determine if this increase is consistent with increased DNA-wall friction due the knot, let us consider a simple model where the total friction consists of the sum of two components: (i) the friction due to the unknotted portion of the confined DNA molecule and (ii) the friction due to a tight knot [13]. For the first contribution,

we assume that the friction due to the unknotted part of the DNA is proportional to the knotted DNA extension X_k in the channel, consistent with the non-draining hydrodynamics in the extended de Gennes regime [92]. This assumption requires that the knotted part of the DNA chain is small so that it does not contribute to the total extension of the knotted DNA chain. For the second contribution, we model the hydrodynamics of the knot as a solid object of radius a confined in a cylindrical channel of diameter $R = \sqrt{D_1 D_2}/2$, corresponding to a channel radius of 161 nm. While this is a crude approximation for the hydrodynamics, it permits a closed form solution. Explicitly, for a closely fitting sphere, the average friction is approximately $6\pi\eta a(R/a-1)^{-5/2}$, where $\eta = 0.89$ cP is the viscosity of water at room temperature [145]. The sum of these two frictions, which is the total friction of knotted DNA, is thus

$$\xi_k = \hat{\xi}_0 X_k + 6\pi\eta a(R/a-1)^{-5/2} \tag{4.6}$$

where $\hat{\xi}_0 = 11.4$ cP is the friction per unit length of unknotted DNA, obtained from the diffusion data in Figure 4.4 using $X_u = 14.8$ μm as the average extension of an unknotted chain. The corresponding friction of an unknotted molecule is $\xi_u = \hat{\xi}_0 X_u$. As a result, the ratio of the friction coefficients is

$$\frac{\xi_k}{\xi_u} = \frac{X_k}{X_u} + \frac{6\pi\eta a}{\hat{\xi}_0 X_u (R/a-1)^{5/2}}. \tag{4.7}$$

The first term in Eq. 4.7, $X_k/X_u = 0.86$, quantifies the reduction in friction due to the shortening of the DNA molecule to $X_k = 12.8$ μm, while the second term in Eq. 4.7 quantifies the increase in friction due to knot formation. To be consistent with the experimental result $\xi_k/\xi_u = 1.7$, the hydrodynamic size of the knot needs to

be $a = 135$ nm, i.e. the knot fills 84% of the channel volume. The knot in this model is small, which justifies the assumption that the friction due to the unknotted part of the DNA molecule is proportional to X_k.

Clearly this model is very simplistic in its treatment of the hydrodynamics. First, decoupling the two contributions to the friction is partially justified by the screening of hydrodynamic interactions at the length scale of the channel [140], but the friction of the knot itself is not quantitatively equivalent to that of a solid sphere. Nevertheless, the arguments made in the context of Eq. 4.7 support the key point of our argument; the formation of a tight knot that fills a significant fraction of the channel size can easily reduce the overall friction two-fold. Second, it is unlikely that the knot can be actually as tight as predicted from this hydrodynamic model (even after accounting for the differences between the radius of gyration and hydrodynamic radius); if the knot were completely dry, its radius $R_g \approx bN^{1/3}$ is around 400 nm based on a Kuhn length $b = 100$ nm and the estimated knot contour length of 9 μm. It is more plausible that the confined knot is an anisotropic, extended object [16] that does not fill the channel as densely as anticipated by our simple model. The details of the knot conformation do not undermine our key idea; this extended knot configuration would still increase DNA friction because the friction increases quickly as the size of the object increases [145]. A detailed understanding of the hydrodynamics of confined knots that leverages tools for computing DNA-wall hydrodynamics [89, 92, 146], is a promising avenue for future computational work.

Our hypothesis for the knotted DNA diffusion in nanochannels is that the dominant contribution to the DNA motion in nanochannels is the moving DNA with a fixed knot ball in the chain which provides extra friction between the knot and chan-

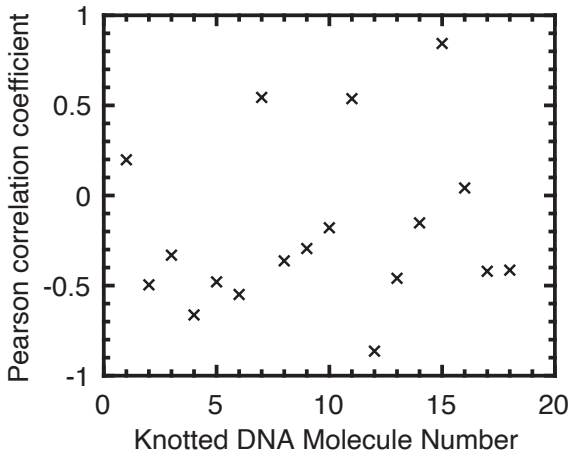

Figure 4.7: Scatter plot of Pearson correlation coefficient between knot motion relative to one of DNA chain ends and center of mass motion of DNA for 18 observed T4 DNA molecules that each contain a single knot. The negative correlation coefficient indicates that the knot moves along the DNA chain in an opposite direction of DNA motion in a nanochannel.

nel wall. The model does not consider knot transport as significant contribution to the knotted DNA chain diffusion. An alternative hypothesis is that the motion of knotted DNA in nanochannels is driven by knot self-reptation along the DNA chain without any superimposed motion of the whole polymer. We thus performed two analyses, one investigating the correlation between center of mass motion of DNA and the motion of the knot within the molecule and the other measuring the magnitude of the knot contribution to the center of mass motion of DNA molecules, to test this hypothesis. The first analysis we performed was to calculate the Pearson correlation coefficient between knot motion relative to one of the DNA chain ends and center of mass motion of DNA for 18 knotted DNA molecules that contain a single knot each. Figure 4.7 shows that the knot motion and DNA center of mass motion are negatively correlated for 13 of the knotted DNA molecules, consistent with the

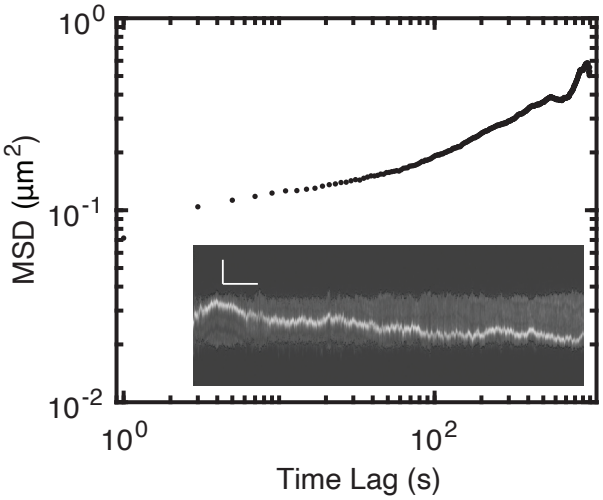

Figure 4.8: A log-log plot of ensemble averaged mean-squared displacement (MSD) as a function of time lag for 20 knotted T4 DNA molecules in nanochannels after shift of positions. The inset shows an example of a kymograph for a knotted DNA in Figure 4.2c after the position of the molecule in each frame is shifted to keep a constant center. The vertical axis is the intensity along the nanochannel with a scale bar of 5 μm and the horizontal axis is the time with a scale bar of 90 s.

knot self-reptation model that the knot tends to move in an opposite direction of the DNA motion, but there is no strong correlation between the motion of knot and center of mass motion of knotted DNA molecules. We then measured the magnitude of the knot contribution to the center of mass motion of knotted DNA molecules. To do so, we centered each knotted DNA molecule in each frame within the same movie. An example of a centered DNA molecule is shown in Figure 4.8. Then, we calculated the intensity weighted center of mass of each fixed DNA molecules. Figure 4.8 shows the ensemble-averaged MSD as a function of time lag of the 20 knotted T4 DNA molecules using the center of mass of fixed knotted DNA chains. The ensemble-averaged MSD caused by motion of the knot along the chain contour is two orders of magnitude smaller than the ensemble-averaged MSD of moving DNA molecules with knots shown in Figure 4.3b. The results from two analyses indicate that the knot

contributes to the knotted DNA in a manner consistent with self-reptation, but the contribution from knot movement to the knotted DNA diffusion in nanochannels is not significant compared with that from the whole chain motion.

The results of decreased chain diffusivity of knotted DNA confined in nanochannels contrast with the free solution data of Kanaeda and Deguchi [136], who found that the ratio of diffusion constants for knotted ring polymers and a linear polymer with the same molecular weight in good solvent increases linearly with the average crossing number of knots, thus suggesting polymers with knots move faster. This discrepancy is plausibly due to the difference in the knot size and topological complexity of knots. They studied simpler small knots with seven crossings and fewer [136]. The topology of knots generated in our experiments cannot be identified through images, but the knots contain a contour length of 9 $\pm$ 2 μm, which is an order of magnitude larger than the size of simple knots with several hundreds nanometers of length [100]. The inconsistency may also be attributed to the absence of polymer-wall friction in free solution. The presence of knots simply reduces the size of the non-draining objects, giving rise to a decreased friction of the object and a resulting increased mobility of the knotted ring polymers in a good solvent.

4.5 Conclusion

We have examined the diffusion of T4 DNA molecules in nanochannels before and after knot formation. The chain diffusivity of knotted T4 DNA molecules confined in nanochannels is found to be 0.014 $\pm$ 0.001 $\mu m^2/s$, which is smaller than the measured diffusivity of 0.0243 $\pm$ 0.0009 $\mu m^2/s$ for the T4 DNA molecules before knot generation. Our experimental results reveal that the presence of knots decreases

the chain diffusivity of DNA molecules in nanochannels, indicating that the DNA-wall friction dominates knotted DNA diffusion under the extedned de Gennes regime in nanochannel confinement.

While our observation of diffusion of DNA with large knots with an estimated contour length of 9 $\pm$ 2 μm indicates that the knots decrease the DNA chain diffusivity in the extended de Gennes regime, a complete understanding of the effect of knot formation on DNA chain diffusion requires a study of diffusion of DNA chain with small knots as well in the confinement regime. Such experiments for probing the diffusion of DNA with small knots are challenging, in terms of identification of small knots using fluorescence microscopy and long duration of image acquisition of small knots, which will move faster along DNA chains [100]. Computational studies, alternatively, could provide insight into the effect of small knots on the DNA chain diffusivity in the extended de Gennes regime because it should be relatively straightforward to precondition the system to a particular knot size. The effect of knot type on DNA chain diffusion is also an intriguing question for theoretical studies because identifying the topology of knots is considerably more straightforward in a simulation than in experiments [5, 19, 21, 105, 130, 133, 134]. Other open questions related with the effect of knots on DNA chain diffusivity in nanochannels also remain, particularly the effect of multiple knots, a more complex and intriguing phenomenon.

Chapter 5

Interactions between Two Knots in Nanochannel-confined DNA

This chapter is based on the publication

Z. Ma and K. D. Dorfman, "Interactions between two knots in nanochannel-confined DNA molecules," *J. Chem. Phys.* **155**, 154901 (2021). [147]

5.1 Introduction

Sufficiently long polymers such as deoxyribonucleic acid (DNA) molecules are susceptible to form knots in the chains [59, 60, 64, 148]. DNA knots have sparked interest in the context of polymer physics [1]. The dynamical properties of individual knots, such as the motion of isolated single knots along polymer chains, have been extensively studied in theoretical and experimental work [18, 19, 98, 100, 103, 105–107]. Composite knots also exist in DNA molecules [64, 149]. The probability of forming multiple simple knots has been predicted to be higher than the knotting probability

of a single complex knot in long DNA chains by a simulation study of DNA knot formation [150]. The physics of composite knots in polymers has recently received attention, in particular regarding the dynamics of knot pairs [151–155]. The knots in a polymer chain can either remain separated or experience an attractive interaction and then be intertwined as shown in Figure 5.1. The interaction between two knots remains an open question: Do the two knots attract one another or remain separated in a polymer chain?

The interaction between two knots in a stretched polymer chain under tension has been studied by simulations [151–154] and experiments [155]. The simulations predict that the knots attract one another with a global minimum free energy in the intertwined knot state [151–154]. One simulation study from Trefz *et al.* [151] further suggested a mechanism that the knots can pass through each other and switch positions after the knots are intertwined. Experimental observations of two-knot interactions in T4 DNA stretched by elongational fields supported the simulation-based predictions that knots in a polymer under tension feel an attractive interaction [155]. Klotz *et al.* [155] also observed that the two knots in stretched DNA under tension can remain close to each other for several minutes after the knots merge together. The two-knot attraction in stretched DNA under tension may be associated with a Casimir, or fluctuation-induced, interaction effect between two knots owing to an analogy between knots and rings along semiflexible polymers [155–157]. Theoretical studies predict that the rings in semiflexible polymers under tension experience an attractive fluctuation-induced force, arising from the restriction of the chain fluctuations in transverse directions by the presence of rings [156, 157].

The mechanism of knot-knot attraction in these studies, however, may be con-

founded by the externally imposed tension used to stretch polymers, thereby linearizing the DNA and enabling measurement of the knot dynamics in experiments. Here we study the interaction between two knots in T4 DNA molecules under nanochannel confinement, which provides an alternative approach to linearize DNA via compression rather than tension [101], resulting in relaxed polymer chains. The nanofluidic knot factory device developed by Amin *et al.* [11] was used to generate multiple knots with high probability in DNA molecules confined in nanochannels. Our experimental results show that (i) widely separated knots in nanochannel-confined DNA feel an attractive interaction, but the knots only stay in close proximity for several seconds and (ii) knots tend to remain separated until one of the knots unravels at the chain end. The interaction between two knots in T4 DNA under nanochannel confinement was quantitatively investigated by analyzing the free energy profile inferred from the separation distances between knots for an ensemble of DNA molecules. The free energy exhibits a global minimum when the knots are separated, indicating that the separated knot state is more stable than the intertwined knot state for knots in nanochannel-confined DNA molecules.

5.2 Experimental Methods

5.2.1 Device fabrication

Our nanofluidic device [103, 135], designed based on the knot factory device developed by Amin *et al.* [11], consists of two U-shaped microchannels (50 μm wide, 0.8 μm deep) connecting 89 nanochannels (304 nm wide, 340 nm deep) to the reservoirs. The nanochannels are 450 μm long with a 32 nm deep slit in the center of each

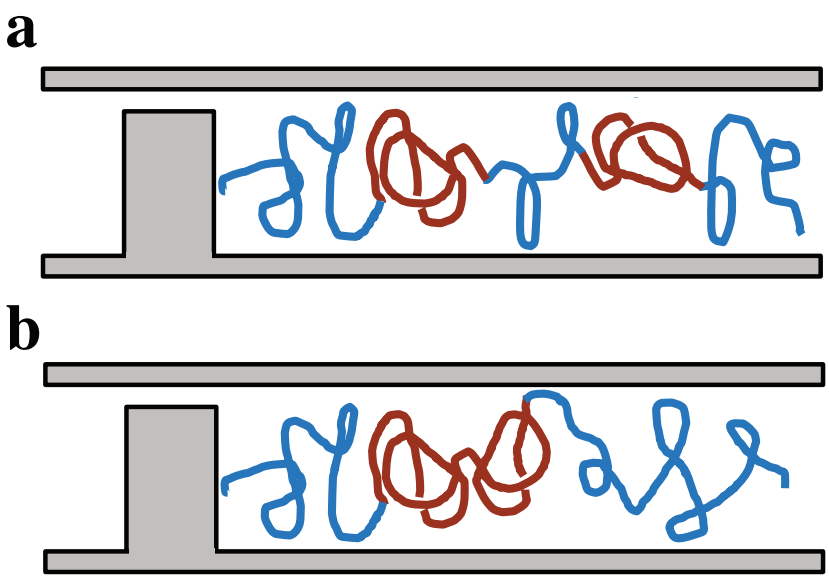

Figure 5.1: Schematic illustration of a DNA molecule containing two knots in a nanochannel (340 nm deep) with a 32 nm deep nanoslit at the device center (not to scale). (a) Two knots shown in red are separated in the DNA chain (blue curve). (b) The knots are in an intertwined state in which they are in close proximity.

nanochannel. A magnified cross-sectional schematic of a nanochannel with a slit barrier is illustrated in Figure 5.1. The devices were fabricated on fused silica substrates (University Wafers) by a combination of two steps of electron beam lithography to define first the nanochannels and then the nanoslits and photolithography to create the microchannels. Each lithography step was subsequently followed by a fluorine (CF_4/CHF_3) reactive ion etching step to transfer the patterns to the substrates. The devices were then sealed via fusion bonding to 170 μm thick fused silica coverslips (University Wafers). Additional details of the nanofluidic device fabrication are described in Ref. [103].

5.2.2 Two-knot interaction experiments

The two microchannels on the nanofluidic device were filled by capillary action with a DNA loading solution containing 0.25× TBE buffer, β-mercaptoethanol (Sigma-Aldrich, 4% v/v) to suppress photobleaching and T4 GT7 DNA (166 kilobase pairs, Nippon Gene) with a contour length of 65 μm when stained with YOYO-1 fluorescent dye (Invitrogen) at an intercalation ratio of 10 base pairs per 1 dye molecule [68, 69]. The ionic strength of the DNA loading solution is estimated to be 18 mM [84, 118]. The DNA molecules in the microchannels were driven into the nanochannels by applying pressure. The pressure was controlled by a microfluidic flow control system (Fluigent MFCS-EZ). The details of loading DNA into nanochannels were described in Ref. [103]. The T4 DNA molecules were then compressed against slit barriers by applying a pressure of 3 kPa for 120 s to generate knots. The DNA molecules before and after the compression step were observed using a blue laser (Coherent OBIS, 473 nm) with a power of 1 mW and a 100× (1.4 N.A.) oil immersion objective on an inverted epifluorescene microscope (Olympus IX73). The images were acquired by an EMCCD camera (Photometrics, Cascade II:512) at 20 fps with a 50 ms exposure time for 60 s for unknotted DNA and at 2 fps with a 200 ms exposure time for DNA containing two knots with the experiment ending when one of the knots unravels at the chain end. After the experiments with multiple cycles of loading, compression and imaging, the device was cleaned and dried for reuse in the next experiment [103].

5.2.3 Data processing

The movies of 16 T4 DNA molecules containing two knots from our previous reports [103, 135] and additional data for 24 two-knotted DNA molecules obtained specifically for this report were processed using custom-written MATLAB codes that output the intensity data of DNA molecules [120]. The intensity profile for each frame was fitted to a convolution of a Gaussian point-spread function with a box function to extract the position of DNA left end, x_{end}, and the extension of DNA, X, in each frame [121]. The position of the knots, x_{knot}, was identified as the brightest pixel using a second custom-written MATLAB code. The dimensionless knot position, x_{KNOT}, was then calculated as

$$x_{\mathrm{KNOT}}(t) = \frac{x_{\mathrm{knot}}(t) - \langle x_{\mathrm{end}}(t) \rangle_{\mathrm{5f}}}{\langle \mathrm{X}(t) \rangle_{\mathrm{5f}}} \tag{5.1}$$

where $\langle \ldots \rangle_{\mathrm{5f}}$ operation is a moving average with a window length of five frames to diminish the effect of chain end fluctuations on the DNA left end position and the extension of DNA [103].

With the dimensionless knot positions, the interaction between two knots was then analyzed by estimating the free energy of the two-knot separations following a previously reported approach [151, 155]. The free energy for knot-knot interactions, $F(x_{\mathrm{kk}})$, is defined as

$$\frac{F(x_{\mathrm{kk}})}{k_{\mathrm{B}}T} = -\log(P(x_{\mathrm{kk}})) \tag{5.2}$$

where x_{kk} is the dimensionless separation distance between two knots and $P(x_{\mathrm{kk}})$ is the probability of observing two knots with a dimensionless separation distance of x_{kk}.

5.3 Results

In our nanofluidic devices, knots were generated efficiently via compression of T4 DNA molecules against nanoslits using a pressure driven flow. The knot formation probability of DNA in nanochannels is a function of channel size, pressure and compression time [8–11]. The effective channel size of our device, D_{eff}, is estimated to be 307 nm using $D_{\text{eff}} = \sqrt{(D_1 - \delta)(D_2 - \delta)}$, where D_1 and D_2 are the height and width of the nanochannels, and δ is the wall depletion length that accounts for the DNA-wall excluded volume and electrostatic interactions [80–82]. Note that δ is estimated to be 14 nm using a model from Bhandari *et al.* [80]. Our effective channel size is close to the effective size of 346 nm for the original knot factory device [11]. The two-knot formation probability in our nanofluidic devices thus can be predicted using the model developed by Amin *et al.* [11] for knot formation in the knot factory device. The predicted probability of generating two knots is about 20% for the compression time and applied pressure in our knot-knot interaction experiments. The observed two-knot formation probability in our devices on 159 T4 DNA molecules is 16 $\pm$ 6% using a Clopper-Pearson interval with a 95% confidence interval [123], which agrees with the model to within experimental uncertainty.

We observed two particular behaviors of knot pairs in nanochannel-confined DNA molecules. Examples of these typical interactions are shown in Figure 5.2. Additional six examples of two-knot interactions are shown in Figure B.2. Figure 5.2a and Figure 5.2c are the kymographs of two knots, identified as bright spots, moving along the T4 DNA molecules over time. The bright streak is the trajectory of the knot. When the knots are in close contact, they appear as a larger bright spot as

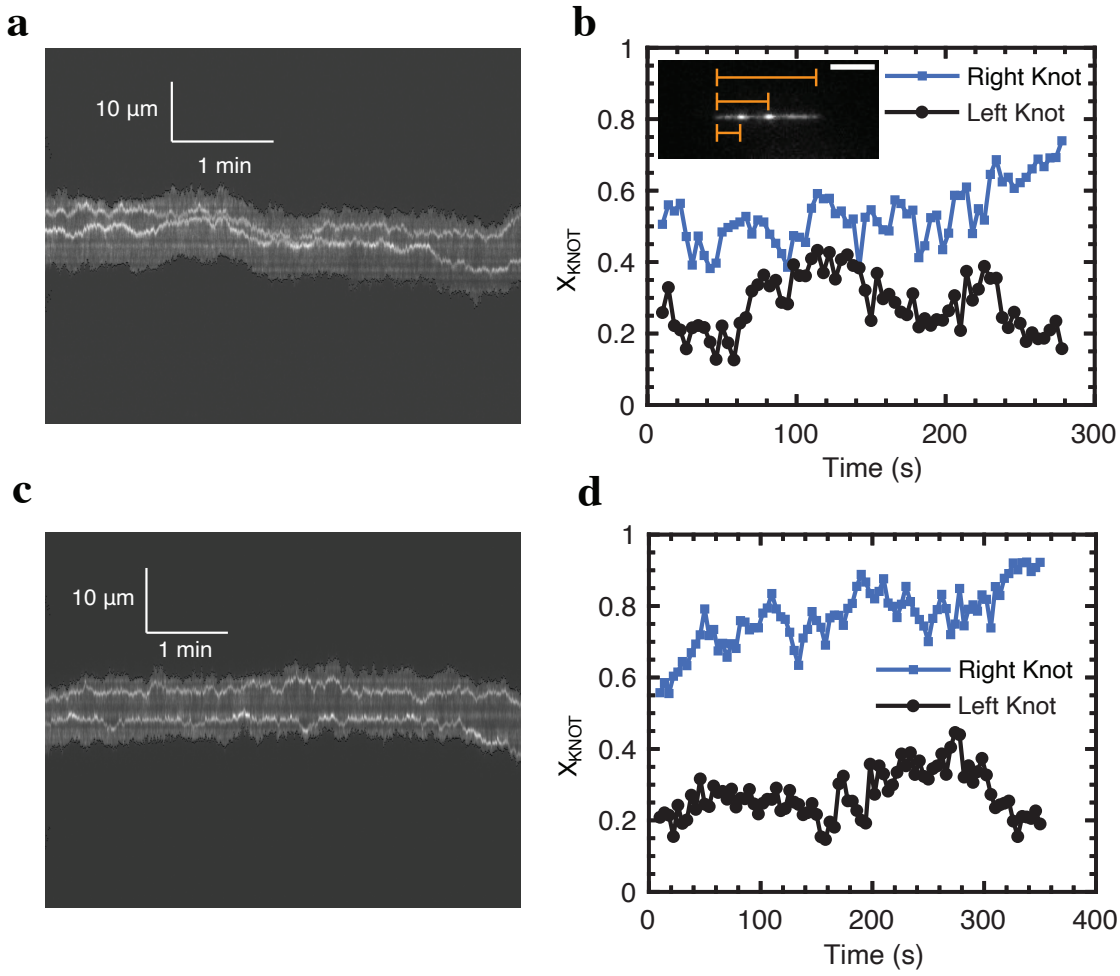

Figure 5.2: Interactions between two knots in nanochannel-confined DNA. (a, c) Kymographs of DNA molecules with two knots in nanochannels. The intensity of knotted DNA is plotted versus time. The bright streak corresponds to the trajectory of a knot moving along the DNA chain. The black dots on the edges of the DNA molecules are the results of the image processing code to locate the DNA. (b, d) Corresponding time evolution of dimensionless positions of the two knots obtained from (a) and (c), respectively. The dimensionless knot position, x_{KNOT}, is calculated as ratio of the distance between the left end of the DNA chain and the knot position to the extension of the DNA as shown in the inset of the two-knotted DNA image. The scale bar is 5 µm. The left end of the chain in the inset image corresponds to the upper end of the knotted DNA chain in the kymographs. The black solid line with circles shows the time trace of the knot close to the left end of the chain as illustrated in the inset, corresponding to the top knot in the kymographs. The blue solid line with squares indicates the dimensionless positions of the knot on the right over time, corresponding to the bottom knot in the kymographs.

shown in Figure 5.2a and are considered to be in an intertwined state. Note that the intertwined knot state is defined in our experiments as the state in which the dimensionless separation distance between two knots is in the range of 0 - 0.02, and one knot may, in principle, include part of the other knot as shown in Figure 5.1b. The definition of the intertwined knot state in our experiments is different from the state defined in the simulation studies, i.e.,that knots are nested [151–154]. The nested knots result in a larger size compared with the knot size in a separated state due to the expansion of a knot that allows the other knot to be inside the expanded knot [151, 152]. The variation of the knot sizes predicted in the simulation studies [151, 152] is inconsistent with our observation that the extension of DNA molecules is independent of the intertwined and separated knot states, which supports that the knots in our experiments only become close to each other rather than become nested together.

Figure 5.2b and Figure 5.2d illustrate the corresponding time evolution of dimensionless knot positions obtained by processing the kymographs in Figure 5.2a and Figure 5.2c, respectively. In the upper example of Figure 5.2, the knots move towards each other, but only remain in close proximity for several seconds. We did not observe that two knots pass through each other and interchange positions; there always appears to be a small region of low fluorescence intensity between the two knots. This observation contradicts the prediction of knot passage from the simulation study of simple knots in semiflexible polymers with ends fixed to walls [151], but is consistent with the observation in the experimental study of two-knot interactions in DNA stretched by elongational fields [155]. The contradiction is probably due to the difference in the topological complexity of knots. Trefz *et al.* [151] studied

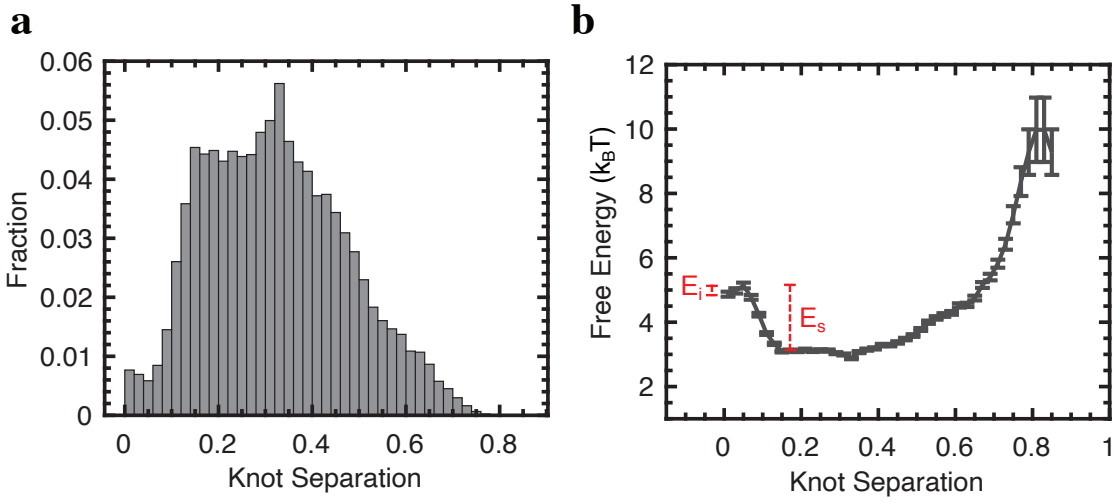

Figure 5.3: Separation between two knots for 40 two-knotted DNA molecules. (a) Normalized histogram of the dimensionless distances between two knots. (b) Corresponding free energy profile obtained from the normalized probability distribution in (a). The energy barrier E_s is the energy difference between the separated knot state, which is the local minimum at knot separation of 0.19, and the transition state, which is the local maximum at the knot separation of 0.05. The energy barrier E_i is the energy difference between the transition state and the intertwined knot state in which the knots have separation distances of about zero. The errors on free energy are estimated by propagating the uncertainties of the histogram bins.

simple trefoil knots in the simulation. The knot topology cannot be identified in our experiments, but our previous studies of single knots have shown that the knots generated in the nanofluidic devices are complex and large [103, 135]. The complex knots need to expand more to allow the other complex and large knot to pass through when compared to the simple trefoil knots. The other type of two-knot interactions is illustrated in the lower example of Figure 5.2. The knots stay separated until one of the knots unravels at the chain end, in agreement with the observation from the experiments of knot-knot interactions in stretched DNA under tension that the knots untie when the knots are initially far apart [155].

The interaction between two knots is quantitatively analyzed by estimating the

free energy from the normalized probability distribution of the dimensionless separation distances between the two knots [151–154]. Figure 5.3 shows the normalized distribution of dimensionless knot-knot separation distances (Figure 5.3a) and the corresponding free energy profile (Figure 5.3b) for 40 DNA molecules containing two knots. At a knot-knot separation distance of about 0.33, there is a global maximum in the two-knot interaction distribution, corresponding to a global minimum in the free energy. This global minimum of the free energy indicates that the most probable state is the separated knot state, and the separated state is more stable than the local minimum corresponding to the intertwined knot state in which the knots have separation distances of approximately zero. When knots are in the stable separated state, the knots need to first overcome the barrier $E_s = 2.0 \pm 0.1\ k_BT$, illustrated in Figure 5.3b to reach the transition state, and then become intertwined as the knot separation decreases further. Note that the energy barrier E_s is defined as the last barrier that the knots need to overcome to reach the transition state, which is the energy difference between the local maximum at the transition state and the local minimum where the knots are close to the transition state. Conversely, when the knots are in the intertwined state, the knots only need to overcome the smaller energy barrier $E_i = 0.3 \pm 0.1\ k_BT$, shown in Figure 5.3b, to move back to the more stable separated state.

Two potential sources of systematic errors in measuring the short-range interaction free energy profile are that (i) the knots tend to unravel when they are close to the chain ends and (ii) knots generated in the knot factory device may have diverse topologies. We thus performed two analyses, one measuring the effect of chain ends and the other examining the knot size, which is a proxy for the knot complexity, on

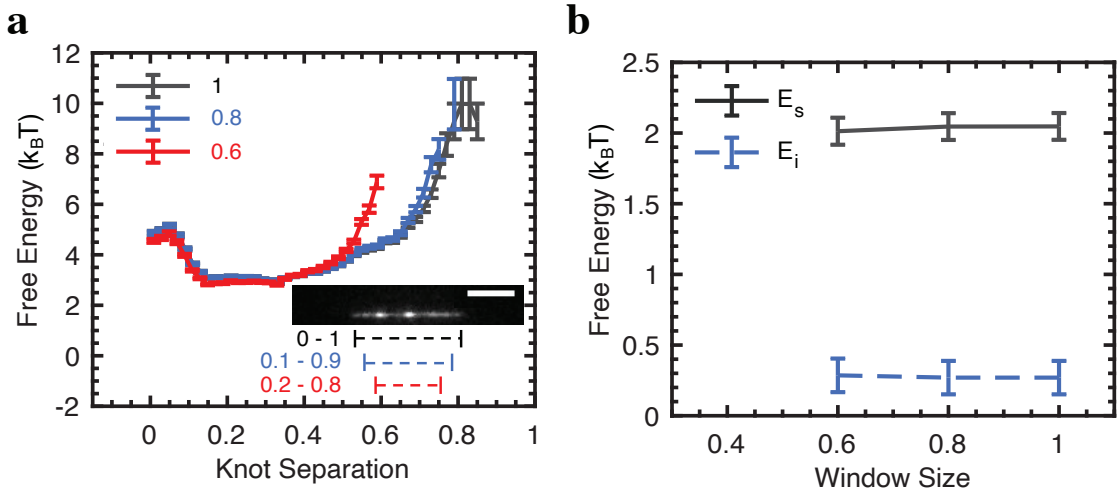

Figure 5.4: Interactions of two knots for 40 DNA molecules computed using window sizes of 0.6, 0.8 and 1 for the range of separation distances between two knots that are both inside the window. (a) Free energy profiles with window size of 0.6 (red solid line), 0.8 (blue solid line) and 1 (black solid line). The window size is defined as a fraction of the knotted DNA molecule, as illustrated in the inset of the knotted DNA image. For example, the energy profile with window size of 0.8 excludes the knot separation data when either of the knots has a dimensionless position outside the window of 0.1 - 0.9. The scale bar is 5 μm. The error in the free energy is estimated by propagating the uncertainty of the histogram bin. (b) Plots of the energy barriers, E_i (blue dashed line) and E_s (black solid line), as a function of window size. The energy barrier E_s is the energy difference between the local maximum at the transition state and the local minimum where the knots are close to the transition state. The energy barrier E_i is the energy difference between the transition state and the intertwined knot state.

the free energy profiles.

The chain edges might affect the short-range interaction between two knots when either of the knots is close to the chain end. To test whether this effect is indeed important for establishing the short-range interaction free energy, Figure 5.4a shows the free energy profiles with different window sizes of 0.6, 0.8 and 1. As illustrated in Figure 5.4a, the window is defined as the central region of the DNA molecule. If either of the knots is outside that region, the knot separation data are excluded. As such, the free energy landscapes with window sizes less than 1 exclude the knot

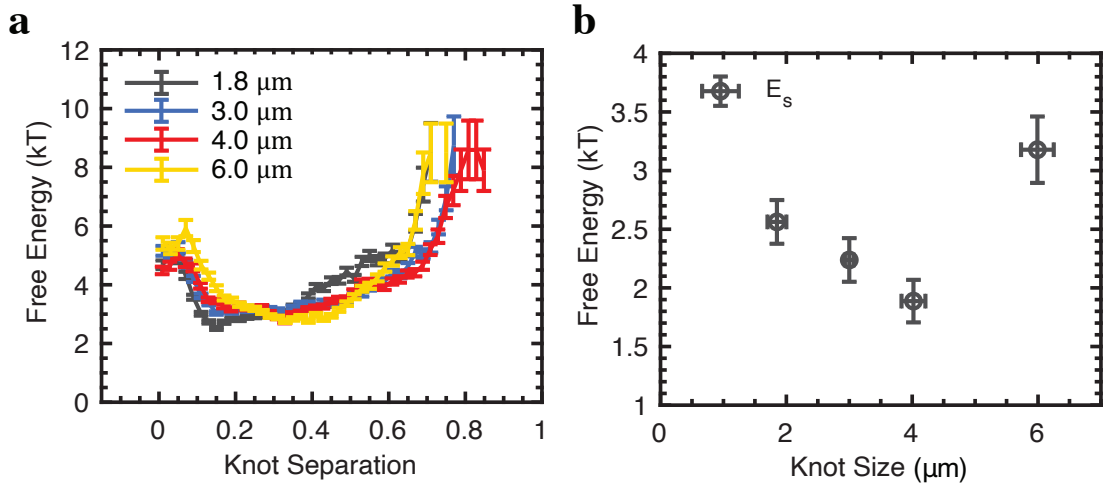

Figure 5.5: Knot-knot interactions in nanochannel-confined DNA for quartiles of 40 knot pairs with size of 1.8 μm, 3.0 μm, 4.0 μm and 6.0 μm. (a) Free energy profiles for ensemble of knots with size knot of 1.8 μm (black line), 3.0 μm (blue line), 4.0 μm (red line) and 6.0 μm (yellow line). The knot size is estimated as the extension difference between knotted and unknotted DNA molecules. (b) Plots of the energy barriers E_s as a function of knot size.

separation distance data when either of the knots is close to a chain end. The different longer-range free energy profiles with knot-knot separation distances larger than 0.4 for window sizes of 0.6, 0.8 and 1 are due to the exclusion of the knot separation data outside the window. For example, the free energy at a knot separation of 0.55 for the window size of 0.6 is larger than the free energy values for a window size of 0.8 and 1 because the free energy profile with the window size of 0.6 excludes the data of knot separation distance of 0.55 when either of the knots is outside the window of 0.2 - 0.8. The important point of Figure 5.4 is that the shorter-range sections of the energy profiles and the energy barriers, E_s and E_i, are independent of the window size. These results indicate that the short-range knot interaction is insensitive to the unravelling of knots near the chain edges.

The knots with different topologies may affect the short-range interactions between

knots. The complexity of knots cannot be directly determined from the knotted DNA images, but we can use the extension difference between unknotted and knotted DNA molecules as a proxy, which is correlated with the knot size, to distinguish between knots with different complexity. To determine whether the knot size affects the short-range interactions between knots, we thus performed an analysis to compare the free energy profiles for quartiles of knot size. Figure 5.5 shows the interactions between knots with averaged size of 1.8 ± 0.1 μm, 3.0 ± 0.1 μm, 4.0 ± 0.2 μm, and 6.0 ± 0.3 μm. The qualitative feature of the free energy profiles is independent of the knot size. Each free energy landscape shows the overall same feature as illustrated in Figure 5.5a: a global minimum when the knots are well separated and a local maximum at a small knot separation distance. One possible qualitative difference with respect to knot size is the existence (or not) of a local minimum at the knot separation distance of approximately zero. In the free energy profiles for knots with size of 1.8 ± 0.1 μm and 4.0 ± 0.2 μm (Figure B.1a and Figure B.1c), a local minimum of free energy exists at a knot separation distance of approximately zero. In contrast, for Figure B.1b and Figure B.1d, there is an overlap between the uncertainties on free energy at knot separation distances of 0.01, 0.03 and 0.05, which indicates that there is no statistically significant minimum at the knot separation distance of approximately zero for knots with size of 3.0 ± 0.1 μm and 6.0 ± 0.3 μm. A local minimum of free energy might exist at the short knot separation distance for knots with size of 3.0 ± 0.1 μm and 6.0 ± 0.3 μm, but there are not sufficient data to reduce the error. Quantitatively, the free energy barrier E_s shows a variation for different knot sizes as shown in Figure 5.5b, but there is no apparent relationship between knot size and energy barrier E_s. The experimental result is thus inconclusive about the effect

of knot size on the knot-knot interactions due to insufficient data.

5.4 Discussion

Our free energy profile of two-knot interactions in nanochannel-confined DNA exhibits a global minimum for separated knots with a smaller energy barrier $E_i = 0.3 \pm 0.1$ k_BT from the intertwined knot state to the transition state between separated and intertwined knots when compared to the energy barrier $E_s = 2.0 \pm 0.1$ k_BT from the separated knot state to the transition state. The overall free energy landscape qualitatively agrees with the results from simulation studies on two-knot interactions in semiflexible polymers stretched between walls separated by a large distance [152, 154]. Explicitly, Najafi *et al.* [152] studied the role of bending rigidity of polymer chains on interactions between knots and presented free energy profiles of knot-knot interactions for polymers with bending rigidity, κ, from 5 to 20 k_BT. Their free energy profiles only show a global minimum when the bending rigidity is less than 10 k_BT [152]. The bending rigidity of 5 k_BT corresponds to a polymer persistence length of 60 nm [151]. Note that the persistence length is computed using $l_\mathrm{p} \approx \kappa\sigma/k_BT$ [151], where σ is the effective diameter of the chain, estimated to be $\sigma = 12$ nm for DNA in a buffer solution with an ionic strength of 18 mM in our experiments [77]. The persistence length for polymers with bending rigidity of 5 k_BT is remarkably close to the calculated DNA persistence length of 60 nm based on the model from Dobrynin [75] in our experiments. The free energy obtained in our experiments using a persistence length of 60 nm shows qualitative agreement with the simulation-based prediction for a bending rigidity of 5 k_BT, both of which produce a global minimum when the knots are separated. Another computational study was that of Richard *et*

al. [154], who presented free energy profiles for knot-knot interactions in polymers with chain ends fixed to walls of varying distances. Their free energy profiles show that the separated knot state becomes more likely when the wall distance is larger, consistent with a stronger stretching of polymer chains. Since simulated free energy profile for knots in polymers with the bending rigidity of 5 k_BT corresponding to the DNA in our experiments is not available in the work of Richard *et al.* [154], we instead compared our experimental result to their free energy profile for polymers with bending rigidity of 10 k_BT. The free energy for knots in polymers with bending rigidity of 10 k_BT stretched between walls with a large distance also exhibits a global minimum for separated knots, which is qualitatively consistent to our experimental result.

While the qualitative agreement between our experiments and the aforementioned simulations [152, 154] is good, the magnitudes of the two energy barriers, E_s and E_i, obtained from our free energy profile, however, are smaller than the energy barriers obtained from the simulations of Najafi *et al.* [152] and Richard *et al.* [154] for strongly stretched chains. Explicitly, the energy barriers E_s and E_i predicted in the computational study from Najafi *et al.* [152] are about 7 k_BT and 1.5 k_BT, respectively, while Richard *et al.* [154] found that the two energy barriers E_s and E_i are about 3.5 k_BT and 3 k_BT, respectively. The inconsistency in the energy barriers between these simulations and our experiments is probably due to the large distance between the walls in the simulation studies [152, 154]. The increased wall distance increases the energy barriers due to tension; the knots need to overcome a larger energy barrier to reach the transition state when the polymer chain is under stronger stretching [151, 154]. In contrast, our DNA is compressed and there is no additional

contribution due to tension that prevents knot motion along the chain.

Our energy barrier E_s for knots to transition from the separated state is, however, in agreement with the results from theoretical studies of interactions between knots in polymers stretched between walls with a small distance [151, 154], where the tension is not very high, and experimental studies of two-knot interactions in polymers under tension induced by an extensional flow [155]. In the former case, Trefz *et al.* [151] simulated interactions between knots in polymers with a bending rigidity from 0 to 20 k_BT stretched between two walls kept at a small distance. The free energy barrier E_s obtained from their study [151] is about 2 k_BT for knots in stretched polymers with bending rigidity of 5 k_BT. Similarly, Richard *et al.* [154] found the energy barrier E_s is about 1 - 2 k_BT for knots in polymers with bending rigidity of 10 k_BT when stretched between walls with a small distance, which is closer to our experiments than their results cited previously for large wall-wall distances. The magnitude of our energy barrier E_s is also close to some of the experimental data of Klotz *et al.* [155], who studied the interaction between two knots in T4 DNA stretched by elongational fields with varied strength in microfludic devices. The fractional extension of the stretched T4 DNA chains by elongational fields is between 0.44 and 0.74, corresponding to the tension of 0.07 - 0.31 pN [98]. The polymer chains under the lower tension are analogous to simulated polymer chains stretched between walls with small distances when the ratio of wall distance to polymer length is between 0.2 and 0.6 [151, 154]. The experimental results from Klotz *et al.* [155] are thus expected to be close to the simulation results for a small wall separation distance [151, 154]. The energy barriers E_s measured in their experiments are between 1 and 3 k_BT [155], consistent with the simulation-based predictions [151, 154] and our experimental results for the energy

barrier E_s for knots in nanochannel-confined T4 DNA.

While the magnitude of our energy barrier E_s is consistent with the results from previous simulations [151, 154] and experiments [155], our experimental observations on behaviors of knot pairs in nanochannel-confined DNA molecules contradict the attractive interaction between knots observed in polymers under tension that leads to the global minimum being the intertwined knot state [151, 154, 155]. Rather, the free energy profile obtained in our experiments exhibits a global minimum for separated knots. The energy barrier $E_i = 0.3 \pm 0.1\ k_BT$ from intertwined knot state to the transition state obtained in our experiments is also smaller than the results of the simulations [151, 154] and experiments [155], which show free energy barriers E_i of about 2 to 3 k_BT. In the experiments from Klotz *et al.* [155], they also observed that the two knots attract each other and can stay in close proximity for several minutes, which is connected to the magnitude of the barrier E_i.

A potential explanation for the observation that knots remain in close for a long time under tension is that the knots may move slower along polymers under tension when compared to knots in nanochannel confinement. The knot mobility is about 0.2 - 3 $\mu m^2/s$ for single knots along DNA molecules under tension with values in the range of 0.07 - 0.31 pN [98]. The knot mobility in nanochannel confinement of about 0.4 $\mu m^2/s$ is within the range of the mobility for knots under tension [103]. The long-time attraction between knots under tension is thus not due to the result of knot mobility along DNA chains.

Rather, we suspect that the tendency for knots to stay close for long times in prior work [98] and the absence of such behavior here is due to the discrepancy in the magnitude of energy barrier E_i between our experimental results and previous

simulation-based [151, 154] and experimental [155] results. Prior work [155] speculated that the long residence time for two proximate knots in an elongational field was due to a Casimir force arising from the transverse fluctuations of the polymer [156, 157]. Inasmuch as we do not observe a similar residence time, we are forced to conclude that, if the Casimir force is the origin of this attraction in flow, it must be much weaker in nanochannel-confined DNA compared with the knots in DNA under tension. This hypothesis is supported by prior work [101] on the magnitude of transverse fluctuations, for stretched DNA and nanochannel-confined DNA, wherein the transverse fluctuations of stretched T4 DNA under tension with values in the range of 0.001 - 0.1 pN are estimated approximately two orders of magnitude greater than the fluctuations of T4 DNA in confinement with an effective channel size of 307 nm. If the Casimir force is indeed the origin of the strong attraction observed for two knots in flow, then the cutoff in transverse fluctuations by the channel walls, and the corresponding reduction in the Casimir force, is consistent with the observation that nanochannel-confined knots do not stay in close proximity for a long time and a smaller free energy barrier E_i from the intertwined knot state to the transition state when compared to knots in polymers under tension.

We can go further in our understanding of the knot-knot interactions, including the importance of a Casimir force, by measuring the probability that two knots attract one another over a short time interval (5 s) as a function of the knot separation distance. If the knots are undergoing uncorrelated random walks along the polymer, we would anticipate an equal probability of moving towards or away from one another over short time intervals. In contrast, if there is a Casimir force between the knots, we would anticipate that the tendency to move towards one another would increase

with decreasing separation distance, since the Casimir force scales like k_BT/d for a separation distance d [156]. Figure 5.6a shows the experimental results for the probability of knot attraction as a function of knot separation distance. Knots that are widely separated have a roughly equal probability of attraction or repulsion over short times, consistent with them performing independent random walks. However, at short distances, the knots tend to repel one another over short times. This behavior is inconsistent with a Casimir force, which would cause the knots to be attractive at short distances. At large separation distances, there is a tendency for the knots to move towards one another because, if one of the knots is close to the chain end, increasing the separation distance by moving that knot would cause it to unravel and no longer remain part of the ensemble of data with two knots.

The boundary layer for the reduction in knot-knot attraction in Figure 5.6a extends out to knot separation distances of approximately $d \approx 0.2$. If the knots cannot pass through one another, which is the observation from our experiments, then there is a reflecting boundary condition at $d = 0$. To see if this decrease in the knot attraction is simply an artifact of that boundary condition, we also performed a numerical simulation of a pair of Gaussian random walkers with a reflecting boundary condition at $d = 0$. Since the knots unravel at the chain ends, we also put adsorbing boundary conditions at DNA chain ends, which is a simplified model for knots unraveling. Figure 5.6b reveals that thickness of the boundary layer due to the reflecting barrier is very narrow, extending out to $d \approx 0.05$. Thus, we conclude that the drop in knot-knot attraction in the experimental data in Figure 5.6a, which extends to $d \approx 0.2$, results from the knot interaction energy rather than the boundary condition.

Our qualitative analysis of difference in transverse fluctuations between DNA un-

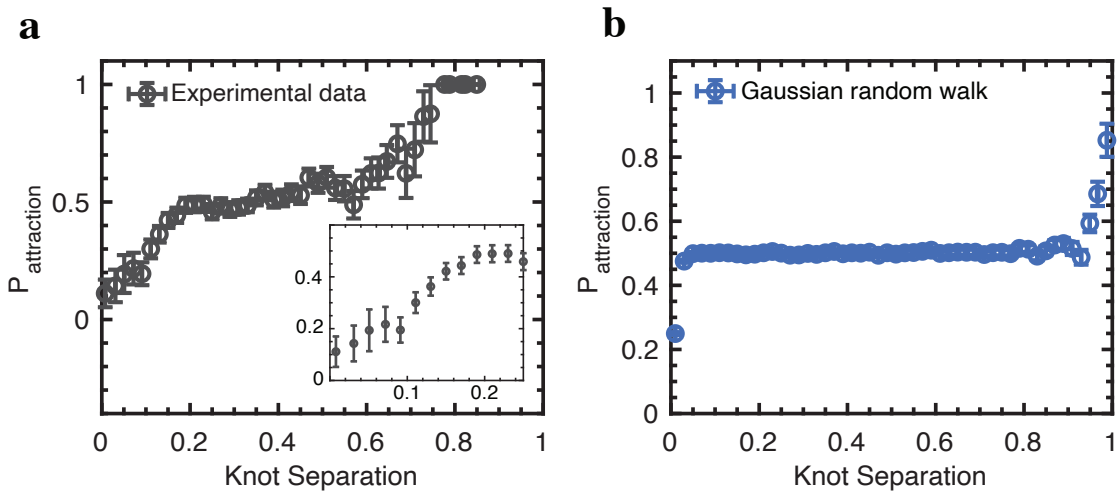

Figure 5.6: Dynamics of knots as a function of knot separation distance. (a) Probability of attraction as a function of dimensionless of knot separation distance obtained from experimental data of knot-knot interactions in 40 DNA molecules. The probability of attraction is estimated as the probability that the knot-knot distance decreases over 5 s. The inset with the axis labels identical to the main plot shows the probability of attraction at small knot separation distances between 0 and 0.25. (b) Simulated probability of attraction as a function of dimensionless of knot separation distance. The plot was obtained by considering knots as two independent Gaussian random walkers with addition of a reflecting boundary condition when the knots come together and an adsorbing boundary when either of knots reaches the chain end. The errors on the probability are calculated using a Clopper-Pearson interval with a 95% confidence interval [123]. The error bar on the knot separation represents the standard error as binned the results with a bin width of 0.02.

der tension and confinement and the quantitative analysis of dynamics of knots at small knot separation distances suggest that the knots in nanochannel-confined DNA experience a much weaker Casimir force compared with knots in DNA under tension, and that there must be some stronger force governing proximate knot-knot interactions because the probability of attraction is inconsistent with a Casimir force. A theory of Casimir interactions in semiflexible polymers under confinement would provide a more detailed quantitative analysis of the Casimir force between knots in nanochannel confinement. The development of such a theory, however, is beyond the

scope of this paper, which provides experimental evidence for knot-knot interactions in polymers under confinement. Our experimental results could motivate theoreticians to develop the new theory of Casimir effect in semiflexible polymers under confinement.

5.5 Conclusion

We have studied the interaction between two knots in nanochannel-confined DNA molecules. Two particular cases of knot-knot interactions were observed in our experiments; (i) widely separated knots in nanochannel-confined DNA attract each other, but the knots only remain in close contact for several seconds and (ii) knots tend to remain separated until one of the knots unravels at the chain end. The associated free energy profile of knot-knot interactions shows a global minimum when the knots are in the separated state and the energy barrier E_i from the intertwined knot state to the transition state is found to be $0.3 \pm 0.1\ k_BT$. This lower barrier leads to our experimental results contradicting the mechanism of two-knot interactions in polymers under tension, where the knots experience an attraction and stay in the intertwined state for a long time [151–155]. Our experimental work provides an initial set of evidence on the knot-knot interaction along DNA confined in nanochannels. A further understanding of this complex and intriguing phenomenon is required to study this for knots with known topology in nanochannels with different channel sizes.

Chapter 6

Conclusions and Outlook

6.1 Summary

In this thesis, we focused on the fundamental questions related to the dynamical properties of knotted DNA in nanochannels. Throughout this work, we use a recently developed nanofluidic knot factory device for efficient DNA knot generation and detection [11]. In the device, the formation of knots utilizes a pressure driven flow to compress single DNA molecules in nanochannels against nanoslits which allow solvent to pass while preventing the passage of long DNA molecules. After the compression process, knots are formed in many of the DNA molecules. The stained knotted DNA molecules confined in nanochannels are then imaged using laser-induced fluorescence microscopy. With the advantage of the nanofluidic knot factory devices and fluorescence microscopy, we (i) determined the knot diffusive behavior along nanochannel-confined DNA to distinguish between two predicted knot diffusion mechanisms [103], (ii) investigated the effect of knots on DNA center-of-mass diffusion in nanochannels in the extended de Gennes regime [135], and (iii) studied the interactions between

knots in nanochannel-confined DNA molecules [147].

We addressed three questions related to knot motion along DNA under nanochannel confinement in the extended de Gennes regime. Those experimental results of dynamical properties of knotted DNA in nanochannels provide deep insights into the mechanism of knot transport under confinement, which could provide some rational strategies based on knot diffusion to remove knots, thus improving the genomic technologies. The experimental evidence gained in this thesis work can even further support theoretical advancements of knotted DNA in nanofluidic systems. However, many intriguing questions still remain in the field of DNA knots, such as the knot formation mechanism in nanofluidic systems and knot transport in different-sized nanochannels and in buffer solutions with different ionic strength. Improved fundamental understanding of knot formation and transport under different degree of confinement will lead to continued improvement of genomic technogies, nanochannel-based genome mapping and nanopore sequencing, as well as manipulation of DNA knots in living cells. Below, we outline several topics related to knot formation and knot transport in nanochannels that may be of interest for future explorations.

6.2 Future Directions

Knot formation mechanism in nanofluidic systems

In the dissertation work, we take advantage of the nanofluidic knot factory device to generate DNA knots in nanochannel confinement. In the device, the knots are generated by compressing DNA using a hydrodynamic flow. The knotting mechanism under confinement, however, is still under investigation. In a linear DNA molecule,

a knot can be generated by passing a free end of DNA through one or several loops within the same linear chain [11]. The kinetic pathway how DNA ends pass through loops is unclear for DNA in the nanofluidic system. Amin *et al.* proposed that Brownian fluctuations may introduce local agitation of DNA chain ends to drive knot formation [158]. It is desirable to investigate the DNA knot formation mechanism experimentally, which could provide deep insights into knotting dynamics of DNA under confinement, thus paving a way to suppress knot formation in genomics technologies and biological systems.

Understanding the kinetic pathway of knotting requires to monitor the movement of DNA backbone and chain ends simultaneously. To do this, we need to stain the DNA backbone and chain ends with two different fluorescent dyes. The idea to construct DNA molecules with different-colored chain ends from the backbone is to attach short DNA fragments labeled with Cy5 fluoresence dyes to the two ends of a long DNA molecule stained with YOYO-1 dyes based on a developed modular stitching protocol [159]. A two-color laser-induced fluorescence microscopy is then used to directly image the movement of DNA ends and backbone simultaneously in nanochannel confinement.

The observation of the simultaneous motion of DNA chain ends and DNA backbone is expected to elucidate the dynamics of chain ends which provides an opportunity to understand the mechanism of DNA knot formation under confinement. Analysis of the experimental data will also explain the process of generating knots in the nanofluidic knot factory device by developing a detailed fluid flow field model. We envision that this knot formation study in nanochannel confinement will also provide an ideal model system for understanding knot formation in crowded biological

environments such as bacteriophage capsids.

Dynamical properties of knotted DNA in different sized nanochannels and ionic strengths of buffer solution

The thesis work focuses on DNA knot transport in the extended de Gennes regime. As described in Chapter 2, the polymers in nanochannel confinement can be roughly differentiated as four regimes, the Odijk regime, the backfolded Odijk regime, the extended de Gennes regime and the de Gennes regime. The dynamical properties of knotted DNA under other regimes of nanochannel confinement still remain unexplored experimentally. In particular, the study of DNA knots in the Odijk regime and the backfolded Odijk regime will be closely related to the genomic technology, nanochannel-based genome mapping with channel sizes less than 50 nm [160].

In Chapter 3, we found knots undergo subdiffusion based on the experimental measurement of knot diffusion projected onto the channel axis, which may not the same as the knot diffusion along the DNA chain contour [103]. In the Odijk regime, DNA molecules feel a strong confinement and the confined chains form deflection segments instead of coils [132]. A study of the more extended DNA chains will provide a more accurate measurement of knot diffusion along chain contour. The experimental study of DNA knots in the Odijk regime is challenging due to the low probability of knot generation [8]. Such challenges could be tackled by using a funnel in a nanochannel, where the knots could be generated in the larger channel and then the knotted DNA molecules are moved into the smaller nanochannels to study DNA knots. It would be also possible to study DNA knots in the Odijk regime using simulation which provides a way to study the diffusion of DNA knots with diverse

known types. Another outcome of knot diffusion study in Chapter 3 is the diffusion rate of knots along DNA molecules in nanochannels with an effective channel size of 308 nm. It would be interesting to further probe the effect of degree of confinement on knot transport. The degree of confinement is measured by the ratio of the channel size to the persistence length of DNA molecules. The persistence length can be varied by changing the ionic strength of buffer solution. It is particularly interesting here to vary the ionic strength at a fixed effective channel size to investigate how DNA stiffness affects the knot transport rate. We hypothesized that the transport rate will increase with decreasing ionic strength of buffer solution which tend to swells the knot, thus decreasing the intra-chain friction inside the knots.

In Chapter 4, we focus on investigating the effect of knots on DNA center-of-mass diffusion in nanochannels in the extended de Gennes regime. It would be intriguing to future probe the effect of knots on DNA center-of-mass diffusion under different regimes of nanochannel confinement. In the experiments, we also observe that the knots generated in the knot factory device have diverse sizes and DNA molecules can form multiple knots on the same chain. Based on the findings in this Chapter 4, we show that the increased single knot size will decrease knotted DNA chain diffusion in the extended de Gennes regime due to the increased friction between the channel wall and the knot region. However, we did not draw a conclusion about the effects of knot number on knotted DNA center-of-mass diffusion due to the limited experimental data of DNA containing knots with diverse numbers [135]. It would be worthwhile to perform a thorough investigation into the effects of numbers of knots on knotted DNA center-of-mass diffusion.

In Chapter 5, we focus on studying interactions between two knots in nanochannel

confinement in the extended de Gennes regime. We postulate the discrepancy between our experimental data under confinement and the results of knot-knot interactions in DNA under tension is due to the smaller transverse fluctuations on DNA under confinement compared with DNA molecules under tension [147]. Our experimental work provides an initial set of evidence on the knot-knot interaction along DNA confined in nanochannels. A further understanding of this complex and intriguing phenomenon is required to study this for knots in nanochannels with different effective channel sizes.

Bibliography

1. Orlandini, E. Statics and dynamics of DNA knotting. *J. Phys. A: Math. Theor.* **51,** 053001 (2018).

2. Turner, J. C. & van de Griend, P. *History and science of knots* (World Scientific, 1996).

3. Vandermonde, A. T. Remarques sur les problèmes de situation. *Mémoires de l'Académie Royal Des Science,* 566–574 (1771).

4. Liu, L. F., Depew, R. E. & Wang, J. C. Knotted single-stranded DNA rings: A novel topological isomer of circular single-stranded DNA formed by treatment with Escherichia coli ω protein. *J. Mol. Biol.* **106,** 439–452 (1976).

5. Dai, L. & Doyle, P. S. Universal knot spectra for confined polymers. *Macromolecules* **51,** 6327–6333 (2018).

6. Dai, L., van der Maarel, J. R. C. & Doyle, P. S. Effect of nanoslit confinement on the knotting probability of circular DNA. *ACS Macro Lett.* **1,** 732–736 (2012).

7. Micheletti, C. & Orlandini, E. Numerical study of linear and circular model DNA chains confined in a slit: metric and topological Properties. *Macromolecules* **45,** 2113–2121 (2012).

8. Jain, A. & Dorfman, K. D. Simulations of knotting of DNA during genome mapping. *Biomicrofluidics* **11,** 024117 (2017).

9. Micheletti, C. & Orlandini, E. Knotting and metric scaling properties of DNA confined in nano-channels: a Monte Carlo study. *Soft Matter* **8,** 10959–10968 (2012).

10. Orlandini, E. & Micheletti, C. Knotting of linear DNA in nano-slits and nano-channels: a numerical study. *J. Biol. Phys.* **39,** 267–275 (2013).

11. Amin, S., Khorshid, A., Zeng, L., Zimny, P. & Reisner, W. A nanofluidic knot factory based on compression of single DNA in nanochannels. *Nat. Commun.* **9,** 1506 (2018).

12. Plesa, C., Verschueren, D., Pud, S., van der Torre, J., Ruitenberg, J. W., Witteveen, M. J., Jonsson, M. P., Grosberg, A. Y., Rabin, Y. & Dekker, C. Direct observation of DNA knots using a solid-state nanopore. *Nat. Nanotechnol.* **11,** 1093–1097 (2016).

13. Grosberg, A. Y. & Rabin, Y. Metastable tight knots in a wormlike polymer. *Phys. Rev. Lett.* **99,** 217801 (2007).

14. Katritch, V., Olson, W. K., Vologodskii, A., Dubochet, J. & Stasiak, A. Tightness of random knotting. *Phys. Rev. E* **61,** 5545 (2000).

15. Dai, L., Renner, C. B. & Doyle, P. S. Origin of metastable knots in single flexible chains. *Phys. Rev. Lett.* **114,** 037801 (2015).

16. Dai, L., Renner, C. B. & Doyle, P. S. Metastable knots in confined semiflexible chains. *Macromolecules* **48,** 2812–2818 (2015).

17. Dai, L., Renner, C. B. & Doyle, P. S. Metastable tight knots in semiflexible chains. *Macromolecules* **47,** 6135–6140 (2014).

18. Metzler, R., Reisner, W., Riehn, R., Austin, R., Tegenfeldt, J. O. & Sokolov, I. M. Diffusion mechanisms of localised knots along a polymer. *Europhys. Lett.* **76,** 696 (2006).

19. Micheletti, C. & Orlandini, E. Knotting and unknotting dynamics of DNA strands in nanochannels. *ACS Macro Lett.* **3,** 876–880 (2014).

20. Suma, A., Orlandini, E. & Micheletti, C. Knotting dynamics of DNA chains of different length confined in nanochannels. *J. Phys.: Condens. Matter* **27,** 354102 (2015).

21. Matthews, R., Louis, A. A. & Yeomans, J. M. Effect of topology on dynamics of knots in polymers under tension. *Europhys. Lett.* **89,** 20001 (2010).

22. Venter, J. C., Adams, M. D., Myers, E. W., Li, P. W., Mural, R. J., Sutton, G. G., Smith, H. O., Yandell, M., Evans, C. A., Holt, R. A., *et al.* The sequence of the human genome. *Science* **291,** 1304–1351 (2001).

23. Pillai, S. K., Wong, J. K. & Barbour, J. D. Turning up the volume on mutational pressure: Is more of a good thing always better? (A case study of HIV-1 Vif and APOBEC3). *Retrovirology* **5,** 1–8 (2008).

24. Sanger, F., Nicklen, S. & Coulson, A. R. DNA sequencing with chain-terminating inhibitors. *Proc. Natl. Acad. Sci. U.S.A.* **74,** 5463–5467 (1977).

25. Morozova, O. & Marra, M. A. Applications of next-generation sequencing technologies in functional genomics. *Genomics* **92,** 255–264 (2008).

26. Metzker, M. L. Emerging technologies in DNA sequencing. *Genome Res.* **15,** 1767–1776 (2005).

27. Metzker, M. L. Sequencing technologies - the next generation. *Nat. Rev. Genet.* **11,** 31–46 (2010).

28. Mardis, E. R. The impact of next-generation sequencing technology on genetics. *Trends Genet.* **24,** 133–141 (2008).

29. Mardis, E. R. Anticipating the $1,000 genome. *Genome Biol.* **7,** 1–5 (2006).

30. Service, R. F. The race for the $1000 genome. *Science* **311,** 1544–1546 (2006).

31. Feuk, L., Carson, A. R. & Scherer, S. W. Structural variation in the human genome. *Nat. Rev. Genet.* **7,** 85–97 (2006).

32. Treangen, T. J. & Salzberg, S. L. Repetitive DNA and next-generation sequencing: computational challenges and solutions. *Nat. Rev. Genet.* **13,** 36–46 (2012).

33. Stankiewicz, P. & Lupski, J. R. Structural variation in the human genome and its role in disease. *Annu. Rev. Med.* **61,** 473–455 (2010).

34. Schmid, C. W. & Deininger, P. L. Sequence organization of the human genome. *Cell* **6,** 345–358 (1975).

35. Batzer, M. A. & Deininger, P. L. Alu repeats and human genomic diversity. *Nat. Rev. Genet.* **3,** 370–379 (2002).

36. Treangen, T. J. & Salzberg, S. L. Repetitive DNA and next-generation sequencing: computational challenges and solutions. *Nat. Rev. Genet.* **13,** 36–46 (2012).

37. Das, S. K., Austin, M. D., Akana, M. C., Deshpande, P., Cao, H. & Xiao, M. Single molecule linear analysis of DNA in nano-channel labeled with sequence specific fuorescent probes. *Nucleic Acids Res.* **38,** e177 (2010).

38. Lam, E. T., Hastie, A., Lin, C., Ehrlich, D., Das, S. K., Austin, M. D., Deshpande, P., Cao, H., Nagarajan, N., Xiao, M. & Kwok, P.-Y. Genome mapping on nanochannel arrays for structural variation analysis and sequence assembly. *Nat. Biotechnol.* **30,** 771–776 (2012).

39. Jain, M., Olsen, H. E., Paten, B. & Akeson, M. The Oxford Nanopore MinION: delivery of nanopore sequencing to the genomics community. *Genome Biol.* **17,** 239 (2016).

40. Howorka, S., Cheley, S. & Bayley, H. Sequence-specific detection of individual DNA strands using engineered nanopores. *Nat. Biotechnol.* **19,** 636–639 (2001).

41. Payne, A., Holmes, N., Rakyan, V. & Loose, M. BulkVis: a graphical viewer for Oxford nanopore bulk FAST5 files. *Bioinformatics* **35,** 2193–2198 (2019).

42. Haque, F., Li, J., Wu, H.-C., Liang, X.-J. & Guo, P. Solid-state and biological nanopore for real-time sensing of single chemical and sequencing of DNA. *Nano Today* **8,** 56–74 (2013).

43. Zheng, G. X. Y., Lau, B. T., Schnall-Levin, M., Jarosz, M., Bell, J. M., Hindson, C. M., Kyriazopoulou-Panagiotopoulou, S., Masquelier, D. A., Merrill, L., Terry, J. M., *et al.* Haplotyping germline and cancer genomes with high-throughput linked-read sequencing. *Nat. Biotechnol.* **34,** 303–311 (2016).

44. Elyanow, R., Wu, H.-T. & Raphael, B. J. Identifying structural variants using linked-read sequencing data. *Bioinformatics* **34,** 353–360 (2018).

45. Reifenberger, J. G., Dorfman, K. D. & Cao, H. Topological events in single molecules of E. coli DNA confined in nanochannels. *Analyst* **140,** 4887–4894 (2015).

46. Sharma, R. K., Agrawal, I., Dai, L., Doyle, P. & Garaj, S. DNA knot malleability in single-digit nanopores. *Nano Lett.* **21,** 3772–3779 (2021).

47. Suma, A., Rosa, A. & Micheletti, C. Pore translocation of knotted polymer chains: How friction depends on knot complexity. *ACS Macro Lett.* **4,** 1420–1424 (2015).

48. Rosa, A., Ventra, M. D. & Micheletti, C. Topological jamming of spontaneously knotted polyelectrolyte chains driven through a nanopore. *Phys. Rev. Lett.* **109,** 118301 (2012).

49. Narsimhan, V., Renner, C. B. & Doyle, P. S. Translocation dynamics of knotted polymers under a constant or periodic external field. *Soft Matter* **12,** 5041–5049 (2016).

50. Cao, H., Hastie, A. R., Cao, D., Lam, E. T., Sun, Y., Huang, H., Liu, X., Lin, L., Andrews, W., Chan, S., *et al.* Rapid detection of structural variation in a human genome using nanochannel-based genome mapping technology. *GigaScience* **3,** 2047-217X-3–34 (2014).

51. Hastie, A. R., Dong, L., Smith, A., Finklestein, J., Lam, E. T., Huo, N., Cao, H., Kwok, P.-Y., Deal, K. R., Dvorak, J., *et al.* Rapid genome mapping in nanochannel arrays for highly complete and accurate *de novo* sequence assembly of the complex *Aegilops tauschii* genome. *PLoS ONE* **8,** e55864 (2013).

52. Dorfman, K. D., Gupta, D., Jain, A., Muralidhar, A. & Tree, D. R. Hydrodynamics of DNA confined in nanoslits and nanochannels. *Eur. Phys. J.: Spec. Top.* **223,** 3179–3200 (2014).

53. Marie, R., Pedersen, J. N., Bauer, D. L. V., Rasmussen, K. H., Yusuf, M., Volpi, E., Flyvbjerg, H., Kristensen, A. & Mir, K. U. Integrated view of genome structure and sequence of a single DNA molecule in a nanofluidic device. *Proc. Natl. Acad. Sci. USA* **110,** 4893–4898 (2013).

54. Marie, R., Pedersen, J. N., Bærlocher, L., Koprowska, K., Pødenphant, M., Sabatel, C., Zalkovskij, M., Mironov, A., Bilenberg, B., Ashley, N., Flyvbjerg, H., Bodmer, W. F., Kristensen, A. & Mir, K. U. Single-molecule DNA-mapping and whole-genome sequencing of individual cells. *Proc. Natl. Acad. Sci. USA* **115,** 11192–11197 (2018).

55. Kounovsky-Shafer, K. L., Hernańdez-Ortiz, J. P., Jo, K., Odijk, T., de Pablo, J. J. & Schwartz, D. C. Presentation of large DNA molecules for analysis as nanoconfined dumbbells. *Macromolecules* **46,** 8356–8368 (2013).

56. Kounovsky-Shafer, K. L., Hernańdez-Ortiz, J. P., Potamousis, K., Tsvid, G., Place, M., Ravindran, P., Jo, K., Zhou, S., Odijk, T., de Pablo, J. J. & Schwartz, D. C. Electrostatic confinement and manipulation of DNA molecules for genome analysis. *Proc. Natl. Acad. Sci. USA* **114,** 13400–13405 (2017).

57. Niedringhaus, T. P., Milanova, D., Kerby, M. B., Snyder, M. P. & Barron, A. E. Landscape of next-generation sequencing technologies. *Anal. Chem.* **83,** 4327–4341 (2011).

58. Kasianowicz, J. J., Robertson, J. W., Chan, E. R., Reiner, J. E. & Stanford, V. M. Nanoscopic porous sensors. *Annu. Rev. Anal. Chem.* **1,** 737–766 (2008).

59. Meluzzi, D., Smith, D. E. & Arya, G. Biophysics of knotting. *Annu. Rev. Biophys.* **39,** 349–366 (2010).

60. Rybenkov, V. V., Cozzarelli, N. R. & Vologodskii, A. V. Probability of DNA knotting and the effective diameter of the DNA double helix. *Proc. Natl. Acad. Sci. USA* **90,** 5307–5311 (1993).

61. Liu, L. F., Perkocha, L., Calendar, R. & Wang, J. C. Knotted DNA from bacteriophage capsids. *Proc. Natl. Acad. Sci. USA* **78,** 5498–5502 (1981).

62. Marenduzzo, D., Micheletti, C., Orlandini, E. & Sumners, D. W. Topological friction strongly affects viral DNA ejection. *Proc. Natl. Acad. Sci. USA* **110,** 20081–20086 (2013).

63. Hiemenz, P. C. & Lodge, T. P. *Polymer chemistry* (CRC Press, 2007).

64. Liu, L. F., Perkocha, L., Calendar, R. & Wang, J. C. Knotted DNA from bacteriophage capsids. *Proc. Natl. Acad. Sci. USA* **78,** 5498–5502 (1981).

65. Reisner, W., Pedersen, J. N. & Austin, R. H. DNA confinement in nanochannels: physics and biological applications. *Rep. Prog. Phys.* **75,** 106601 (2012).

66. Bates, A. D. & Maxwell, A. *DNA Topology* (Oxford University Press, 2005).

67. Murade, C. U., Subramaniam, V., Otto, C. & Bennink, M. L. Force spectroscopy and fluorescence microscopy of dsDNA–YOYO-1 complexes: implications for the structure of dsDNA in the overstretching region. *Nucleic Acids Res.* **38,** 3423–3431 (2010).

68. Günther, K., Mertig, M. & Seidel, R. Mechanical and structural properties of YOYO-1 complexed DNA. *Nucleic Acids Res.* **38,** 6526–6532 (2010).

69. Kundukad, B., Yan, J. & Doyle, P. S. Effect of YOYO-1 on the mechanical properties of DNA. *Soft Matter* **10,** 9721–9728 (2014).

70. Wenner, J. R., Williams, M. C., Rouzina, I. & Bloomfield, V. A. Salt dependence of the elasticity and overstretching transition of single DNA molecules. *Biophys. J.* **82,** 3160–3169 (2002).

71. Baumann, C. G., Smith, S. B., Bloomfield, V. A. & Bustamante, C. Ionic effects on the elasticity of single DNA molecules. *Biophys. J.* **94,** 6185–6190 (1997).

72. Odijk, T. Stiff chains and filaments under tension. *Macromolecules* **28,** 7016–7018 (1995).

73. Skolnick, J. & Fixman, M. Electrostatic persistence length of a wormlike polyelectrolyte. *Macromolecules* **10,** 944–948 (1977).

74. Odijk, T. Polyelectrolytes near the rod limit. *J. Polym. Phys. Edn* **15,** 477–483 (1977).

75. Dobrynin, A. V. Effect of counterion condensation on rigidity of semiflexible polyelectrolytes. *Macromolecules* **39,** 9519–9527 (2006).

76. Dobrynin, A. V. Electrostatic persistence length of semiflexible and flexible polyelectrolytes. *Macromolecules* **38,** 9304–9314 (2005).

77. Stigter, D. Interactions of highly charged colloidal cylinders with applications to double-stranded DNA. *Biopolymers* **16,** 1435–1448 (1977).

78. Nicolai, T. & Mandel, M. Ionic strength dependence of the second virial coefficient of low molar mass DNA fragments in aqueous solutions. *Macromolecules* **22,** 438–444 (1988).

79. Brian, A. A., Frisch, H. L. & Lerman, L. S. Thermodynamics and equilibrium sedimentation analysis of the close approach of DNA molecules and a molecular ordering transition. *Biopolymers* **20,** 1305–1328 (1981).

80. Bhandari, A. B., Reifenberger, J. G., Chuang, H.-M., Cao, H. & Dorfman, K. D. Measuring the wall depletion length of nanoconfined DNA. *J. Chem. Phys.* **149,** 104901 (2018).

81. Gupta, D., Bhandari, A. B. & Dorfman, K. D. Evaluation of Blob theory for the diffusion of DNA in nanochannels. *Macromolecules* **51,** 1748–1755 (2018).

82. Gupta, D., Miller, J. J., Muralidhar, A., Mahshid, S., Reisner, W. & Dorfman, K. D. Experimental evidence of weak excluded volume effects for nanochannel confined DNA. *ACS Macro Lett.* **4,** 759–763 (2015).

83. Iarko, V., Werner, E., Nyberg, L. K., Müller, V., Fritzsche, J., Ambjörnsson, T., Beech, J. P., Tegenfeldt, J. O., Mehlig, K., Westerlund, F. & Mehlig, B. Extension of nanoconfined DNA: Quantitative comparison between experiment and theory. *Phys. Rev. E* **92,** 062701 (2015).

84. Gupta, D., Sheats, J., Muralidhar, A., Miller, J. J., Huang, D. E., Mahshid, S., Dorfman, K. D. & Reisner, W. Mixed confinement regimes during equilibrium confinement spectroscopy of DNA. *J. Chem. Phys.* **140,** 214901 (2014).

85. De Gennes, P.-G. *Scaling Concepts in Polymer Physics* (Cornell University Press, 1979).

86. Daoud, M. & Gennes, P. G. D. Statistics of macromolecular solutions trapped in small pores. *J. Phys. France* **38,** 85–93 (1977).

87. Wang, Y., Tree, D. R. & Dorfman, K. D. Simulation of DNA extension in nanochannels. *Macromolecules* **44,** 6594–6604 (2011).

88. Odijk, T. Scaling theory of DNA confined in nanochannels and nanoslits. *Phys. Rev. E* **77,** 060901(R) (2008).

89. Tree, D. R., Wang, Y. & Dorfman, K. D. Mobility of a semiflexible chain confined in a nanochannel. *Phys. Rev. Lett.* **108,** 228105 (2012).

90. Odijk, T. On the statistics and dynamics of confined or entangled stiff polymers. *Macromolecules* **16,** 1340–1344 (1983).

91. Dai, L., van der Maarel, J. & Doyle, P. S. Extended de Gennes regime of DNA confined in a nanochannel. *Macromolecules* **47,** 2445–2450 (2014).

92. Muralidhar, A. & Dorfman, K. D. Kirkwood diffusivity of long semiflexible chains in nanochannel confinement. *Macromolecules* **48,** 2829–2839 (2015).

93. Metzler, R., Ambjörnsson, T., Hanke, A., Zhang, Y. & Levene, S. Single DNA conformations and biological function. *J. Comput. Theor. Nanosci.* **4,** 1–49 (2007).

94. Adams, C. C. *The knot book: An elementary introduction to the mathematical theory of knots* (American Mathematical Society, 2004).

95. Arai, Y., Yasuda, R., Akashi, K.-i., Harada, Y., Miyata, H., Kinosita, K. & Itoh, H. Tying a molecular knot with optical tweezers. *Nature* **399,** 446–448 (1999).

96. Soh, B. W., Narsimhan, V., Klotz, A. R. & Doyle, P. S. Knots modify the coil–stretch transition in linear DNA polymers. *Soft Matter* **14,** 1689–1698 (2018).

97. Soh, B. W., Klotz, A. R. & Doyle, P. S. Untying of complex knots on stretched polymers in elongational fields. *Macromolecules* **51,** 9562–9571 (2018).

98. Klotz, A. R., Soh, B. W. & Doyle, P. S. Motion of knots in DNA stretched by elongational fields. *Phys. Rev. Lett.* **120,** 188003 (2018).

99. Tang, J., Du, N. & Doyle, P. S. Compression and self-entanglement of single DNA molecules under uniform electric field. *Proc. Natl Acad. Sci. USA* **108,** 16153–16158 (2011).

100. Bao, X. R., Lee, H. J. & Quake, S. R. Behavior of complex knots in single DNA molecules. *Phys. Rev. Lett.* **91,** 265506 (2003).

101. Dai, L. & Doyle, P. S. Comparisons of a polymer in confinement versus applied force. *Macromolecules* **46,** 6336–6344 (2013).

102. Levy, S. L., Mannion, J. T., Cheng, J., Reccius, C. H. & Craighead, H. G. Entropic unfolding of DNA molecules in nanofluidic channels. *Nano Lett.* **8,** 3839–3844 (2008).

103. Ma, Z. & Dorfman, K. D. Diffusion of knots along DNA confined in nanochannels. *Macromolecules* **53,** 6461–6468 (2020).

104. Taylor, W. R. & Lin, K. Protein knots: a tangled problem. *Nature* **421,** 25–25 (2003).

105. Vologodskii, A. Brownian dynamics simulation of knot diffusion along a stretched DNA molecule. *Biophys. J.* **90,** 1594–1597 (2006).

106. Dommersnes, P. G., Kantor, Y. & Kardar, M. Knots in charged polymers. *Phys. Rev. E* **66,** 031802 (2002).

107. Möbius, W., Frey, E. & Gerland, U. Spontaneous unknotting of a polymer confined in a nanochannel. *Nano Lett.* **8,** 4518–4522 (2008).

108. Chuang, J., Kantor, Y. & Kardar, M. Anomalous dynamics of translocation. *Phys. Rev. E* **65,** 011802 (2001).

109. Kantor, Y. & Kardar, M. Anomalous dynamics of forced translocation. *Phys. Rev. E* **69,** 021806 (2004).

110. Soh, B. W., Narsimhan, V., Klotz, A. R. & Doyle, P. S. Knots modify the coil-stretch transition in linear DNA polymers. *Soft Matter* **14,** 1689–1698 (2018).

111. Narsimhan, V., Klotz, A. R. & Doyle, P. S. Steady-state and transient behavior of knotted chains in extensional fields. *ACS Macro Lett.* **6,** 1285–1289 (2017).

112. Klotz, A. R., Narsimhan, V., Soh, B. W. & Doyle, P. S. Dynamics of DNA knots during chain relaxation. *Macromolecules* **50,** 4074–4082 (2017).

113. Suma, A., Orlandini, E. & Micheletti, C. Knotting dynamics of DNA chains of different length confined in nanochannels. *J. Phys: Condens. Matter* **27,** 354102 (2015).

114. Tubiana, L., Rosa, A., Fragiacomo, F. & Micheletti, C. Spontaneous knotting and unknotting of flexible linear polymers: equilibrium and kinetic aspects. *Macromolecules* **46,** 3669–3678 (2013).

115. Nyberg, L., Persson, F., Åkerman, B. & Westerlund, F. Heterogeneous staining: a tool for studies of how fluorescent dyes affect the physical properties of DNA. *Nucleic Acids Res.* **41,** e184 (2013).

116. Carisson, C., Johnson, M. & Åkerman, B. Double bands in DNA gel electrophoresis caused by bis-intercalating dyes. *Nucleic Acids Res.* **23,** 2413–2420 (1995).

117. Lund, A. H., Duch, M. & Pedersen, F. S. Increased cloning efficiency by temperature - cycle ligation. *Nucleic Acids Res.* **24,** 800–801 (1996).

118. See `http://microfluidics.stanford.edu/download/CalcEquilibriumLoCv1p1.m` for the program for equilibrium reaction calculations.

119. Perssona, F. & Tegenfeldt, J. O. DNA in nanochannels - directly visualizing genomic information. *Chem. Soc. Rev.* **39,** 985–999 (2010).

120. Reisner, W., Morton, K. J., Riehn, R., Wang, Y. M., Yu, Z., Rosen, M., Sturm, J. C., Chou, S. Y., Frey, E. & Austin, R. H. Statics and dynamics of single DNA molecules confined in nanochannels. *Phys. Rev. Lett.* **94,** 196101 (2005).

121. Tegenfeldt, J. O., Prinz, C., Cao, H., Chou, S., Reisner, W. W., Riehn, R., Wang, Y. M., Cox, E. C., Sturm, J. C., Silberzan, P. & Austin, R. H. The dynamics of genomic-length DNA molecules in 100-nm channels. *Proc. Natl. Acad. Sci. USA* **101,** 10979–10983 (2004).

122. Savin, T. & Doyle, P. S. Static and dynamic errors in particle tracking microrheology. *Biophys. J.* **88,** 623–638 (2005).

123. Clopper, C. J. & Pearson, E. S. The use of confidence or fiducial limits illustrated in the case of the binomial. *Biometrika* **26,** 404–413 (1934).

124. Davison, P. F. The effect of hydrodynamic shear on the deoxyribonucleic acid from T2 and T4 bacteriophages. *Proc. Natl. Acad. Sci. USA* **45,** 1560–1568 (1959).

125. Muralidhar, A., Tree, D. R., Wang, Y. & Dorfman, K. D. Interplay between chain stiffness and excluded volume of semiflexible polymers confined in nanochannels. *J. Chem. Phys.* **140,** 084905 (2014).

126. Werner, E. & Mehlig, B. Confined polymers in the extended de Gennes regime. *Phys. Rev. E* **90,** 062602 (2014).

127. Reifenberger, J. G., Cao, H. & Dorfman, K. D. Odijk excluded volume interactions during the unfolding of DNA confined in a nanochannel. *Macromolecules* **51,** 1172–1180 (2013).

128. Kepten, E., Bronshtein, I. & Garini, Y. Improved estimation of anomalous diffusion exponents in single-particle tracking experiments. *Phys. Rev. E* **87,** 052713 (2013).

129. Uehara, E. & Deguchi, T. Knotting probability of self-avoiding polygons under a topological constraint. *J. Chem. Phys.* **147,** 094901 (2017).

130. Huang, L. & Makarov, D. E. Langevin dynamics simulations of the diffusion of molecular knots in tensioned polymer chains. *J. Chem. Phys.* **111,** 10338–10344 (2007).

131. Martin, D. S., Forstner, M. B. & Käs, J. A. Apparent subdiffusion inherent to single particle tracking. *Biophys. J.* **83,** 2109–2117 (2002).

132. Odijk, T. The statistics and dynamics of confined or entangled stiff polymers. *Macromolecules* **16,** 1340–1344 (1983).

133. Narsimhan, V., Renner, C. B. & Doyle, P. S. Jamming of knots along a tensioned chain. *ACS Macro Lett.* **5,** 123–127 (2016).

134. Vandans, O., Yang, K., Wu, Z. & Dai, L. Identifying knot types of polymer conformations by machine learning. *Phys. Rev. E* **101,** 022502 (2020).

135. Ma, Z. & Dorfman, K. D. Diffusion of knotted DNA molecules in nanochannels in the extended de Gennes regime. *Macromolecules* **54,** 4211–4218 (2021).

136. Kanaeda, N. & Deguchi, T. Universality in the diffusion of knots. *Phys. Rev. E* **79,** 021806 (2009).

137. Croxton, C. A. & Turner, R. M. Iterative convolution determination of the mobility of knotted macromolecules. *Macromolecules* **24,** 177–183 (1991).

138. Matuschek, D. W. & Blumen, A. Increase of the mobility of knotted macromolecules. *Macromolecules* **22,** 1490–1491 (1989).

139. Daoud, M. & De Gennes, P. G. Statistics of macromolecular solutions trapped in small pores. *J. Phys.* **38,** 85–93 (1977).

140. Brochard, F. & de Gennes, P. G. Dynamics of confined polymer chains. *J. Chem. Phys.* **67,** 52–56 (1977).

141. Dai, L., Tree, D. R., van der Maarel, J. R. C., Dorfman, K. D. & Doyle, P. S. Revisiting blob theory for DNA diffusivity in slitlike confinement. *Phys. Rev. Lett.* **110,** 168105 (2013).

142. Strychalski, E. A., Levy, S. L. & Craighead, H. G. Diffusion of DNA in nanoslits. *Macromolecules* **41,** 7716–7721 (2008).

143. Akerman, B. & Tuite, E. Single- and double-strand photocleavage of DNA by YO, YOYO and TOTO. *Nucleic Acids Res.* **24,** 1080–1090 (1996).

144. York, D., Evensen, N. M., Martínez, M. L. & Delgado, J. D. B. Unified equations for the slope, intercept, and standard errors of the best straight line. *Am. J. Phys.* **72,** 367–375 (2004).

145. Mavrovouniotis, G. M. & Brenner, H. Hindered sedimentation, diffusion, and dispersion coefficients for brownian spheres in circular cylindrical pores. *J. Colloid Interface Sci.* **124,** 269–283 (1988).

146. Hernández-Ortiz, J. P., de Pablo, J. J. & Graham, M. D. Fast computation of many-particle hydrodynamic and electrostatic interactions in a confined geometry. *Phys. Rev. Lett.* **98,** 140602 (2007).

147. Ma, Z. & Dorfman, K. D. Interactions between two knots in nanochannel-confined DNA molecules. *J. Chem. Phys.* **155,** 154901 (2021).

148. Sumners, D. & Whittington, S. G. Knots in self-avoiding walks. *J. Phys. A: Math. Gen.* **21,** 1689 (1988).

149. Ercolini, E., Valle, F., Adamcik, J., Witz, G., Metzler, R., Rios, P. D. L., Roca, J. & Dietler, G. Fractal dimension and localization of DNA knots. *Phys. Rev. Lett.* **98,** 058102 (2007).

150. Rieger, F. C. & Virnau, P. A Monte Carlo study of knots in long double-stranded DNA chains. *PLoS Comput. Biol.* **12,** e1005029 (2016).

151. Trefz, B., Siebert, J. & Virnau, P. How molecular knots can pass through each other. *Proc. Natl. Acad. Sci. USA* **111,** 7948–7951 (2014).

152. Najafi, S., Podgornik, R., Potestio, R. & Tubiana, L. Role of bending energy and Knot chirality in knot distribution and their effective interaction along stretched semiflexible polymers. *Polymers* **8,** 347 (2016).

153. Najafi, S., Tubiana, L., Podgornik, R. & Potestio, R. Chirality modifies the interaction between knots. *Europhys. Lett.* **114,** 50007 (2016).

154. Richard, D., Stalter, S., Siebert, J. T., Rieger, F., Trefz, B. & Virnau, P. Entropic interactions between two knots on a semiflexible polymer. *Polymers* **9,** 55 (2017).

155. Klotz, A. R., Soh, B. W. & Doyle, P. S. An experimental investigation of attraction between knots in a stretched DNA molecule. *Europhys. Lett.* **129,** 68001 (2020).

156. Kachan, D., Bruinsma, R. & Levine, A. J. Casimir interactions in semiflexible polymers. *Phys. Rev. E* **87,** 032719 (2013).

157. Gilles, F. M., Llubaroff, R. & Pastorino, C. Fluctuation-induced forces between rings threaded around a polymer chain under tension. *Phys. Rev. E* **94,** 032503 (2016).

158. Amin, S. Knot formation on nanochannel-confined DNA and flow-assisted DNA disentanglement and linearization. *PhD Thesis, McGill University Libraries* (2018).

159. Guan, J., Wang, B., Bae, S. C. & Granick, S. Modular stitching to image single-molecule DNA transport. *J. Am. Chem. Soc* **135,** 6006–6009 (2013).

160. Chuang, H.-M., Reifenberger, J. G., Cao, H. & Dorfman, K. D. Sequence-dependent persistence length of long DNA. *Phys. Rev. Lett.* **119,** 227802 (2017).

Appendix A

Supporting Information to Chapter 4

This appendix includes the supporting figures of k-means clustering analysis and determination of upper and lower bounds for fitting the T4 DNA chain diffusivity before and after knot generation for Chapter 4.

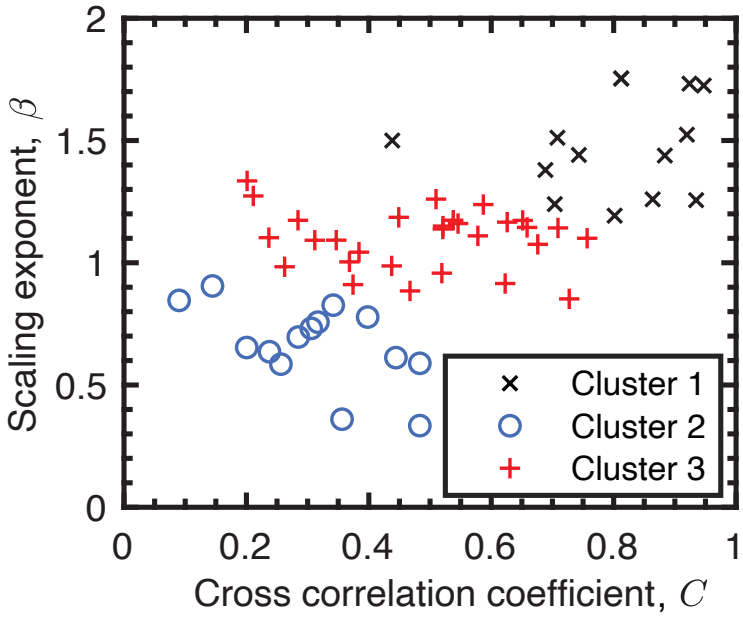

Figure A.1: k-means clustering result for the data of scaling exponent, β, and average cross correlation coefficient, C, for an ensemble of T4 DNA molecules in each movie. The k-means clustering analysis partition the data into three clusters that molecules are highly correlated and superdiffusive, relatively uncorrelated, and very uncorrelated. The cluster 1 (black $\times$) is the data set of DNA molecules with high β and C values. These molecules are highly correlated with all of the other molecules within the same movie and exhibit strongly superdiffusive behavior, and were excluded from the subsequent DNA diffusion analysis. Clusters 2 (blue $\bigcirc$) is the data set of very uncorrelated molecules with relatively small beta values. The molecules in cluster 3 (red $+$) are relatively uncorrelated DNA molecules with beta values between 0.8 and 1.4. The intact T4 DNA molecules with knots formed after the compression process in cluster 2 and cluster 3 are used for DNA diffusion analysis.

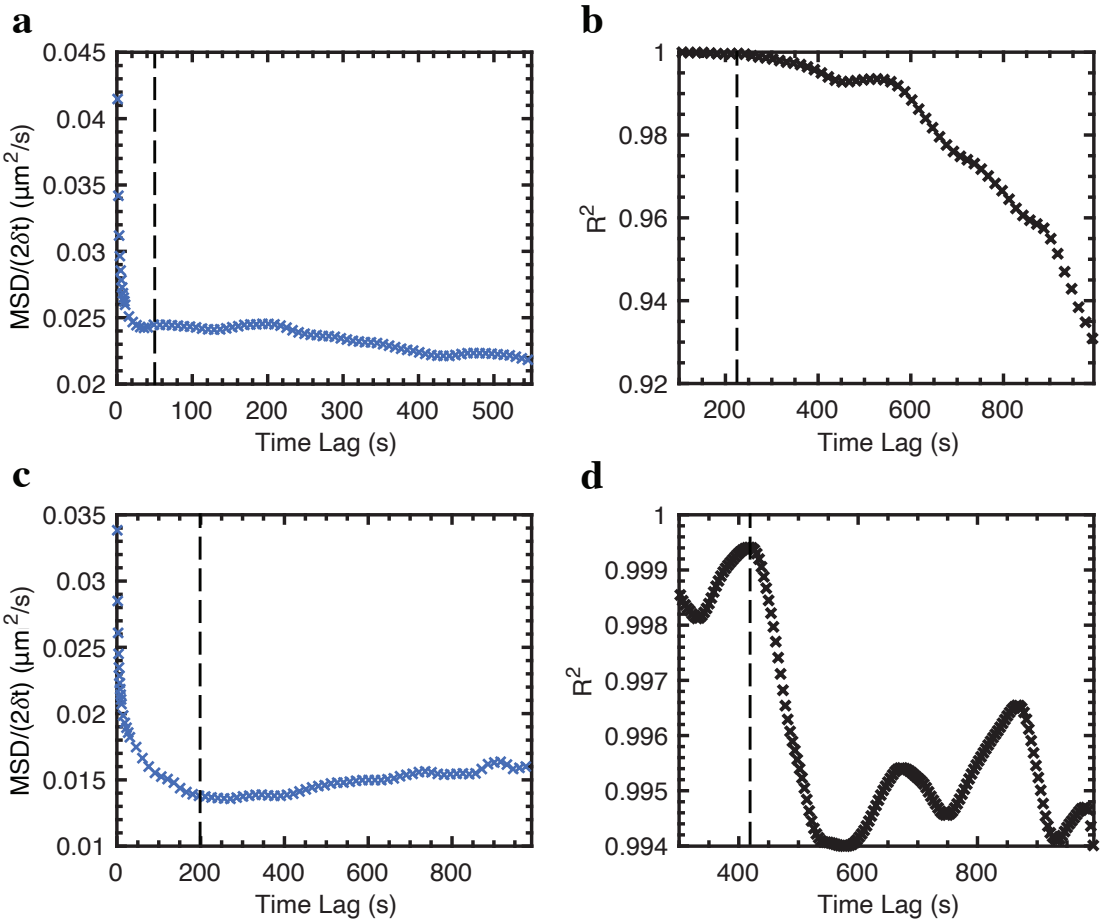

Figure A.2: Determination of upper and lower bounds of the time lag used for fitting the T4 DNA chain diffusivity in nanochannels before and after knotting. (a, c) The dynamic diffusion coefficient, MSD/$2\delta t$, as a function of time lag and (b, d) the correlation coefficient, R^2, of the linear fit line Eq. 5 with different upper bounds and a fixed lower bound for unknotted DNA (a, b) and knotted DNA molecules (c, d). The MSD/$2\delta t$ curve decays continuously until the time lag of 50 s for unknotted DNA molecules and 200 s for DNA with knots. The initial decay is due to a dynamical error from the DNA motion during finite exposure time [122]. The lower bound thus is 50 s for the DNA before knotting and 200 s for the knotted DNA molecules. The upper bound for fitting the ensemble-averaged MSD data to obtain the DNA chain diffusivity, D, is determined by calculating the R^2 of the linear fit function Eq. 5 with different upper bounds and a fixed lower bound of 50 s for unknotted DNA and 200 s for knotted DNA. The R^2 curve of unknotted DNA starts to decay at the time lag of 227 s which is determined to be the upper bound for the unknotted DNA. For DNA with knots, the upper bound is 418 s, which is the point with the largest value of R^2. The lower and upper bounds are indicated by the black vertical dashed lines.

Appendix B

Supporting Information to Chapter 5

This appendix presents the supporting figures of free energy profiles of two-knot interactions for knots with diverse sizes and motion of two knots in nanochannel-confined DNA molecules.

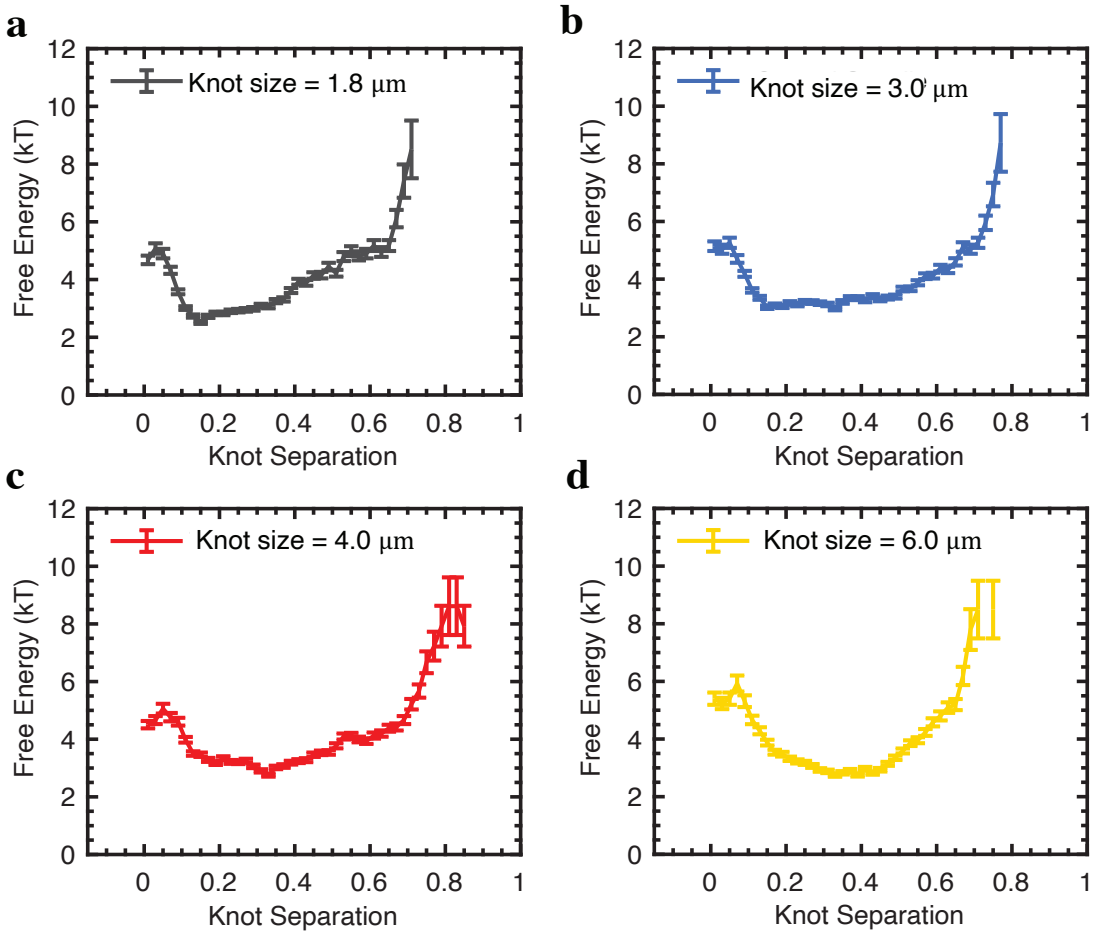

Figure B.1: Free energy profiles of knot-knot interactions in nanochannel-confined DNA for quartiles of knots with size of (a) 1.8 μm (black line), (b) 3.0 μm (blue line), (c) 4.0 μm (red line) and (d) 6.0 μm (yellow line). The knot size is estimated as the extension difference between knotted and unknotted DNA molecules.

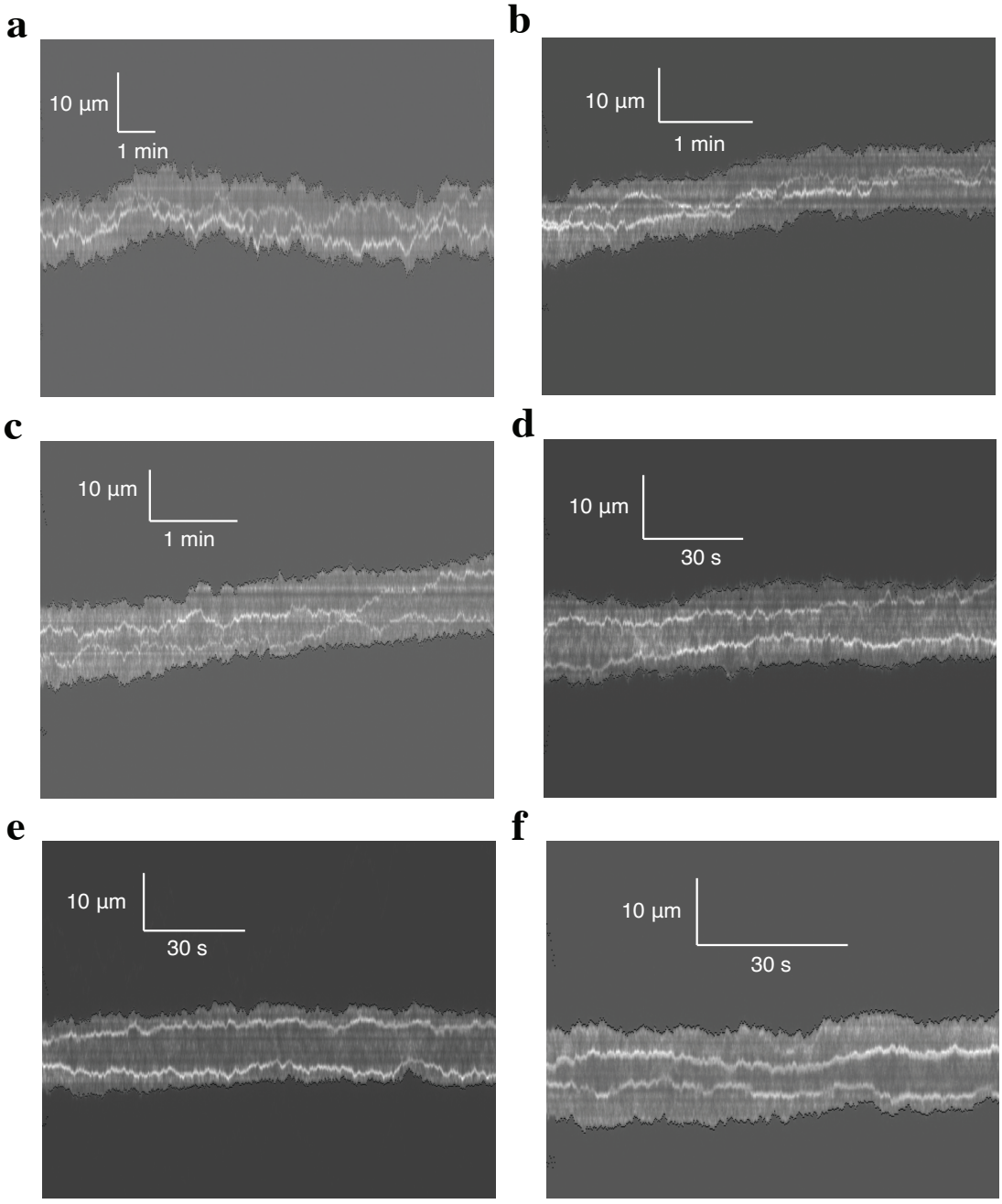

Figure B.2: Six kymographs of DNA molecules containing two knots. The vertical axis is the intensity along a nanochannel and the horizontal axis is the time. The knots are identified as bright spots, moving along the DNA molecules. (a, b, c) The widely separated knots attract each other but only remain in close for several seconds. (d, e, f) The knots tend to remain separated until one of the knots unravels at the chain end.

Appendix C

Protocols

In this appendix, we describe details of the steps and tips for the nanofluidic knot factory device fabrication in Minnesota Nano Center (MNC) cleanroom, T4 GT7 DNA sample preparation and knot experiments presented in the dissertation.

C.1 Device Fabrication

The devices are fabrciated on fused silica substrates using a combination of electron beam (E-beam) lithography to first create nanochannels and then nanoslits and subsequent optical photolithography to fabricate microchannels. The workflow to fabricate the nanofluidic devices is shown in Figure C.1.

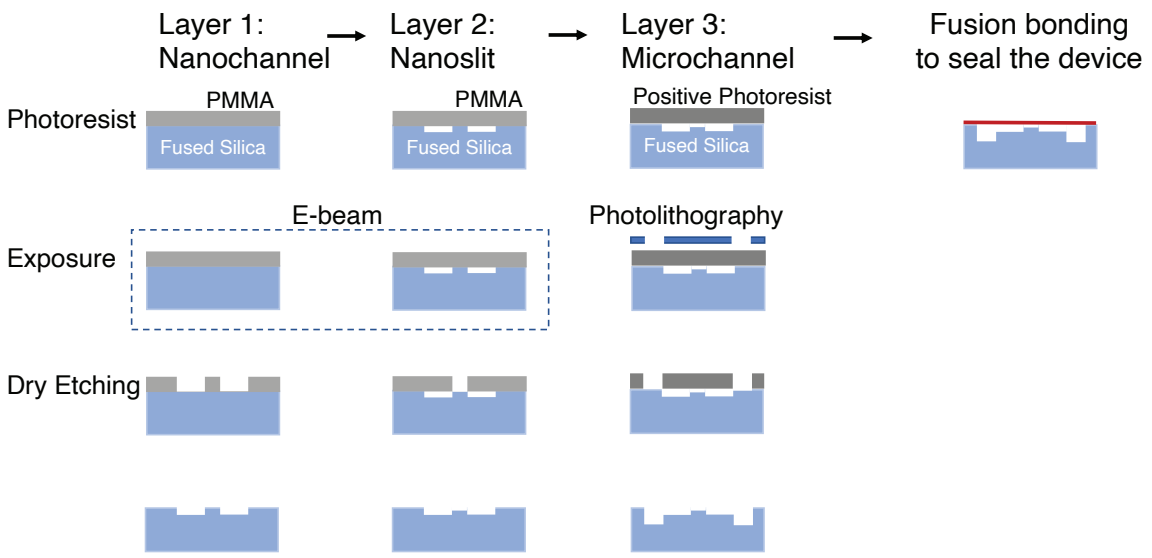

Figure C.1: Schematic illustration of workflow for fabricating nanofluidic knot factory devices.

Nanochannels and Nanoslits

1. Design of nanochannels and nanoslits

   (a) Create nine patterns consisting of 89 nanochannels and 89 nanoslits with four alignment marks next to each of the patterns using CleWin software and save the file in GDS format. Note here the nanochannels with alignment marks and nanoslits are in separate layers of the design in CleWin. The GDS file is then transferred to CAD server using FileZilla.

   (b) On the CAD server, fracture the nanochannels with algnment marks and nanoslits separately using LayoutBEAMER. First drag the "Import" box and select the pattern in the GDS file. Then, connect "Healing" over the bottom of the "Import" box and then drag "PEC" over the bottom of the

"Healing" box. Finally, add the "Export" box to ouput the GDS file to GDF file.

(c) Generate job file using CJOB on the CAD server. First, drag a "Substrate" object into the work area of CJOB and choose wafer 100 100 0° 32.5 as the substrate. Then, drag an "Exposure" object under the "Substrate" for the file with nanochannels. For the file with nanoslits, drag an "Exposure" object under the "Substrate" and enter the global alignment mark locations. Next, drag a "Pattern" object under the "Exposure" object and set the dose and the beam current. Finally, export the file as JOB file.

2. Fabrication of nanochannels using non-aligned writing and nanoslits using aligned writing of the electron-beam lithography followed by a reactive ion etching

(a) Clean 4″ fused silica wafer and 4″ silicon wafer in acid piranha for 1 hour. Wash the wafers twice using DI water. Then, dry the wafers using Spin Rinse Dryer equipment.

(b) Prepare PMMA C 6.5 - 950 Resist using resist-thinner rinsed glasswares. Add 13 ml 950 PMMA C 9 and 5 ml chlorobenzene into a clean bottle and then mix the solution by moving the bottle up and down.

(c) Dehydration bake of the 4″ fused silica wafer at 180°C for 1 - 2 minutes. Apply the PMMA C 6.5 - 950 resist and imprint the resist uniformly on the substrate using CEE spinner. Set the spin speed to be 4000 rpm, acceleration to be 1000 rpm/s and spin time to be 30 s. Before using one hand to remove the coated wafer from the spinner, wait for 2 minutes. Then, soft bake the wafer at 180°C for 5 minutes.

(d) Deposit gold onto the fused silica wafer using Cressigton sputter coater with a 15 s cyclic process for 90 s. The thickness of the gold layer is about 30 nm.

(e) Create nanochannel pattern using Vistec E-Beam. Load the wafer in the 4″ wafer holder. Locate the center of wafer, which is the write location for creating nanochannel patterns, using the alignment microscope. For creating nanoslits through aligned writing, written locations are the three positions where the three global alignment marks are in the approximate center of the monitor. Load the holder into the system and execute the JOB file to create the nanochannel pattern using non-aligned writing and the nanoslit pattern using aligned writing. Unload the wafer holder and then the wafer.

(f) Etch the gold layer first by immersing the wafer into the diluted gold etchant containing 40 ml of gold etchant and 40 ml DI water for 2 minutes.

(g) After removing the gold layer, develop the wafer by first submerging the wafer in isopropyl alcohol (IPA)/methyl isobutyl ketone (MIBK) 3 : 1 Developer for 30 s with gentle string, rinsing with IPA for 30 s, and then drying with nitrogen. After each developing process, check all the patterns on the fused silica wafer using the microscope. To inspect the transparent wafer, a cleaned silicon wafer is placed at the bottom of the fused silica wafer. If the patterns are not clear, repeat the developing process but for 10 s in each step instead of 30 s. Heat the developed wafer at 90°C for 90 s.

(h) Etch the patterns into the substrate using a plasma etching with a 1 min

cyclic process. First, etch the wafer using oxygen clean for 10 s and then etch the wafer using a fluorine reactive ion etching. The parameters used for the etching step called pjsoxide in MNC cleanroom are 50 sccm argon, 50 sccm trifluoromethane and 25 sccm tetrafluoromethane at 75 millitorr pressure with 150 watts. The etching time depends on the etching rate. To create the nanochannles with 340 nm depth, the etching time is 22 minutes. For nanoslites with 32 nm depth, the etching time is 2 minutes and 10 seconds. The suggestions to etch channels with a targeted depth are to measure the etching rate first before etching a new pattern.

(i) After the etching process, lift off the PMMA resist by soaking the etched wafer into a n-methylpyrrolidone (NMP) solution for 30 - 60 minutes at 180 °C. Then, rinse the wafer using acetone, methanol and then IPA. Finally, clean the wafer in acid piranha for 1 hour.

(j) Measure the thickness of the nanochannels using a KLA Tensor P-7 profilometer.

(k) After creating the nanochannels, repeat step 2(b - j) in this section to create the nanoslits pattern.

Microchannels

1. Fabrication of microchannels using optical photolithography

   (a) Draw arrows near marks on the back side of the fused silica wafer to locate wafer alignment marks.

   (b) Dehydration bake the wafer at 150 °C for 3 minutes. Then, the wafer

is placed into a chamber for hexamethyldisilizane (HMDS) process for 3 minutes. Spin coat AZ 1512 positive photoresist on the wafer at 3000 rpm speed and 3000 rpm/s acceleration for 30 s. Soft bake the coated wafer at 100 °C for 60 s. Expose the wafer with the patterned mask to create microchannels using MA6 mask aligner for 5 s with 25 μm align gap and soft contact mode. Note here the chrome mask is fabricated using the Heidelberg laser writer.

(c) Post-bake the exposed wafer at 95 °C for 60 s. Then, develop the wafer in 351 developer with developer to DI water ratio of 1 : 5 for 30 s by gently shaking the crystallizing dish and rinse the wafer with DI water for 2 minutes. Inspect the microchannel patterns using microscope.

(d) Etch the patterns into the substrate using a plasma etching with a 20 min cyclic process. The parameters used for the etching step called pjsoxide in MNC cleanroom are 50 sccm argon, 50 sccm trifluoromethane and 25 sccm tetrafluoromethane at 75 millitorr pressure with 150 watts. The etching time depends on the etching rate. To create the microchannels with 0.8 μm depth, the etching time is 70 minutes.

(e) Strip off the photoresist by soaking the etched wafer into NMP for 30 - 60 minutes at 180 °C. Then, rinse the wafer using acetone, methanol and then IPA. Finally, clean the wafer in acid piranha for 1 hour.

(f) Measure the thickness of the nanochannels using a KLA Tensor P-7 profilometer.

Device Bonding

1. Wafer Saw

   (a) Spin coat the wafer with a photoresist to protect the patterns on the wafer during the cutting process. Then, mark the cutting line from the top side of the wafer using a Sharpie marker. Mount the substrate on a blue dicing tape with thickness of 75 μm.

   (b) Cut the fused silica wafer using Disco DAC-522 wafer dicing saw.

2. Sandblasting

   (a) Denote hole locations using a Sharpie marker on both sides of the cut device. Place masking tape on both sides of the device. Draw hole locations again and mark the front side of the device. Cut away squares at the hole locations with a new razor blade. Note here cut away larger squares on the back side of the device compared to the squares on the front side of the chip.

   (b) Add sand to a gun reservoir. Start sandblasting at a 90 degree angle with respect to the backside of the device in 1 - 2 mm away for several minutes. Check periodically if the hole is sandblasted.

   (c) After sandblasting all the holes, wet the chip using acetone and remove the tapes.

3. Fusion Bonding

   (a) Place a coverslip rack with the devices and coverslips in a crystallizing dish. First add 660 ml sulfuric acid and then add 220 ml hydrogen peroxide

slowly. Soak the devices and coverslips for 15 - 20 minutes. Rinse with DI water and then dry with nitrogen.

(b) Add 700 ml DI water into another crystallizing dish and heat to 85 °C. Place the devices and coverslips in the container. After the temperature reaches 85 °C, add 140 ml hydrogen chloride and then 140 ml hydrogen peroxide. The devices and coverslips are immersed for 20 minutes at about 80 °C. Rinse with DI water and then dry with nitrogen.

(c) Add 750 ml DI water into another crystallizing dish and heat to 75 °C. Place the devices and coverslips in the container. After the temperature reaches 75 °C, add 150 ml ammonia hydroxide and then 150 ml hydrogen peroxide. The devices and coverslips are immersed for 20 minutes at about 70 °C. Rinse with DI water and then dry with nitrogen.

(d) Temporally bond the device with a coverslip by pressing the two pieces of glasses together using two fingers first and then use a tweezer to remove access air between the device and the coverslip.

(e) Permanently bond the device by placing it in the Thermo Scientific - Lindberg Blue M oven. Program the oven to heat the device according to the following instructions:

- Start at 25 °C.
- Ramp to 1000 °C over 4 hours.
- Hold at 1000 °C for 6 hours.
- Cool down to 25 °C over 4 hours.
- Hold at 25 °C indefinitely.

(f) The device is ready for the knot experiments.

C.2 Nanochannel Experiments

In this work, T4 GT7 DNA was stained with YOYO-1 fluorescent dye at a dye-to-DNA base pair ratio of 10:1 in a 5× TBE solution and subsequently diluted to a 0.25× TBE. The detailed workflow for generating DNA knots and imaging knotted DNA in the fabricated nanofluidic devices is also presented in this section.

DNA Sample Preparation

1. DNA stock solution

   (a) Filter out 2 ml of 5× TBE buffer into a microcentrifuge tube using 0.2 μm pore size filter. Remove 0.01 mM YOYO-1 solution from the freezer to defrost and heat T4 GT7 DNA with a concentration of 760 μg/ml solution at 40 °C for 5 minutes in water bath to defrost.

   (b) Pipette 73.1 μl of ultrapure water and 100 μl of filtered 5× TBE buffer into an amber microcentrifuge tube. Then, pipette 2.1 μl of T4 GT7 DNA using a wide bore pipette tip. Add 24.8 μl 0.01 mM YOYO-1 solution into the same tube and mix the solution via slow motion of the pipette tip to avoid DNA shear.

   (c) To ensure the uniform staining of DNA molecules with YOYO-1, heat the solution in water bath at 50 °C for 3 hours. After 3 hours, remove the centrifuge tube from the water bath, cool it to room temperature and then store it in 4 °C refrigerator.

2. DNA loading solution

   (a) The DNA loading solution is prepared before the start of the experiments. Pipette 86 µl of ultrapure water, 10 µl of DNA stock solution and 4 µl of β-mercaptoethanol into an amber microcentrifuge tube. Mix the solution by gently stirring the solution with the pipette tip.

3. Buffer loading solution

   (a) The buffer loading solution is prepared before the start of the experiments. Pipette 227.5 µl of ultrapure water, 12.5 µl of filtered 5× TBE buffer and 10 µl of β-mercaptoethanol into a microcentrifuge tube. Mix the solution by vortexing the tube for 1 minute.

Knot experiments

1. Knot generation and detection

   (a) Load one device reservior at a time with 4 µl of the DNA loading solution. Wait for one microchannel to fill completely before moving onto the next reservoir of the other microchannel.

   (b) Mount the wet nanofluidic device onto the chuck. Then, load 6 µl of buffer loading solution with the same ionic strength as the DNA loading solution in each well of the pressure chuck to avoid drying using gel loading pipette tips. Completely seal the pressure chuck with screws.

   (c) Add oil on the 100× objective. Connect air lines from Fluigent, which is the microfluidic flow control system, to the pressure chuck. Then, mount the pressure chuck on the laser microscope.

(d) Image microchannels near the nanochannel to check if there are bubbles in the microchannels using bright field option of the microscope. If there are bubbles, use a pulsed 25 psi pressure to remove them. Then, wait for 1 hour for flow inside the device to reach an equilibrium.

(e) Load intact T4 GT7 DNA from one microchannel to nanochannels using 35 kPa pressure. Make sure there is only one DNA per nanochannel and then drive the DNA molecules using 10 kPa pressure until the DNA are close to the slit barriers. Compress the DNA molecules using 5 kPa pressure and wait for 1 minute. The pressure and waiting time can be changed to modify the probability of knot generation.

(f) After 1 minute of waiting time, move DNA away from the slit barriers using 5 kPa pressure. Then, stop the pressure, pause the microfluidic flow control system, and wait for 2 minutes to allow DNA molecules to relax.

(g) Image the DNA molecules after the compression process to check if there are knots formed in the DNA chains using a 0.5 mW blue class III laser (Coherent OBIS, 473 nm) with 50 ms exposure time.

(h) Set desired imaging condition, which depends on the application and image the knotted DNA in nanochannels.

(i) After image acquisition, unload the knotted DNA molecules using 5 kPa pressure and repeat step 1(e - h) in this section for imaging new DNA molecules.

2. Device clean with base piranha solution

(a) After the knot experiments, place the device in ultrapure water overnight

to reduce the ionic strength in channels. Then, dry the surface of the device with Kim Wipes.

(b) Dry the channels using filtered air. Then, flush the channels with ultrapure water by pipetting 2 μl of ultrapure water into one reservoir at a time. Wait for one microchannel to completely wet before adding ultrapure water into another reservoir.

(c) Repeat step 2(b) in this section two more times. In the third time, wet the device using base piranha solution (hydrogen peroxide : ammonium hydroxide = 1 : 2) instead of ultrapure water. Then, submerge the device in the base piranha solution with the holes of the device facing up at 80 °C for 40 minutes.

(d) Remove the device from the base piranha solution and rinse the device with ultrapure water. Then, repeat step 2(b) in the section twice.

(e) Dry the device by following the step 3(e) in the section of Device Bonding. The dried device is ready for the next knot experiments.